Automated analysis approaches for coronary CT angiography : labeling, quality assessment and plaque thickness comparison

Cao, Q.

Automated Analysis Approaches for Coronary CT Angiography

Labeling, Quality Assessment and Plaque Thickness Comparison

Qing Cao

Automated Analysis Approaches for Coronary CT Angiography: Labeling, Quality Assessment and Plaque Thickness Comparison

Cover design Qing Cao

Layout Qing Cao

Printed by Ridderprint BV

ISBN: 978-94-6375-747-8

Automated Analysis Approaches for Coronary CT Angiography

Labeling, Quality Assessment and Plaque Thickness Comparison

Proefschrift

ter verkrijging van
de graad van Doctor aan de Universiteit Leiden,
op gezag van prof. mr. C.J.J.M. Stolker,
volgens besluit van het College voor Promoties
te verdedigen op dinsdag, 21 januari 2020
klokke 10:00 uur

door

Qing Cao

geboren te Jiangyan, P.R. China

in 1990

Promotor	**Prof.dr.ir. B.P.F. Lelieveldt**
Copromotor	**Dr.ir. J.Dijkstra**
Leden promotiecommissie	**Prof.dr. P. Knappen** *Amsterdam University Medical Center* **Dr. J.J. Wentzel** *Erasmus Medical Center* **Prof.dr. P.H.A. Quax** *Leiden University Medical Center*

The research presented in this thesis was performed at the Division of Image Processing, Department of Radiology of Leiden University Medical Center, The Netherlands.

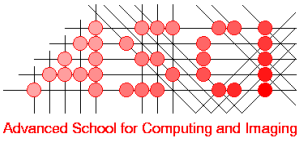

This work was carried out in the ASCI graduate school.
ASCI dissertation series number 411

Financial support by the Dutch Heart Foundation for the publication of this thesis is gratefully acknowledged.

Financial support for the publication of this thesis was kindly provided by:

The Dutch Heart Foundation

ASCI graduate school

Leiden University Library

GE Medical Systems (China)

CONTENTS

CHAPTER 1

General Introduction

CORONARY ARTERY DISEASE

Coronary artery disease (CAD) is still one of the leading causes of death worldwide [1] which is usually caused by the build-up of plaque in the walls of the coronary arteries resulting in limited blood flow to the heart muscle.

Coronary Arteries

Coronary arteries are the blood vessels around the heart which supply blood to different parts of the heart muscle (Figure 1.1). There are two major coronary arteries, the right coronary artery (RCA) and the left coronary artery (LCA). The LCA is further separated into left anterior descending (LAD) and the left circumflex (LCX). Their common part is called the left main (LM) artery. Some side branches, such as septal perforator, obtuse marginal (OM), and diagonals (D) are derived from RCA and LCA.

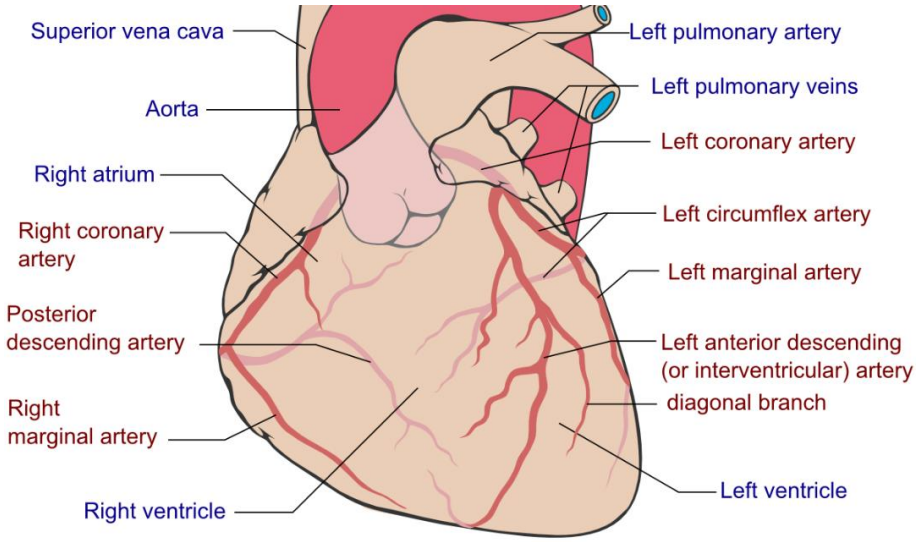

Figure 1.1 Heart and coronary arteries from a right dominance type coronary circulation. Coronary segments are marked with corresponding anatomical names. When posterior descending artery is supplied by left circumflex artery, it is called left dominance type. From: (https://commons.wikimedia.org/wiki/File:Coronary_arteries.svg)

Coronary Circulation

Coronary circulation has major importance in the system circulation since it supports not only the heart but also the entire body. The main artery, RCA or LCX, that supplies the posterior descending artery (PDA) determines the dominance type of the coronary circulation [2]. In the general population, there are three categories of coronary circulations: the right dominant (RD, 86.6% of the population) in which the PDA is supplied by the RCA and is called right posterior descending artery (RPDA); the left dominant (LD, 9.2%) in which the PDA is supplied by the LCX and is called left posterior descending artery (LPDA); and the balanced

type (4.2%) in which both RCA and LCX supplies PDA [3]. Figure 1.1 shows a right dominant coronary artery circulations. The anatomical names of corresponding coronary arteries are marked.

Coronary Artery Plaque

Due to several processes, and also depending on life style and age, plaques build up in the coronary arteries, which eventually may result in lumen stenosis. If the plaque grows large enough, a semi-blockage or full blockage of the artery will cause a chest pain or a heart attack (Figure 1.2). Coronary plaques can develop at different locations in the coronary arteries with a different size. Furthermore, a build-up of plaque in the arteries not only puts people at risk for heart and vascular disease but also makes them vulnerable to cancer, kidney, and lung diseases [4].

CAD often develops over decades. An early diagnosis of the plaque location, size and type will help the risk stratification, early treatment, and prognosis. Due to the rapid development of imaging techniques, a more advanced and detailed diagnosis of CAD is available nowadays.

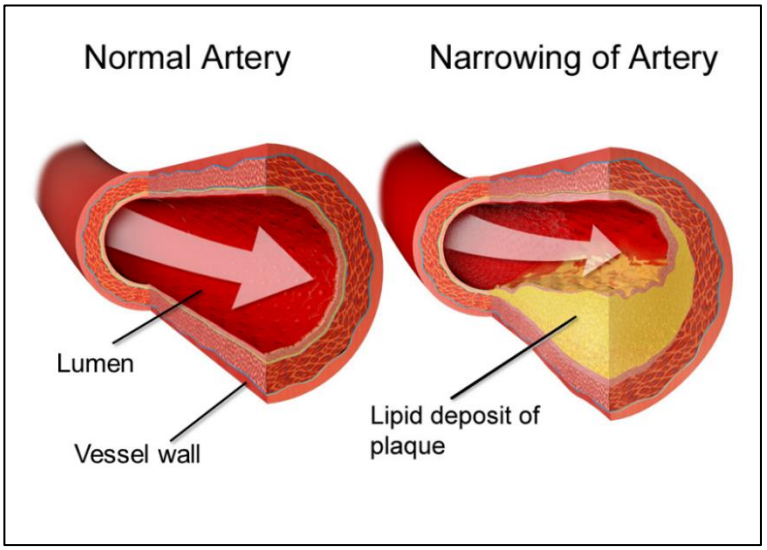

Figure 1.2 Coronary lumen and Vessel wall [5].

IMAGING TECHNIQUES

Different imaging modalities are available for CAD diagnosis and plaque characterization [6, 7]. The choice of the imaging modality depends on the goal and varies among different countries, regions and even hospitals. In the following sections, we categorize the imaging techniques as invasive and non-invasive imaging modality to give a brief introduction.

Invasive Coronary Angiography (ICA)

X-Ray Angiography uses x-ray as imaging source and makes use of that different tissues absorb different amounts of x-rays. To ensure adequate opacification of the coronary lumen, a contrast agent is administered into the arteries by an intracoronary catheter to enhance the lumen. X-ray angiography is still the most commonly used technique in the catheterization laboratories for the visualization of the coronary arteries and to guide the treatment when necessary [8]. However, the vessel wall (plaque) cannot be visualized by X-ray images, which limits its application for CAD early diagnosis. Furthermore, X-ray angiography is limited by its 2D projection of the lumen in a moving coronary arterial tree. The C-arm based x-ray angiography provides views from different viewing angles. Therefore, the angiography images from different viewing angles allows for the possibility of a 3D/4D reconstruction for the coronary arteries [9].

During the last decades, other invasive imaging technologies have been developed, intravascular ultrasonography (IVUS) [10], optical computed tomography (OCT) [11], and near-infrared spectroscopy (NIRS) [12]. They are all catheter-based techniques. A detector is placed inside of the coronary artery with the guidance of the x-ray angiography which enables its ability to evaluate the vessel wall.

Intravascular ultrasonography (IVUS) uses ultrasound as imaging source to provide real-time cross-sectional images with a resolution of about 0.1 to 0.2 mm, which is able to view the vessel wall and enables an early detection of plaques. IVUS is highly accurate for detecting and quantifying CAD and has become an integral tool in the catheter laboratory for the characterization of intermediate angiographic stenosis [10]. IVUS remains the gold standard for plaque quantification [13].

Intravascular optical coherence tomography uses near-infrared (NIR) light, typically with wavelengths of approximately 1.3 μm, as the imaging source in in which a catheter is inserted in to coronary artery [11]. The acquired OCT images provides higher resolution (10-20μm) cross-sectional images compared to IVUS which enables the capability of plaque composition and thin fibrous cap analysis. However, the penetration of OCT is limited due to high light attenuation, which makes OCT only assess the superficial layers of the vessel wall. It also requires blood-free field of view which may add significant complexity to the procedure.

Near-infrared spectroscopy system (NIRS) is based on the principle that different substances absorb NIR light to different degrees at different wavelengths (from 800 ~2500 *nm*) when the light interacts with certain molecular bonds [12]. NIRS is used for the identification of lipid-rich and potentially vulnerable atherosclerotic plaques. The main limitation of NIRS is the lack of information regarding the lumen, plaque anatomy, and the status of the fibrous cap or its attenuation. NIRS is combined with IVUS to enable a complete assessment of patient's arteries, including vessel size and structure, plaque volume, area, and composition [14].

All of these are invasive imaging techniques which rely on arterial catheterization under the guidance of X-ray to gain direct access of the coronary vasculature. Since these technologies are invasive, they are often used for patients with intermediate or advanced CAD which are candidates to undergo an intervention. For routine check, or stable chest pain doing an invasive check is costly and not patient-friendly.

Noninvasive Coronary Angiography

Although invasive coronary angiography has been the gold standard in establishing the diagnosis of CAD, there is a growing shift towards using noninvasive imaging modalities for more efficient use of the cardiac catheterization laboratory to perform interventional procedures once a diagnosis of CAD has been established.

***Coronary computed tomography angiography* (*CCTA*)** is a noninvasive technique and uses x-ray as imaging source to do a slice scanning which later can be reformatted into a 3D image. To provide a contrast in the coronary artery, a contrast agent is injected into the coronary intravenously. CCTA is widely used for the assessment of patients with suspected CAD because of its high specificity and sensitivity [15, 16]. It provides detailed information about the anatomy of the coronary arteries and the characteristics of coronary atherosclerosis such as the extent of calcifications, the volumetric plaque burden, plaque composition, degree of stenosis and occlusions.

Magnetic resonance angiography (MRA) uses strong magnetic fields to generate images of the organs and therefore does not involve radiation. However, the relatively long image acquisition time and operator dependency have limited the widespread use of coronary MRA. It is not frequently used in coronary arteries since coronary arteries are tortuous and smaller in size, and both the heart motion and respiratory motion affect the image quality [17]. The use of coronary MRA is more on the blood flow of the coronary artery for a functional check [6]. Moreover, most experts and clinical guidelines support the use of coronary MRA only for the assessment of anomalous coronary arteries and coronary artery aneurysms in patients with Kawasaki disease.

Nuclear Medical Imaging Single-photon emission computed tomography (SPECT) and positron emission tomography (PET) are nuclear medicine techniques which provide measurements of myocardial disease through functional imaging. SPECT uses gamma emitting radionuclides which can reconstruct 3D images from different 2D images of distribution of radionuclides in the targeted organ taken by a gamma camera from different angles. SPECT allows for a qualitative or semi-quantitative assessment of regional perfusion defects. PET uses positron emitting radionuclides, which are labelled to biological compounds of interest, to generate images of physiological processes [18]. Different from SPECT, PET is able to provide absolute quantitative of myocardial flow and coronary flow reserve. SPECT and PET are often accomplished with the aid of CT scans or MRI scans which are obtained in the same session and provide both anatomic and metabolic information.

It is difficult to make a general conclusion on the optimal imaging technique. The optimal choice for the right modality for diagnosing CAD is a combination of the purpose of the test, patient situation, health care budget and the experience of the doctor.

In this thesis, we are discussing the use of CCTA images in terms of its non-invasively early diagnosis that is fast and has a high resolution together with its feasibility for precise plaque quantification.

CORONARY COMPUTED TOMOGRAPHY ANGIOGRAPHY (CCTA)

CCTA is widely used for the assessment of patients with suspected CAD [15, 16]. From 2009, CCTA was introduced as a new, alternative option for emergency department evaluation of non-acute coronary syndrome cardiac chest pain [19]. It provides detailed information about the anatomy of the coronary arteries and the characteristics of coronary atherosclerosis such as the extent of calcifications, the volumetric plaque burden, degree of stenosis and occlusions.

Patient management Despite the non-invasive and high-speed imaging, CCTA has advantages in health care resource utilization which reduced unnecessary hospital admissions and emergency department length of stay [19]. From a point of patient management view, CCTA also enables the long-term prognostic assessment for patients with suspected CAD.

Apart from identifying coronary artery narrowing as the cause of chest discomfort, it can also detect other possible causes of symptoms, such as a collapsed lung, blood clot in the vessels leading to the lungs, or acute aortic abnormalities.

Dose Reduction Strategies The main drawbacks of using CCTA includes radiation and contrast exposure. Various strategies have been proposed to reduce the radiation dose, such as lowering tube voltage, or prospective electrocardiogram-gated tube current modulation, while preserving diagnostic accuracy [20, 21]. Recent developments in low-dose CT reduces the radiation without deteriorate the imaging quality.

Reporting System For standardizing the interpretation and reporting of coronary CT angiography, the first guideline was made in 2009 and then updated in 2014 by the Society of Cardiovascular Computed Tomography Guidelines Committee (SCCT) [22, 23]. In clinical practice, radiologists and cardiologists usually report pathological findings from CCTA images according to the SCCT guidelines in which a coronary artery segment model based on the American Heart Association (AHA) is widely used (Figure 1.1). Recently, a reporting system, named CAD-RADS^{TM} was proposed to standardize the CCTA reporting and facilitate patient management after CCTA [24].

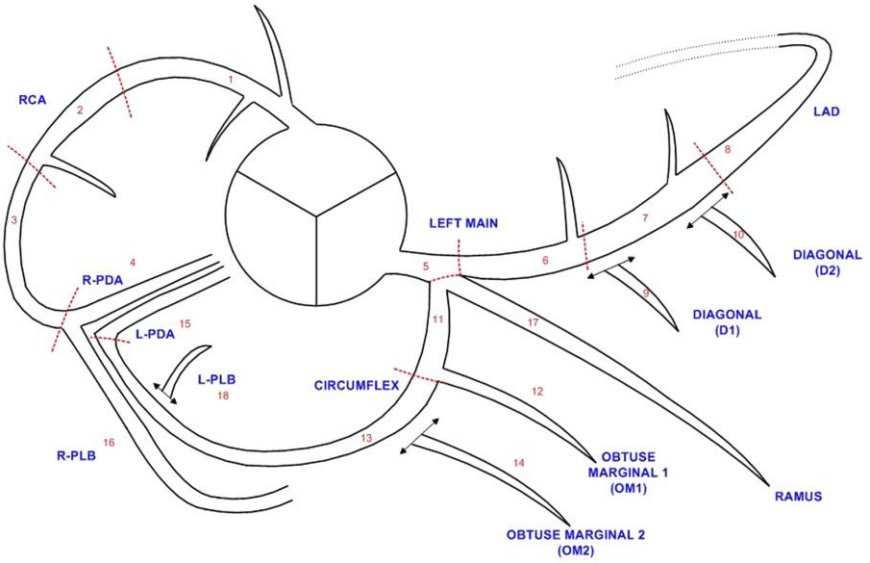

Figure 1.3 Society of Cardiovascular Computed Tomography (SCCT) coronary segmentation diagram. Dashed lines represent division between RCA, LAD, and LCX and the end of the LM. PLB= posterior-lateral branch; PLV= posterior left ventricular branch. Definitions derived and adjusted from the American Heart Association Model. SCCT Guidelines 2014

QUANTITATIVE ANALYSIS ON CCTA IMAGES

For the purpose of increasing the reproducibility of the analysis on CCTA images, reducing user interaction and manual bias, approaches for quantitative analysis of coronary arteries on CCTA images have been studied during the past decades. In the following section, some approaches to aid quantitative analysis on CCTA images are described.

Coronary Artery Tree Extraction

Coronary artery trees (CATs) are often extracted before doing automatic analysis of coronary arteries on CCTA images. A number of automatic CAT extraction methods have been published in the literature [25-33]. Lesage et al. [34] presented an overview of the previous studies in CAT extractions. Regardless of the specific applied segmentation method, vesselness measurements are often designed to describe the features of the targeted coronary arteries on CCTA images. One of the most widely used vesselness measurements is Frangi's vesselness filter which enhances the long shape tubular structures in the image and is often modified to improve the extraction results [35-37]. Besides feature measurements based on prior knowledge of the appearance of coronary arteries, vesselness features can also be obtained based on machine learning without any prior assumption [28]. More and more CCTA images with experts' annotations enable the possibility of using deep learning related algorithms. Recently, Wolterink et al. [32] presented a work using a convolutional neural network (CNN) based orientation classifier for CAT centerline extraction which shows the

feasibility of applying deep learning for vessel feature from image data directly without hand-crafted vesselness representations.

Coronary Artery Lumen and Vessel Wall Contours Detection

One benefit from CCTA is that it enables the visualization of the lumen and vessel wall (Figure 1.4). Marquering et al. [38] presented a method to automatically detect longitudinal and transversal contours for coronary arteries based on the image gradient, and then connect the candidates using a minimal cost approach. Automatic detection of lumen and vessel wall contours for coronary arteries could help the automatic quantification of coronary plaques. After a comparison with the gold standard IVUS, Boogers et al. [39] showed the feasibility of doing automated quantification of coronary plaques on CCTA images using a dedicated registration algorithm.

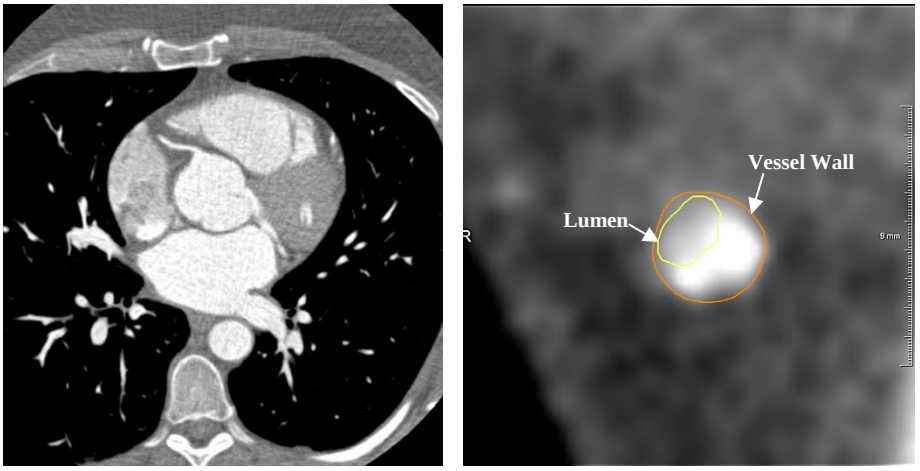

(a) (b)

Figure 1.4 The coronary CTA image. (a) a slice of a coronary CTA image; (b) a close-up image of the coronary artery on 2D axial view with lumen and vessel wall contour highlighted.

Coronary Artery Plaques Analysis

The location of a coronary artery plaque has different clinical significance. Compared to more distally located lesions, a proximal located lesion has a worse prognosis for patients with acute myocardial infarction [40, 41]. For example, on each coronary segment, a different weight factor is applied in the SYNTAX score which was designed to determine the extent and complexity of CAD [42]. Therefore, it is necessary to do a localization of the stenosis on a coronary artery.

Automated quantification of coronary plaques on CCTA images has become feasible due to the development of automatic extraction, labeling, quality assessment for CATs and lumen and vessel wall segmentation methods [39, 43-46]. Changes of plaques between a coronary artery tree at baseline (*CAT-BL*) and coronary artery tree at follow-up (*CAT-FU*) are assessed

on CCTA images to investigate the plaque development after a treatment, or to study the association with long-term mortality [47, 48]. Currently, plaque changes are measured manually [45].

IMAGE PROCESSING CHALLENGES

There are several challenges in extracting, identifying, quality assessment for coronary artery trees and automatic plaque comparison of the coronary arteries on CCTA images.

Coronary Artery Tree Extraction Since vesselness filters for coronary artery extraction are designed based on assumptions about the appearance of the coronary arteries, they may not fully grasp the information available in the data, especially in low-contrast regions of the image due to stenosis. Even with an improved vesselness filter, there are gaps in the filtered vesselness image when there is a low contrast due to a severe occlusion in the coronary artery. Furthermore, surrounding veins could be wrongly extracted as arteries because of their similar appearance to the arteries. These typical situations can create unwanted shorter or longer extractions.

The extracted CATs containing wrong extractions often require corrections from experts. The method in [37] presented a branch searching method to overcome gaps and include disconnected branches. In some studies, statistical models or 3D CAT models were used as prior information to deal with the gaps or early termination of the search. A method called active searching was proposed by Han et al. [49] to solve the discontinuity in the automatically extracted CAT. A statistical branch occurrence location model was used in the study to predict the position of the branch. However, the detection of the discontinuity and different types of vessels in the extracted CAT were not described. Furthermore, the statistical branch occurrence model is used only for the LM artery. Zheng et al. [50] used a 3D coronary tree model to predict the initial position of the major centerlines, but information for side branches was not included.

Identification of Coronary Artery Tree Anatomy Identification of the coronary tree anatomy, i.e. automatically assigning labels to the segments of coronary trees was limited to the RD coronary trees in most previous studies [51-54]. Although ~86% of patients have a RD [3] coronary system, a widely applicable system should also be able to deal with LD coronary trees [55-57].

Another issue is that in most applications, the dominance type of the studied cases is manually determined [53, 58-60]. With the aim for processing large cohorts for multi-center studies, the manual dominance type determination limits the fully automatic processing of the whole pipeline, such as the automatic identification of the extracted coronary artery trees.

Quality Assessment Standardization Even though methods were proposed for coronary artery tree centerline or lumen segmentation, the evaluation measurements for the extracted coronary artery tree are quite limited. The coronary artery centerline extraction challenge at

the MICCAI 2008 provided a platform to evaluate coronary artery centerline extraction methods [25]. The evaluation is in terms of the distance from the given ground truth extractions which were limited to the three main arteries and some selected smaller arteries. The standardized evaluation framework sets a benchmark of state-of-the-art techniques while the evaluation for the extracted coronary tree itself is limited, such as the completeness of the tree.

Automatic Analysis of Coronary Plaque Changes Coronary plaque changes between *CAT-BL* and *CAT-FU* are currently manually compared on CCTA images. The corresponding arteries from the *CAT-BL* and *CAT-FU* are first visually assessed from a similar longitudinal viewing angle, and then aligned using anatomical landmarks, for instance, bifurcation points. Afterwards, coronary plaque differences are calculated based on the 2D transversal view and experts visually assess and grade the changes. However, manually selecting a viewing angle and landmarks for the alignment is time consuming and potentially introduces bias. Moreover, calculating plaque changes in 2D does not utilize the 3D topology information.

AIM AND SCOPE OF THIS THESIS

The main focus of this thesis is to develop approaches to help achieving fully automatic analysis of coronary arteries on coronary CT angiography images.

Previous studies have demonstrated the clinical significance of stenosis localization. Therefore, automated lesion reporting and risk stratification requires an automatic coronary identification algorithm. In **Chapter 2**, an automatic coronary artery tree labeling algorithm is presented to identify the anatomical segments for extracted coronary arteries from both RD and LD cases.

CATs are often extracted before the detection and quantifications of coronary arteries. The quality of the extracted CATs is very important since it will affect the successive steps. However, automatically extracted CATs often miss some arteries or include wrong extractions which require manual corrections before further steps. For analyzing a large number of datasets, a manual quality check of the extraction results is time-consuming and labor-intensive. Therefore in **Chapter 3,** a scoring system is developed to assess the CAT extraction quality using the clinical importance of the artery segments described in the AHA model and the completeness of the extracted CAT.

Based on the designed scoring system, it is able to assess the quality of the extracted CAT. Still, experts need to do manual corrections for the extracted CAT before using the CAT for the analysis which are very tedious. **Chapter 4** describes a model-guided method to detect potential incorrect extractions and automatically improve the extracted CAT, and the designed scoring system is used to monitor the improved extraction quality.

Coronary plaque changes between baseline and follow-up coronary artery trees are important for investigating the association of plaque changes after treatment, and studying the

association with long-term mortality. Therefore, **Chapter 5** describes a method to automatically measure the plaque thickness changes between *CAT-BL* and *CAT-FU* which allows the automatic comparison of plaque progression or regression.

This thesis ends with a summary of results, a general discussion and a future outlook in **Chapter 6** in English, Dutch and Chinese.

CHAPTER 2

Automatic Identification of Coronary Tree Anatomy in Coronary Computed Tomography Angiography

Qing Cao, Alexander Broersen, Michiel A. de Graaf, Pieter H. Kitslaar, Guanyu Yang, Arthur J. Scholte, Boudewijn P.F. Lelieveldt, Johan H.C. Reiber, Jouke Dijkstra

Int J Cardiovasc Imaging, vol. 33, no. 11, pp. 1809-1819, Jun 24, 2017

ABSTRACT

***Purpose*:** An automatic coronary artery tree labeling algorithm is described to identify the anatomical segments of the extracted centerlines from coronary computed tomography angiography (CCTA) images. This method will facilitate the automatic lesion reporting and risk stratification of cardiovascular disease.

***Methods*:** Three-dimensional (3D) models for both right dominant (RD) and left dominant (LD) coronary circulations were built. All labels in the model were matched with their possible candidates in the extracted tree to find the optimal labeling result. In total, 83 CCTA datasets with 1149 segments were included in the testing of the algorithm. The results of the automatic labeling were compared with those by two experts.

***Results*:** In all cases, the proximal parts of main branches including LM were labeled correctly. The automatic labeling algorithm was able to identify and assign labels to 89.2% RD and 83.6% LD coronary tree segments in comparison with the agreements of the two experts (97.6% RD, 87.6% LD). The average precision of start and end points of segments was 92.0% for RD and 90.7% for LD in comparison with the manual identification by two experts while average differences in experts is 1.0% in RD and 2.2% in LD cases. All cases got similar clinical risk scores as the two experts.

***Conclusion*:** The presented fully automatic labeling algorithm can identify and assign labels to the extracted coronary centerlines for both RD and LD circulations.

INTRODUCTION

As a non-invasive imaging modality, coronary computed tomography angiography (CCTA) is widely used for the diagnosis of cardiovascular disease [15]. It provides detailed information about the anatomy of the coronary arteries and the characteristics of coronary atherosclerosis such as the extent of calcifications, the volumetric plaque burden, degree of stenosis and occlusions. In clinical practice, radiologists and cardiologists usually report these pathological findings per artery or per segment according to the society of cardiovascular computed tomography (SCCT) image guidelines [23] and CAD-RADS^{TM} reporting system [61].

Previous studies have demonstrated the clinical significance of stenosis localization. For example, a different weight factor is applied to each coronary segment in the SYNTAX score [42] which is designed to determine the extent and complexity of coronary artery disease (CAD). A worse prognosis for patients with acute myocardial infarction is caused by a proximal located lesion compared to more distal located lesions [40, 41]. Also, previous studies have shown that automatic quantification of CCTA images is feasible [62, 63]. Therefore, automated lesion reporting and risk stratification requires an automatic coronary artery extraction and identification algorithm.

Identification of the coronary tree anatomy, i.e. automatically assigning labels to the segments of coronary trees was limited to the right dominant (RD) coronary trees in most previous studies [51-54]. Although ~86% of patients have a RD [3] coronary system, a widely applicable system should also be able to deal with left dominant (LD) coronary trees [55-57].

A number of previous methods have shown that the centerlines of coronary arteries in CCTA images can be extracted automatically [25, 26, 37]. This paper presents a labeling method to automatically identify and assign labels to the anatomical segments of the entire coronary tree. The assigned label and the location of the start and end points of the label are compared with the results from human observers. Furthermore, current clinical risk scores are computed to show the performance of the identification method in risk score assessment.

MATERIALS AND METHODS

Patients

The patient population consisted of 100 clinical datasets (62 RD cases and 38 LD cases), including: five RD cases to refine the RD model which was derived from Dodge et al. [59]; 11 LD cases to build and train the LD model; and the remaining 84 cases for testing and evaluation of the method. The 100 datasets did not include cases with severe lesions at the proximal parts of the main branches or coronary anomalies. The institutional review board of the Leiden University Medical Center approved this retrospective evaluation of clinically collected data. The need for written informed patient consent was waived.

The labeling method was applied to the extracted centerlines of the coronary trees. Cases with heavily calcified plaques or step/motion artifacts were handled similarly as long as the centerlines were successfully extracted or manually corrected by experts. The coronary centerlines for all the 100 datasets were extracted by a method presented by Yang et al. [37].

CTA acquisition

Data acquisitions were performed with a 64–detector row CT scanner (Aquilion 64, Toshiba Medical Systems, Tokyo, Japan) or 320-detector row CT scanner (Aquilion One, Toshiba Medical Systems, Tokyo, Japan) according to a previous described protocol [64]. In short, if the heart rate was higher than 65 beats per minute, oral or intravenous β blockers were administered, if not contra-indicated. In total, 60-110 mL non-ionic contrast material (Iomeron 400, Bracco, Milan, Italy or Ultravist 370, Bayer Schering Pharma AG Berlin, Germany) was administered followed by a saline flush with a flow rate of 5 mL/second. Thereafter, images were reconstructed at the best phase of the R-R interval. The average image size and voxel size of the datasets were 512x512x512 and 0.307x0.307x0.25 mm, respectively.

Automatic tree labeling method

Figure 2.1 displays different steps in the identification of all the segments in the coronary artery tree. A three-dimensional (3D) coronary tree model provides anatomical *a priori* knowledge of coronary arteries. With the 3D model, a three-step labeling method is used to perform the identification: (1) Align the model with the patient coronary tree to identify the main branches, and separate the coronary tree into sub-trees according to the main branches; (2) Evaluate the matching costs for the segments in each sub-tree to find optimal correspondence between model and patient tree; and (3) Apply logical rules which were translated from the clinical experience to adjust and refine the labels on all segments to obtain the final labeling.

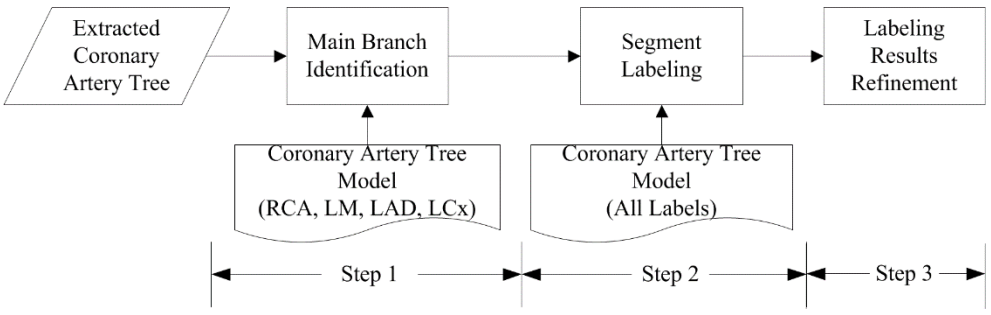

Figure 2.1 Different steps in the identification of all the segments in the coronary artery tree

Coronary artery tree model

Both RD and LD models are composed of three main branches: right coronary artery (RCA), left anterior descending (LAD), left circumflex (LCX), and their derived side-branches. The labels in the models are based on the 15-segments model defined by the American Heart Association (AHA) [65], which is widely adopted in the clinical practice. Additionally, ramus intermedius (RI) arteries which originate near the LAD-LCX bifurcation are added to the models. Furthermore, the obtuse marginal (OM) branches are distinguished as the first obtuse marginal (OM1) and the second marginal (OM2) according to the SCCT guidelines [23]. All the labels used in this paper are summarized in Table 2.1.

Table 2.1 Labels used in the coronary artery tree labeling
(p = proximal, m = mid, d = distal)

	Main branch	Labels of main branch	Labels of side-branches
		LM	/
Sub-trees	RCA	pRCA, mRCA, dRCA	Right Posterior Lateral (RPLB) branch *RD type*: Right Posterior Descending (RPDA) artery
	LAD	pLAD, mLAD, dLAD	two Diagonal arteries (D1, D2)
	LCX	pLCx, LCx	two Obtuse Marginal (OM1, OM2) arteries, Left Posterior Lateral (LPLB) branch Anterolateral (AL) artery or Ramus Intermedius (RI) arteries *LD type*: Left Posterior Descending (LPDA) artery

Note: LM=Left Main Artery; RCA=Right Coronary Artery; LAD=Left Anterior Descending; LCX= Left Circumflex; LD= Left Dominant; RD= Right Dominant

Right dominant model. The initial 3D RD model was created using the 2D angiography statistical information from Dodge et al. [59]. Then five randomly selected RD cases were used to refine and obtain the final RD model. The initial results of this RD model were presented by Yang et al. [54]. The balanced type cases were treated as RD in this paper.

Left dominant model. Coronary artery dominance is defined in terms of which artery supplies the posterior descending artery (PDA) [2]. Because of the difference in PDA and LD cases were not included in Dodge et al. [59], a separate LD model was created. The LD model

was built from 11 randomly selected training-datasets using a leave-one-in cross validation scheme as follows. Each time, one of the 11 cases was chosen as the initial LD model, after which the lengths of the branches of the model were normalized to the average lengths of the 11 training datasets. The remaining 10 training cases were used to validate the model. Finally, the model with the best validation results was defined to be the final LD model. Additionally, the LPDA was defined as the end of the LCX. The distal part (dRCA) of the RCA was excluded from the LD model, since the dRCA was not present in the selected training datasets. From a clinical point of view, the discrimination of proximal (p-), mid (m-) or distal (d-) RCA segment is not important in LD cases.

Main branch identification

The patient coronary tree has a different location, orientation and size compared to the model, so a point-set registration method [66] is introduced to align the 3D model with it. Before the alignment, centerlines of the patient coronary tree and the model are normalized and re-sampled to remove scale variance; all side-branches from the 3D model are removed to reduce their influence on the registration. Weight factors, defined as the number of all child arteries originating from the current segment, are assigned to the points in the patient coronary tree to ensure that their main branches attract the main branches in the model.

RCA, LAD, or LCX is identified as the centerline in the patient coronary tree with the minimal distance to the corresponding main branch in the aligned model. The overlapping part of the identified LAD and LCX is marked as LM. Branches derived from the LAD-LCX bifurcation are labeled as RI arteries. This step provides an initial identification of the main branches in the patient coronary tree, because the distal parts of the main branches have a lower weight factor as their side-branches. In the next section, an iterative algorithm is described to find the optimal correspondence of each label in the 3D model.

Segment labeling

Before labeling all the segments, short side-branches (less than 1 cm) and side-branches that have obtuse angles (more than 120 degrees away from the main branches) at the bifurcations are removed. The rigid transformation obtained in the previous step is used to deform the 3D model with all side-branches.

By minimizing a cost function, an iterative algorithm is applied to find the optimal labeling result from all possible labeling results [54]. According to the identified three main branches, the extracted coronary tree can be separated into three sub-trees with each sub-tree containing one identified main branch and several side-branches. Figure 2.2 illustrates the iterative process of labeling one of the sub-trees. Three sub-trees are subsequently matched with the corresponding sub-trees in the model to get all the segments labeled.

Labeling results refinement

In clinical practice, the proximal, mid and distal parts of LAD and LCX are separated at the bifurcations of the specific side-branches according to AHA coronary artery classification [65]. The labeling result obtained from the previous two steps as shown in Figure 2.2 may not satisfy these requirements. Some criteria were defined in Yang et al. [54] to adjust the obtained labeling result.

Additionally, by transforming clinical experience into logic rules, RI branches are discriminated into RI and anterolateral (AL) branches based on the distance of their origin from the LAD-LCX bifurcation. The distance threshold for RI branches is defined as 0.5 cm according to the clinical experience of cardiologists. If the side-branches originate from the LCX and the distance from its opening to the LAD-LCX bifurcation is less than 2 cm, these side-branches are labeled as AL branches. Branches bifurcating after more than 2 cm from the LCX ostium are treated as OM branches.

If these cases mentioned above are not present in the labeling result, the initial labeling result will not be changed.

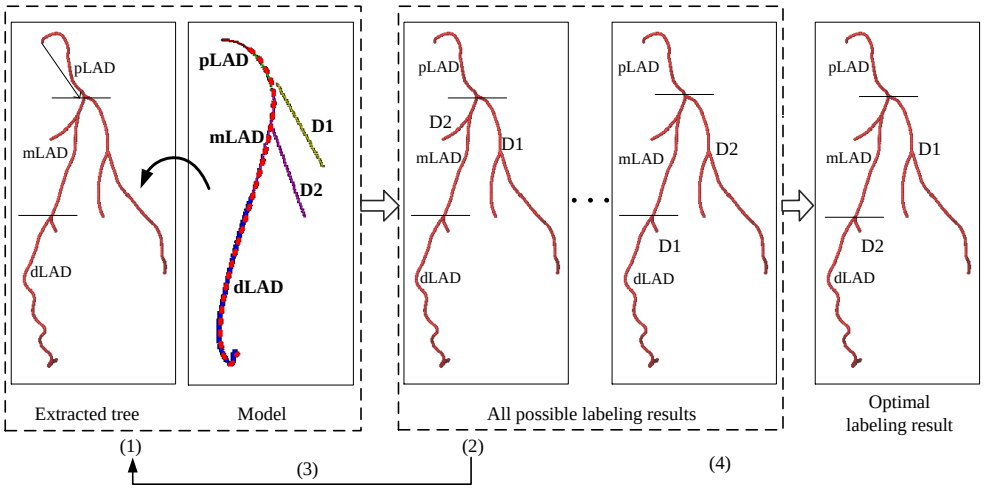

Figure 2.2 The iterative algorithm for labeling all segments. Abbreviations can be found in Table1.

Evaluation measures

For each label, the presence and the accuracy of the start and end points are evaluated. In order to validate the clinical performance of the identification method on each patient or each coronary tree in the aspect of risk score assessment, the accuracy for clinical risk scores is also calculated. Automatic labeling results were compared with the manual labeling from two experts. Two experts with at least four years of experience in cardiac CT imaging independently assigned labels to the coronary tree segments, and subsequently verified the

results for each other to correct any mistakes. As differences between the experts remained after their verification, inter-observer variability of the manual labeling is also analyzed.

Presence

In this step, evaluate the labels in Table 2.1 present or not. As the automatic method may omit or wrongly assign the label on some segments and different opinions also exist between the two experts, three situations are considered. For each label: (1) If both experts agreed with the result of the automatic method, the automatic assigned label is treated as definitely correct; (2) If both experts disagreed with the results of automatic method, automatic assigned label is treated as definitely wrong; (3) If expert1 disagreed with expert2, this means either of them would agree with the automatic method. In this situation, the presence of the label is ambiguous, automatic assigned label is treated as a semi-correct.

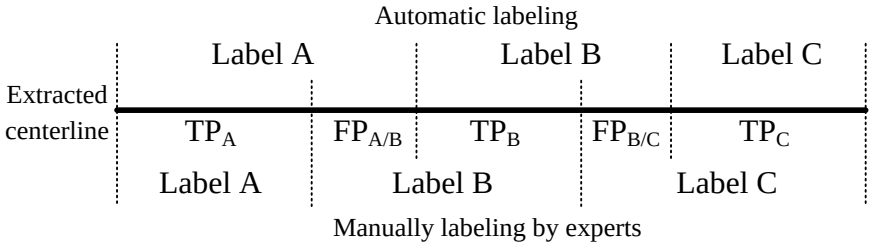

Figure 2.3 Definition of the overlap measure used in the evaluation. TP= True Positive; FP= False Positive.

Overlap

After the evaluation of the presence of labels, the start and end points of a labeled segment are compared with the results of the two experts. An overlap measurement is defined in Figure 2.3 to quantify the labeling accuracy for each presented label. Along the extracted centerline, the points with the same label in both automatic and experts labeling results are marked as true positive (TP), otherwise (i.e. longer or shorter part of the segments), marked as false positive (FP). The overlap measure for the label A between automatic and experts labeling results is defined as,

$$OV_A = \frac{\|TP_A\|}{\|TP_A\| + \|FP_A\|}$$

Accuracy for clinical risk scores

The labeling accuracy for current clinical risk scoring models is evaluated for all patients. In current literature, several risk scores of the coronary plaques in the coronary tree are available to provide an estimate of prognosis of cardiovascular diseases [67, 68].

In order to fit the clinical meaning, assume that all the segments have plaques in this method, four scores are calculated. (1) The ability to identify all segments of the three main branches (i.e. RCA, LAD, LCX). (2) The ability to label the proximal segments of these three main branches including LM. (3) The segment involvement score (SIS) [69] per patient is calculated. SIS is defined as the total number of correctly labeled segments with regard to the segments labeled by experts. (4) The Leaman score [67], as also applied in the SYNTAX-Score [42], is computed by assigning a weight factor ranging from 6 (LM in LD) to 0 (p-, m-, d-RCA in LD) to each coronary segment. For each patient, the Leaman scores are calculated as the summation of the weight factors of all the correctly labeled segments. The labeling of OM in the Leaman score is correct if one of the OM1 or OM2 is labeled correctly. Both SIS and the Leaman score are shown as the proportion compared to the results of experts.

Statistical Analysis

The presence of each label is reported as an absolute number. Agreements or disagreements of the presence are expressed as percentages. The accuracy for overlap and clinical risk scores are illustrated as absolute numbers or percentages ± standard deviation (SD) where appropriate.

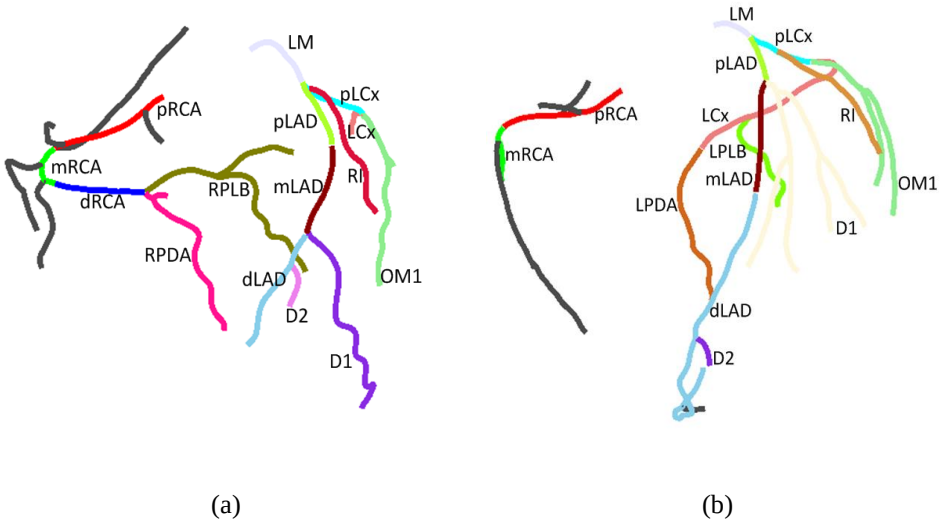

(a) (b)

Figure 2.4 Coronary artery tree labeling result with their labels surrounded by. (a) RD coronary tree; (b) LD coronary tree. All segments including proximal, mid and distal parts as well as side-branches were labeled correctly.

RESULTS

The automatic labeling of one coronary tree took less than 3 seconds on a PC with a Quad Core 2.4Ghz processor and 8GB RAM. One dataset was excluded from the RD evaluation

datasets because of an extraction problem of LAD. In total, 83 (56 RD and 27 LD) cases were used in the evaluation. Baseline characteristics of the 83 patients are depicted in Table 2. 61 patients were male and the mean age was 59.9. A total number of 1149 (795 for the RD cases and 354 for the LD) segments were included on which the automatic method or experts assigned any labels. Figure 2.4 shows the results of applying the automatic labeling approach on a RD and a LD case.

Table 2.2 Patient characteristics

	Total (83)
Age (years)	59.9 ± 11.4
Gender (% male)	61 (73%)
Diabetes	20 (24%)
Hypertension†	34 (41%)
Hypercholesterolemia‡	37 (45%)
Family history of CAD*	26 (31%)
Smoking	15 (18%)
Obesity	22 (27%)

Note: Data are represented as mean ± SD or as number and percentages of patients.
†Defined as systolic blood pressure ≥140 mm Hg and/or diastolic blood pressure ≥90 mmHg or the use of antihypertensive medication.
‡Defined as serum total cholesterol ≥230 mg/dL or serum triglycerides ≥200 mg/dL or treatment with lipid lowering medication.
*Defined as the presence of coronary artery disease in first-degree family members at age <55 years in men and <65 years in women.
CAD: coronary artery disease

Figure 2.5 and Figure 2.6 show an overview of agreements and disagreements on the presence of labels among the automatic method, expert1 and expert2 for RD and LD coronary trees, respectively. For each label, numbers show the amount of agreed or disagreed segments, and by adding all the numbers in a, b and c, one can get the total numbers of the segments involved. For instance, in the RD datasets (Figure 2.5) the total number of segments with label OM2 can be computed as follows. Starting with 11 segments in which all agree from Figure 2.5a plus 9 where the experts disagree with the automatic from Figure 2.5b, and plus 3 where both

experts disagree from Figure 2.5c makes a total of 23 segments. The percentages of these agreements and disagreements with respect to the total segments involved are illustrated in different colors, and green color shows a 100.0% agreement (Figure 2.5a) or 0.0% disagreement (Figure 2.5b and c).

Presence

The agreement on the labeling of the two experts is 776 (97.6%) RD segments and 310 (87.6%) LD segments by adding the numbers in Figure 2.5a and b and Figure 2.6a and b, respectively. Seen from Figure 2.5a and Figure 2.6a, the presence of the labels on 709 (89.2%) RD and 296 (83.6%) LD segments were definitely correct, on which both experts and the automatic approach assigned the same labels. For all the cases, the labels of the proximal segments (pRCA, pLAD and pLCx) including LM were always present and got a 100.0% agreement.

Figure 2.5b and Figure 2.6b show the segments with definitely wrong labels where both experts disagreed with automatic method. However, only 67 (8.4%) RD and 14 (4.0%) LD segments had definitely wrong labels and most of the differences (RD 55.2%; LD 78.6%) were on diagonal and OM branches.

Figure 2.5c and Figure 2.6c show the segments (91.6% in RD, and 96.0% in LD) with semi-correct labels where expert1 disagreed with expert2 but either of them agreed with automatically assigned labels. Expert1 disagreed with expert2 about the presence of the labels on 19 (2.4%) RD segments and 44 (12.4%) LD segments. Specifically, for segments with OM2 labels in the LD cases, expert1 disagreed with expert2 on 12 (75.0%) out of 16 segments.

In RD cases, 0 out of 3 segments with LPLB labels were definitely correct, while the disagreements between expert1 and expert2 were also 33.3%. In LD cases, no OM2 segments got definitely correct labels, and 4 (25.0%) got definitely wrong labels, while on the remaining 12 (75.0%) OM2 segments, either expert1 or expert2 agreed with the automatic method.

Overlap

The average overlap accuracy of the definitely correct labeled segments (as shown in Figure 2.5a and Figure 2.6a) is depicted in Figure 2.7. All labels got at least 70.0% overlap and the LM even has a 100.0% overlap. 18 labeled RD segments and 7 LD segments have no overlapping regions which appeared more often in certain segments, such as D2 (3 in RD, 2 in LD), LCx (4 in RD), and the posterior branch (4 RPLB and 2 LPLB).

There are also inter-observer differences in the overlap on some labels as shown in Figure 2.7, which is 1.0% in RD cases and 2.2% in LD cases in average. In both RD and LD cases, there was a larger inter-observer variability on the labels of LCX sub-tree segments, especially on LPDA segments of LD cases that there was an average 10.0% overlap difference.

By averaging the overlap differences between the experts, the average overlap accuracy on RD labeling is 92.0% (±6.7%), and on LD is 90.7% (±9.5%).

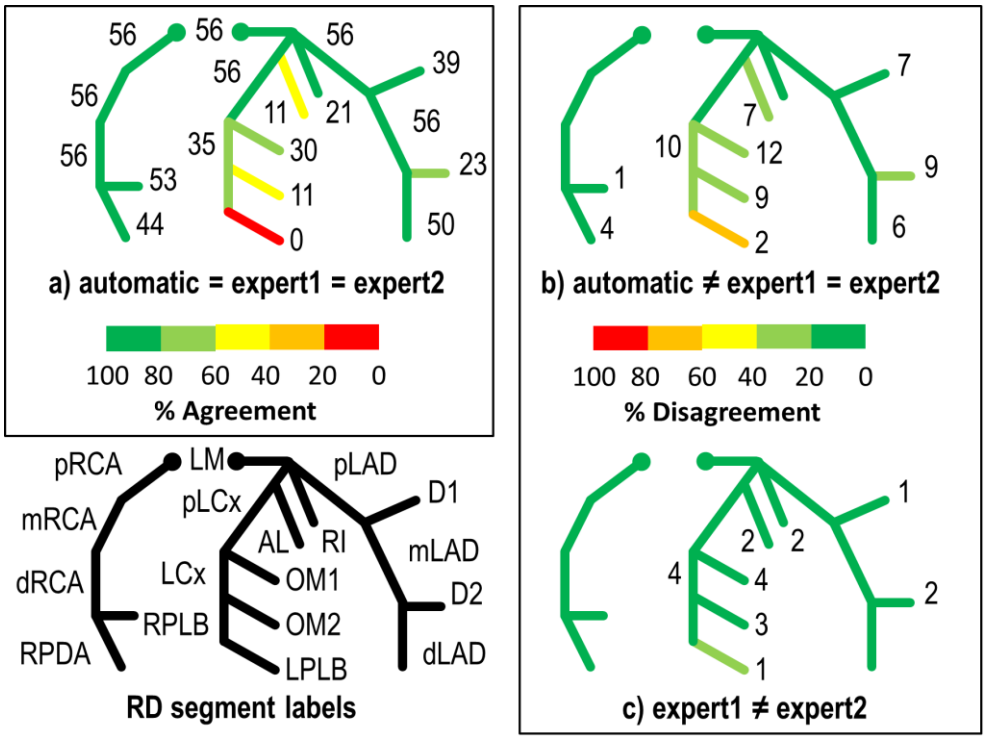

Figure 2.5 Agreements and disagreements among expert1, expert2 and the automatic method for RD cases. (a) agreements among expert1, expert2 and automatic method; (b) disagreements between experts and automatic method; (c) disagreements between expert1 and expert2. For each label, numbers show the amount of agreed or disagreed segments, and by adding all the numbers in (a), (b) and (c) can get the total numbers of the segments involved. The percentages of agreement and disagreement in comparison with the total segments involved are illustrated in different colors, and green color shows a 100.0% agreement (a) or 0.0% disagreement (b) and (c). For instance, 0 (100.0%) out of total 3 LPLB segments get agreements among both experts and automatic method in (a) while in 2 (66.6%) LPLB segments, both experts disagreed with automatic method in (b) and in 1 (33.3%) LPLB segment that expert1 didn't agree with expert2 in (c). Abbreviations can be found in Table 1.

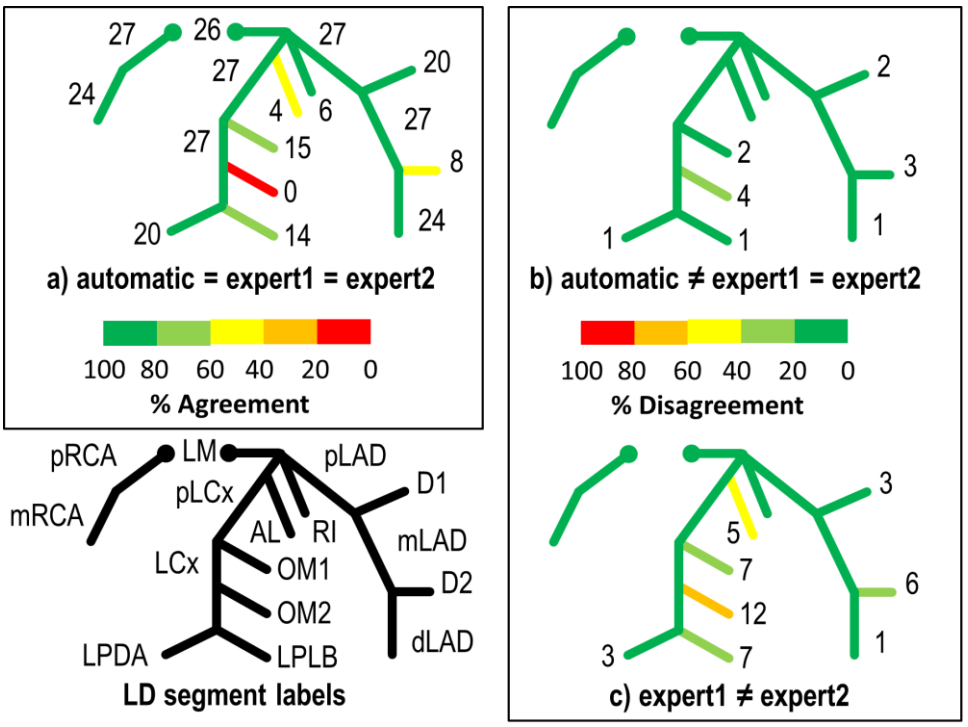

Figure 2.6 Agreements and disagreements among expert1, expert2 and automatic method for LD cases. (a) agreements among expert1, expert2 and automatic method; (b) disagreements between experts and automatic method; (c) disagreements between expert1 and expert2. For each label, numbers show the amount of agreed or disagreed segments, and by adding all the numbers in (a), (b) and (c) can get the total numbers of the segments involved. The percentages of agreement and disagreement in comparison with the total segments involved are illustrated in different colors, and green color shows a 100.0% agreement in (a) or 0.0% disagreement in (b) and (c). Abbreviations can be found in Table 1.

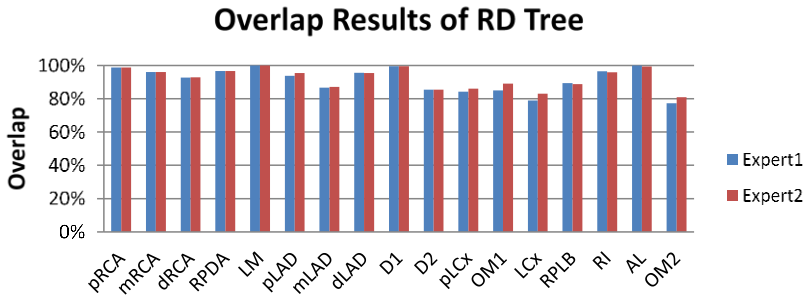

(a)

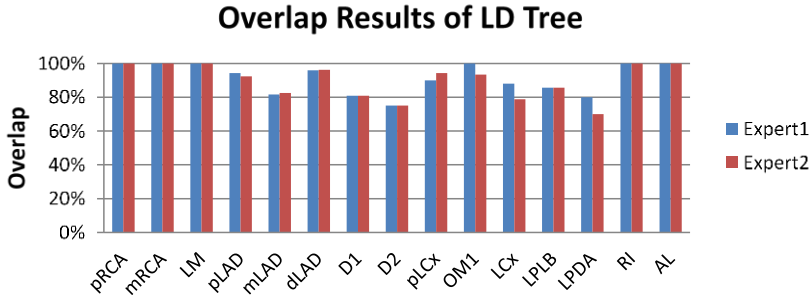

(b)

Figure 2.7 Overall overlap results of the methods. (a) and (b) show the overlap of each segment with two experts for RD tree and LD tree, respectively. RD= Right Dominant; LD=Left dominant; The other abbreviations used here are the same as in Table 1.

Accuracy for clinical risk scores

Clinical risk scores of RD and LD cases are shown in Table 2.3 with the differences in experts averaged. The tree labeling method was able to accurately identify all the proximal segments and LM segments for all patients and at least one main branch was labeled correctly. From all clinical risk scores listed in Table 2.3, RD and LD coronary trees got similar labeling results.

All segments of the three main branches were identified in more than 70.5% of the RD cases and 96.3% of the LD cases and the wrongly labeled segments all occurred in the distal part (dLAD or dLCx). The SIS percentages are 92.6% (±7.3%, RD) and 93.3% (±8.1%, LD) in comparison with manual labeling results. Specifically, in only 1.8% of the RD patients and 9.3% of the LD patients, the SIS score is less than 80.0% compared to the experts. For the segments which have a weight>0 in the Leaman score system, the automatic method got at least 96.0% similar Leaman scores compared to the manual labeling results. In only 4.5% of the RD patients and 3.7% of the LD patients, the automatic method is less than 90.0% similar to the Leaman scores from the experts.

Table 2.3 Clinical risk scores of RD and LD cases

		RD	LD
		Patients (n=56)	Patients (n=27)
Identify three main branches	N=1	100.0%	100.0%
	N=2	98.2%	98.1%
	N=3	70.5%	96.3%
Proximal Segments &LM		100.0%	100.0%
SIS	mean(±SD)	92.6% (±7.3%)	93.3% (±8.1%)
	=100.0%	37.5%	46.3%
	>=90.0%	68.8%	70.4%
	>=80.0%	98.2%	90.7%
	<80.0%	1.8%	9.3%
Leaman Score	mean(±SD)	96.0% (±3.8%)	96.7% (±4.1%)
	=100.0%	37.5%	50%
	>=95.0%	67.9%	70.4%
	>=90.0%	95.5%	96.3%
	<90.0%	4.5%	3.7%

Note: Data are represented as percentages or mean ± SD. N represent the numbers of branches. The SIS and Leaman scores are shown as the percentages of automatic method results in comparison with the averaged results of experts. For example, there were 37.5% RD and 46.3% LD patients got the same SIS score as the experts.

RD= Right Dominant; LD= Left Dominant; LM=Left Main Branch; SIS= Segment Involvement Score; SD=Standard Deviation.

DISCUSSION

In this paper, an automatic coronary artery tree labeling algorithm for centerlines extracted from CCTA images is presented. The labeling algorithm can automatically identify coronary tree segments and assign labels to the identified segments for both RD and LD circulations. This can be used to facilitate automatic lesion reporting and risk stratification in a large cohort of patients [63] and allow automatic follow-up comparison of quantitative parameters on certain segments.

Evaluation of the algorithm

Presence

The accuracy for the presence of D1, D2, OM1 and OM2 labels are lower compared to other segments, because labels of the D1 or D2 and OM1 or OM2 were often switched, especially when one of the diagonal branches or marginal branches did not exist or were absent from the extraction. More disagreements in experts on these segments show that it is also difficult for human experts to discriminate the D1 or D2 and also OM1 or OM2 segments. However, with regard to risk assessment, whether it is the D1 or D2 is not important as long as they are identified as diagonal branches. The same applies to the marginal branches.

Overlap

On LPDA segments of LD cases, there is a large overlap inter-observer variability (10.0%) which is caused by the different start point definition of LPDA. In this method, the start point of LPDA is defined at the position where LCx starts to go to the ventricle groove which is consistent with expert1, while expert2 used the bifurcation point of LCx and LPLB as a start point.

In general, the middle segment of a branch usually has a lower overlap score compared to the proximal segment of the same branch. Due to the definition of pLAD, a missing label of the D1 or the lack of extraction of the D1 will create an incorrect end point for the pLAD. Similarly, if the D2 and OM1 are not extracted, it will influence the accuracy of the mLAD and pLCx. Furthermore, if one of the segments was assigned the wrong label or wrong start and end points, the following segment will inherit or even enlarge this error.

Accuracy for clinical risk scores

The presented labeling method is capable to accurately identify all the proximal segments of main branches and can get similar results as the experts with respect to SIS and Leaman scores. Although, only 70.5% RD cases were labeled correctly in all three main branches compared to experts, the errors all occurred in distal parts of the main branches. It should be taken into account that the lesions in the distal parts have less clinical relevance than in the proximal parts [40, 41].

Comparison to other labeling methods

Several approaches [51, 70] focused on the coronary tree labeling in 2D X-ray angiography. Since 2D X-ray angiography is a different imaging modality with CCTA, assigning the anatomical labels to coronary arteries in CCTA images has different challenges. To the best of our knowledge, the literature on automatic coronary tree labeling in CCTA images is very limited.

Akinyemi et al. [52] presented an automatic labeling method which used geometric features of coronary arteries to train a multivariate Gaussian classifier. In this method, the large anatomical variation of the training datasets such as the size of the heart might decrease the accuracy of the labeling results, while our method is robust to the scale of the coronary trees. The proximal, mid and distal parts of the main coronary arteries were not identified, which is widely adopted in clinical practice for CCTA image reporting and evaluating.

Recently, Mehmet et al. [53] proposed a coronary labeling method through calculating the geodesic paths between coronary tree of a standard model and the patient. In the method, labeling a whole coronary tree took 3 minutes by parallelized implementation, while we only need less than 3 seconds without parallelization. Anatomical prior location, such as the position of four chambers, was used to set the coordinates of the coronary tree, while only coronary centerline points were needed in our automatic method. Furthermore, their approach was not used on LD cases or on cases with a RI. A similar overlap measurement was used to evaluate the labeling accuracy. Compared to their labeling results (87.0% for left coronary tree and 86.0% for right coronary) on automatic detected centerlines, our method got a slightly higher labeling score (92.0%, RD). Since the datasets, the centerline detection methods and coronary segments model are different, it's hard to put these results side-by-side.

Limitations

The following limitations of the present study should be considered. First, two models for RD and LD cases are needed, thus the dominance type of the coronary tree should be known before labeling. Automatic detection of the dominancy to choose the correct model or building a generic model for all the three main dominant types will be investigated in future work. Second, the quality of the tree labeling is highly dependent on the automatic extraction results. In follow up work, we will study if the method could determine whether there are missing, shortened or wrongly extracted arteries. In this way, the labeling of the coronary arteries will allow to improve the tree extraction results by automatically extending short branches and remove veins from an extracted tree.

CONCLUSION

The presented labeling algorithm can successfully identify the coronary tree anatomy in CCTA automatically for both RD and LD cases in a fully automatic manner.

CHAPTER 3

A Quality Score for Coronary Artery Tree Extraction Results

Qing Cao, Alexander Broersen, Pieter H. Kitslaar, Boudewijn P.F. Lelieveldt, Jouke Dijkstra

In: Proc. SPIE 10575, Medical Imaging 2018: Computer-Aided Diagnosis, Houston, Texas United States, 27 February 2018. p 105750V

ABSTRACT

Coronary artery trees (CATs) are often extracted to aid the fully automatic analysis of coronary artery disease on coronary computed tomography angiography (CCTA) images. Automatically extracted CATs often miss some arteries or include wrong extractions which require manual corrections before performing successive steps. For analyzing a large number of datasets, a manual quality check of the extraction results is time-consuming. This paper presents a method to automatically calculate quality scores for extracted CATs in terms of clinical significance of the extracted arteries and the completeness of the extracted CAT. Both right dominant (RD) and left dominant (LD) anatomical statistical models are generated and exploited in developing the quality score. To automatically determine which model should be used, a dominance type detection method is also designed. Experiments are performed on the automatically extracted and manually refined CATs from 42 datasets to evaluate the proposed quality score. In 39 (92.9%) cases, the proposed method is able to measure the quality of the manually refined CATs with higher scores than the automatically extracted CATs. In a 100-point scale system, the average scores for automatically and manually refined CATs are 82.0 (±15.8) and 88.9 (±5.4) respectively. The proposed quality score will assist the automatic processing of the CAT extractions for large cohorts which contain both RD and LD cases. To the best of our knowledge, this is the first time that a general quality score for an extracted CAT is presented.

INTRODUCTION

Coronary computed tomography angiography (CCTA) is widely used for the analysis of the coronary artery disease (CAD) as a non-invasive imaging modality [15]. Coronary artery trees (CAT) are often extracted before the detection and quantification of the CAD. To facilitate the automatic analysis of CAD from CCTA images, a number of methods have shown that CATs can be extracted automatically [25, 26, 37]. The extraction quality of the CATs is very important since it will affect the successive steps. However, automatically extracted CATs often miss some arteries due to their small sizes or low spatial resolution of the CCTA images. Veins or surrounding tissues which are similar to arteries are easily included in the automatically extracted CATs. These incorrect extractions require the user to manually add or remove vessels on the automatically extracted results.

The requirements for the arteries in the extracted CATs are different, depending on the purpose. In clinical practice, pathological findings in the coronary arteries are often reported per artery or per segment based upon a widely adopted 17-segments model defined by the American Heart Association (AHA) [23, 61, 65]. The arteries in the AHA model are considered to have high clinical significance in CAD risk scoring. On the other hand, the arteries not considered part of the AHA model are also treated important for some applications. For example, fractional flow reserve derived from CCTA (FFR_{CT}) is a recent approach which enables the determination of physiologic significance of a suspected CAD by a single non-invasive test [71, 72]. In order to calculate the FFR_{CT}, an anatomical model of the CAT with all the available vessels including side branches which are not in the AHA model is required [73].

The coronary circulations can be categorized into three groups: the right dominant (RD, 86.6%), the left dominant (LD, 9.2%) and the balanced type (4.2%) circulation [3]. The artery that supplies the posterior descending artery (PDA) determines the coronary arterial dominance [2]. Thus, the CATs from different dominance type (DT) cases have different topologies. Moreover, the DT is related to the prognostic value of the significant CAD [55]. In most applications, the DTs of the studied cases is manually determined or only the RD cases are included [53, 58-60]. With the aim at processing large cohorts for multicenter studies, the manual DT determination and quality check of the CAT extractions are very labor-intensive and time-consuming.

In this paper, a method is presented to automatically calculate quality scores for extracted CATs. The presented score measures the extraction quality from the clinical significance aspect of the arteries in the AHA model and the completeness aspect of the extracted CAT. A score weight factor is used to weigh the importance between the two aspects. Anatomical statistical models for both RD and LD types are generated and compared with extracted CATs. An automatic DT detection method is also presented to determine which anatomical statistical model should be used for calculating the score. Experiments were conducted on automatically extracted and manually refined CATs to give an evaluation for the proposed quality score.

METHODS

The proposed score method consists of the following steps. Firstly, the anatomical statistical information for each segment/vessel either in or not in the AHA model is calculated and analyzed. Secondly, a dominance type (DT) detection method is developed based on the analysis of the statistics. With the automatically determined DT, the corresponding anatomical statistical model is used to compare with the newly extracted CAT. The comparison is first performed for the vessels in the AHA model (Part 1) and then the remaining vessels (Part 2). For each comparison, a sub-score function is defined to calculate a value for the comparison result. Lastly, the sub-scores are combined to build a final score for the extraction quality.

Anatomical statistical model

Coronary artery trees

The CAT contains three main coronary branches, the right coronary artery (RCA), the left anterior descending (LAD), the left circumflex (LCX), and their derived side-branches. According to the three main arteries, the CAT is separated into three sub-trees with each sub-tree containing one main branch and several side branches. Furthermore, all vessels in the CATs are grouped into two categories: **vessels with labels** in the AHA model which have higher clinical significance, and **vessels without a label** which are not considered part of the AHA model. Specifically, Figure 3.1 shows the schematic figure of vessels with labels in the AHA model for both RD and LD cases together with the sub-trees RCA, LCX, and LAD divided by dashed lines. Additionally, a balanced-type case is treated as a RD in this paper since the balanced-type doesn't exist as an option in current CAD risk scoring models [42, 67] and the RD is the most prevalent DT in the general population.

Datasets for Statistics

The CATs of 83 cases, including 56 RD cases and 27 LD cases were automatically extracted and assigned labels based on the AHA model as previously described in Cao et al. [58]. In their study, experts manually corrected all automatically extracted CATs and then assigned the labels. In this paper, the 83 manually corrected and labeled CATs are used to generate the statistics. Details of the calculation and analysis of the anatomical statistical information will be described below.

Statistics Calculation and Analysis

The anatomical statistical information is calculated and analyzed for all arteries in the CATs, all arteries in each sub-tree, each vessel with a label and all vessels without a label.

In CATs, a pathline is defined as starting from the ostium and continuing all the way to the end of the vessel branch. Figure 3.2 shows a histogram of the length for all 1116 pathlines in the 83 extracted CATs with an average length of 162 ± 60 mm. The average, minimum and

maximum lengths for all pathlines in both RD and LD CATs are listed in the first two rows of Table 3.1. The average length of the pathline from a RD case (164 ± 60 mm) is slightly longer than the pathline from a LD case (157 ± 62 mm). Pathlines in RD and LD cases have a similar minimum length (RD 14 mm vs LD 12 mm) and a similar maximum length (RD 331 mm vs LD 299 mm). Since there are no obvious differences in the length of RD and LD pathlines, the minimum length 12 mm and the maximum length 331 mm of all are used as boundaries to measure whether a pathline in the extracted CAT is too long or too short.

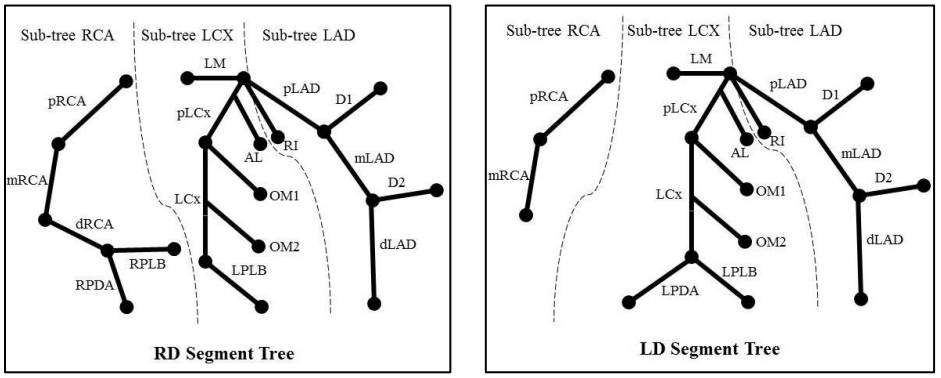

(a) (b)

Figure 3.1 RD and LD coronary artery tree segments. Dashed lines represent division between sub-trees RCA, LAD, and LCX. LD= Left Dominant; RD= Right Dominant; RCA=Right Coronary Artery; LAD=Left Anterior Descending; LCX=Left Circumflex; LM=Left Main; D=Diagonal; OM=Obtuse Marginal; RI=Ramus Intermedius; AL=Anterior Lateral; RPDA= Right Posterior Descending Artery; RPLB= Right Posterior Lateral Branch; LPDA= Left Posterior Descending Artery; LPLB= Left Posterior Lateral Branch; p=proximal; m=middle; d=distal

For each label and the three main branches in both RD and LD cases, box plots in Figure 3.3 show the distribution of their lengths. All boxplots we use in this paper are Tukey boxplots which use the 1.5 times of the interquartile range (IQR) to define the outliers [74]. Moreover, when calculating the lengths of the three main branches, the proximal (p-), middle (m-), distal (d-) part of the RCA, LAD and LCX, the right posterior descending artery (RPDA) and the left posterior descending artery (LPDA) are included. The average, minimum and maximum lengths for all labels and the three main branches are listed in Table 3.1. Compared to the p- and m- segments of the main branches, side branches or d- segments of the main branches have a larger standard deviation in the length. We consider the extracted side branches or last segments of the main branches as correct if their length is within the corresponding minimum and maximum range.

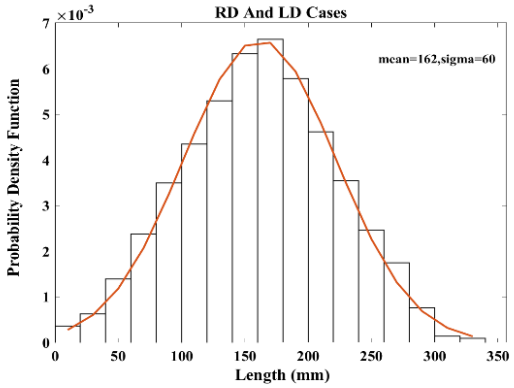

Figure 3.2 Histogram of all extracted pathlines in 83 cases including RD and LD cases. LD= Left Dominant; RD= Right Dominant

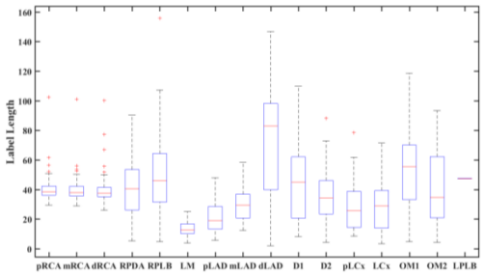

(a). RD segments

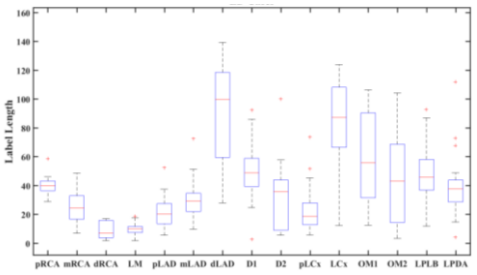

(b). LD segments

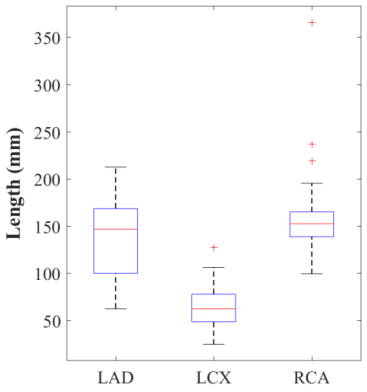

(c). RD main branches

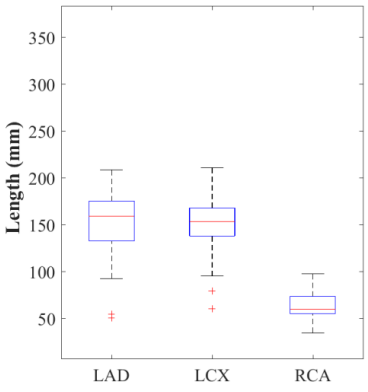

(d). LD main branches

Figure 3.3 Box-plots of the lengths for 17-segments in the AHA model, and three main branches for both RD and LD coronary artery trees. RCA= Right Coronary Artery; LAD= Left Anterior Descending; LCX= Left Circumflex; LD= Left Dominant; RD= Right Dominant the other abbreviations used here are the same as in Figure 3.1

Additionally, the frequency of each label being extracted in the 56 RD and the 27 LD CATs is also given in Table 3.1 which is further referred as the occurrence of the label. In the extracted CATs, the absence of a label with a high occurrence indicates a high probability of a miss-extraction while the absence of a label with a low occurrence implicates a low probability of a miss-extraction. Taking a RD case as an example, the absence of the proximal RCA (pRCA) means a high chance of a miss-extraction in the pRCA since the occurrence of pRCA is 56 out of 56 cases, whereas the absence of left posterior lateral branch (LPLB) might be treated as correct since the occurrence of LPLB is only 2 out of 56 cases.

The average length of the three main branches as listed in Table 3.1 (last three rows) is similar to the length as reported in Hurst's The Heart [2]. Furthermore, Figure 3.3(c-d) and Table 3.1 (last three rows) show that there are obvious differences in the average length of the RCA (RD 122 mm vs LD 64 mm) and the LCX (RD 64 mm vs LD 118 mm) for the RD and LD cases. This indicates that the length of the RCA and the LCX can be used as a feature to determine the dominance type of a CAT.

Figure 3.4 presents the box plots for the number of vessels without a label in each sub-tree for both RD and LD CATs. There is a large variation in the number of vessels without a label in each sub-tree. The minimum and maximum number of vessels for each sub-tree (LAD, LCX and RCA) are [0, 4], [0, 2], [1, 4] and [0, 4], [0, 3], [0, 5] for both RD and LD cases, respectively. These values are used as reference while measuring the quality of extracted CATs to avoid that extracted CATs omit some important arteries or contain too many wrong extractions.

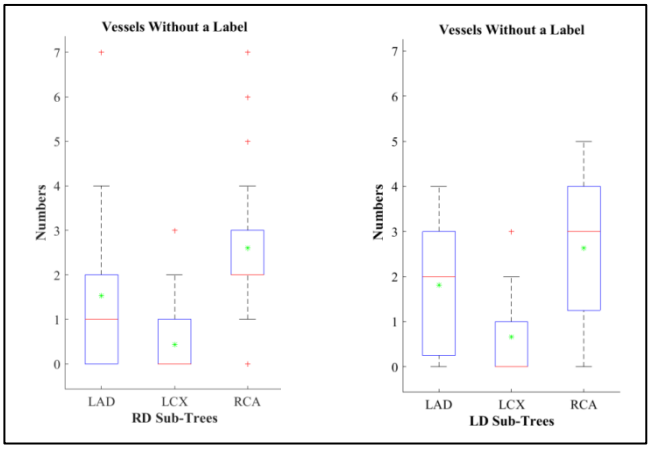

Figure 3.4 Boxplots of the number of vessels without a label in each sub-tree for both RD and LD CAT. The average number is plotted in green which is LAD=3, LCX=2, RCA=1 for both RD and LD cases. RCA= Right Coronary Artery; LAD= Left Anterior Descending; LCX= Left Circumflex; LD= Left Dominant; RD= Right Dominant

Table 3.1 The statistics for all pathlines, labels and the three main branches in both RD and LD cases.

		RD				LD			
		n	Length (mm)			n	Length (mm)		
			AVG	MIN	MAX		AVG	MIN	MAX
Pathlines		763	164(±60)	14	331	353	157(±62)	12	299
Labels	pRCA	56	41(±10)	27	52	27	41(±6)	26	54
	mRCA	56	40(±10)	26	52	24	24(±10)	1	57
	dRCA	56	41(±12)	26	51				
	RPLB	53	51(±28)	1	112				
	RPDA	47	42(±21)	1	93				
	LM	56	14(±5)	1	27	26	10(±4)	1	18
	pLAD	56	21(±10)	1	48	27	22(±11)	1	47
	mLAD	56	30(±11)	1	60	27	31(±13)	1	53
	dLAD	55	74(±41)	1	187	25	95(±33)	5	206
	D1	44	45(±24)	1	124	22	51(±22)	1	88
	D2	30	36(±20)	1	80	14	34(±26)	11	96
	pLCx	56	29(±16)	1	70	27	24(±16)	1	49
	LCx	40	29(±16)	1	78	27	84(±28)	7	167
	OM1	42	54(±30)	1	121	20	59(±31)	1	179
	OM2	16	41(±28)	1	124	11	46(±34)	1	148
	LPLB	2	48(±0)	40	60	16	47(±22)	5	91
	LPDA					22	40(±22)	6	67
Main Branches	RCA	56	122(±31)	100	196	27	64(±15)	35	98
	LAD	56	137(±38)	63	213	27	156(±54)	93	209
	LCX	56	64(±22)	25	106	27	118(±28)	95	211

Note: Data is represented as average ± standard deviation. n represents the occurrence of the segments. AVG= Average; MIN= Minimum; MAX= Maximum; LD= Left Dominant; RD= Right Dominant; the other abbreviations used here are the same as in Figure 3.1.

The statistics can be summarized and used as follows. (1) The minimum and maximum lengths of all pathlines and all labels indicate the possible length ranges for a pathline/segment in a new CAT. (2) The occurrence of each label shows the probability of a miss-extraction when the label is absent. (3) In each sub-tree, the minimum and maximum numbers of vessels without a label provide the reference values while comparing with the corresponding part in a new CAT. Finally, (4) the length of the RCA and the LCX is a feature to differentiate between the RD and the LD.

Automatic dominance type detection

The segment identification method from Cao et al. [58] is able to automatically assign the labels of the 17-segments AHA model to the CAT. All labels in the 3D anatomical model (RD or LD) are matched with their possible candidates in the extracted CAT to find the optimal labeling result. However, the dominance type (DT) should be used as prior knowledge before the matching.

An automatic DT detection method is developed based on the analysis of the statistics. Since the PDA determines the DT, the RPDA on the RCA and the LPDA on the LCX can differentiate between RD and LD cases. Moreover, there are obvious differences in the average length of the RCA and the LCX for the RD and LD cases as described in **Anatomical Statistical Model** section. Accordingly, the difference in the length of the RCA and the LCX from a CAT is selected as the feature to determine the DT.

Before the lengths of the RCA and the LCX can be calculated, they need to be identified in the CAT. The RD model is set as the initial DT to perform an initial automatic identification since 86.6% of the hearts in the whole population are the RD type [3]. Only the main branches are identified in the initial identification and then their lengths are calculated. However, the distal part of the main branches could be missed due to their small size and limited spatial resolution of CCTA. When comparing the length of the LCX with the length of the RCA without the distal part in the RD case, the DT could be wrongly determined as LD. Similarly, the DT could be wrongly determined as RD if the distal part of the LCX is not extracted in a LD case. Hence, 95 mm, which is the minimum length between the RCA (100 mm, RD) and the LCX (95 mm, LD), is chosen as the threshold to give a rough estimation that the RCA and LCX are fully extracted (see Table 3.1, last three rows).

If the RCA is fully extracted (the length > 95mm) and longer than the LCX, the CAT is determined as a RD case; If the LCX is fully extracted (the length > 95mm) and longer than the RCA, the CAT is determined as a LD case; If both RCA and LCX are not fully extracted, the DT of the CAT is initially marked as “hard to decide”. In order to be able to perform successive steps, the CAT marked as “hard to decide” is temporarily set as a RD case considering that RD is the most prevalent DT in the general population.

For a newly extracted CAT, the presented DT detection method is applied to determine its DT automatically. Afterwards, the CAT is compared with the anatomical statistical model of

the determined DT to measure the quality. The comparison, described in the following sections, is performed in two steps and quantified by two sub-score functions.

Part 1: Vessels with labels

With an automatically detected DT, the vessels with labels in the new CAT are identified by using the automatic segment identification method [58]. The 3D anatomical models used for the automatic identification are the CATs containing all 17-segments as well as their labels, positions and directions. Afterwards, the number of present vessels with labels in the newly extracted CAT is obtained by comparing them with the 3D anatomical models. However, the information of which label is present remains unknown. Different labels have their different clinical relevance. Accordingly, a weight for each label is defined to distinguish the presence of different labels.

In the extracted CATs, the absence of a label with high occurrence indicates a high probability of a miss-extraction while the absence of a label with low occurrence implies a low probability of a miss-extraction. Therefore, the weight of each label is defined as the percentage of its occurrence (see the first column of Table 3.1) compared to the total number of datasets. This ensures that the correct extraction of a more frequently present label gains a higher weight. The weights of each label for both RD and LD cases are shown in Figure 3.5(a) and Figure 3.5(b), respectively.

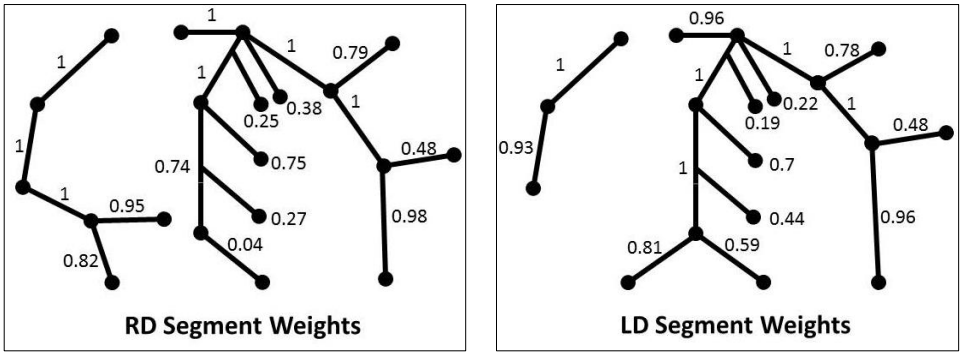

(a) (b)

Figure 3.5 Weights of the 17-segments in the AHA model for both the RD and LD cases. LD= Left Dominant; RD= Right Dominant

The overall weight of a CAT is the summation of the individual label weights in it. A CAT consists of the three sub-trees and they contribute differently to the blood circulation as described by Leaman et al. [67]. The overall weight is calculated for each sub-tree with the aim of building a score which shows the sub-tree differences. In addition to the three sub-trees, the left main (LM) as the common part of the LAD and LCX, and ramus intermedius (RI) or anterior lateral (AL) originating from the bifurcation of the LAD and LCX are treated

as the fourth and fifth sub-tree, respectively. Thus, the differences of the RI/AL among the extracted CATs can also be distinguished.

The overall weight of a sub-tree in the 3D anatomical model is calculated as W_0 and used as a reference to compare with the corresponding sub-tree overall weight W_{new} in the newly extracted CAT. A sub-score function *S1* of a sub-tree describing the difference between W_0 and W_{new} is calculated as follows (Scale: 0-100),

$$S1 = \frac{W_{new}}{W_0} * 100 \quad (1)$$

Part 2: vessels without a label

Similar to the Part 1, the extraction quality of vessels without a label is measured by the comparison with their anatomical statistics. A sub-score function *S2* is defined to quantify the comparison results.

First of all, the total number of vessels without a label in a sub-tree is calculated as N_0. After that, the path lines of the vessels without a label are treated as wrong extractions if their lengths are outside the minimum and maximum range [12 mm, 323 mm]. Then, along the pathline, the angles where the vessels bifurcate from the main branches are calculated and further referred as the bifurcation angles. In this paper, 120 degrees is set as the bifurcation angle threshold to make sure that a vessel doesn't have a sudden change in direction. Excluding wrong lengths and bifurcation angles from the total number N_0, the number of vessels without a label is computed as N_1. The ratio of N_1 to N_0 describes the difference. A CAT will have a smaller ratio if it includes more incorrect extractions.

There are some wrong extractions which not fulfil the above criteria. Some big veins nearby the arteries are easily extracted and connected to the CATs. They usually have similar length and bifurcation angles as arteries. Accordingly, the minimum and maximum number of vessels without a label in each sub-tree is used as reference to ensure that an extraction contains more arteries and fewer veins. In a sub-tree, if N_1 (excluding vessels with wrong length and bifurcation angles) from the newly extracted CAT is in the range of [minimum, maximum], N_1 is considered as reasonable; If N_1 is outside the range, it will not be treated as a wrong extraction immediately considering the variances in CATs within a population. Alternatively, the distance between N_1 and the average number N_μ is calculated using the Gaussian function. There are more wrong extracted arteries in the extracted CAT if the N_1 deviates more from the N_μ. The values of the average number N_μ for each sub-tree is shown in Table 3.2.

Based on the above information, a sub-score function *S2* for vessels without a label in one sub-tree is defined as follows (Scale: 0-100),

$$S2 = \left(\frac{\omega + N_1}{\omega + N_0}\right) * 100 * \begin{cases} 1 & , N1 \in [N_{\min}, N_{\max}] \\ e^{-(N_1 - N_\mu)/2\delta^2} & , \quad otherwise \end{cases} \tag{2}$$

ω is set to 0.001 for regularization in case N_0=0 which means that there aren't any vessels without a label in the extraction; The Gaussian distribution $e^{-(N_1 - N_\mu)^2/2\delta^2}$ is used to measure the distance between N_1 and N_μ; δ^2 is empirically set to 2 in this paper.

The quality score

The Part 1 and Part 2 described the details of *S1* and *S2* for measuring the extraction quality of vessels with labels and vessels without a label, respectively. However, there is a *S1* and a *S2* for each sub-tree in the extracted CAT. In this section, we combine *S1* and *S2* from all sub-trees to build the quality score *S* for a whole CAT.

For each sub-tree, the sub-scores *S1* and *S2* are combined to describe the clinical significance and completeness of it. To start with, a score weight factor α is set to weigh the importance of *S1* and *S2*. Specifically, the sub-score *S1* is treated as more important since the vessels with labels have higher clinical relevance. Afterwards, the *S1* and *S2* are multiplied by the score weight factor α, respectively. The sum of the weighted *S1* and *S2* is the score for this sub-tree.

Similarly, the score of all sub-trees are integrated together by using a sub-tree weight factor γ. γ shows the clinical significance of the sub-tree. The Leaman risk score model, as one of the widely used risk scoring models, provides a set of weight factor for the coronary segments [67, 68]. The Leaman weight factor of each segment describes its clinical significance in supplying the blood for the coronary circulation. Consequently, the sub-tree weight factor γ is acquired by adding up the Leaman weight factors of all segments in the sub-tree. The γ of all sub-trees are then normalized to [0, 1] to make them sum up to 1. Finally, the summation of the score from each sub-tree multiplied with its corresponding sub-tree weight factor γ forms the final score of the CAT.

The final formulation of the quality score function *S* is defined as follows,

$$S = \sum_{sub-tree=1}^{5} (\gamma * [\alpha * S1 + (1-\alpha) * S2])_{sub-tree} \tag{3}$$

α∈[0,1] is the weight representing the importance of *S1* and *S2*, and is empirically set as 0.8 in this study; γ weighs the importance of the different sub-trees with $\sum_{sub-tree=1}^{5} (\gamma)_{sub-tree} = 1$. Additionally, the calculation of the score for RD and LD cases is performed separately since there are different anatomical models and different sets of weight factors are provided in the Leaman risk score model [67].

For each sub-tree in both RD and LD CATs, the overall weight of 3D anatomical models W_0, average number of vessels without a label N_μ and the sub-tree weight factor γ are shown in Table 3.2.

Table 3.2 Statistics of each sub-tree for both RD and LD coronary tree

		RD			LD		
		W_0	N_μ	γ	W_0	N_μ	γ
Sub-trees	RCA	4.82	3	0.20	1.89	3	0.05
	LAD	4.56	2	0.37	4.56	2	0.37
	LCX	3.11	1	0.17	5.14	1	0.28
	LM	1	0	0.22	0.96	0	0.26
	RI/AL	0.38/0.25	0	0.04	0.22/0.19	0	0.04

Note: RCA=Right Coronary Artery; LAD=Left Anterior Descending; LCX= Left Circumflex; RI/AL=Intermediate Ramus/Anterior Lateral; LD= Left Dominant; RD= Right Dominant

EXPERIMENTS AND RESULTS

3

Datasets and parameters

42 cases, including 18 training datasets (No. 0-17) and 24 testing datasets (No. 18-34) have been provided by MICCAI segmentation challenge workshop [75]. The LUMC/Medis team (Leiden, Netherlands) extracted CAT centerlines for all cases using the method presented by Yang et al. [37] and then manually refined the extracted CAT centerlines if necessary. The DTs of all cases were also manually assessed. The proposed quality score is applied on the automatically extracted CATs and the manually refined CATs of the 42 cases to do the evaluation.

Firstly, the proposed automatic DT detection method identifies the DTs for all automatically extracted and manually refined CATs from the 42 cases. Afterwards, the anatomical statistical model of the identified DT is chosen to compare with the extracted CATs to calculate the quality scores. It is to be expected that a well-defined quality score should show a higher value for the manually refined CTA than the corresponding automatically extracted CAT.

Results

The proposed automatic DT detection method is performed on automatically extracted and manually refined CATs from the 42 cases before calculating the quality scores. In all automatic extracted CATs, the DT detection method successfully identifies 30 RD cases and 11 LD cases. One of the 42 automatic extractions is identified as “Hard to Decide” since the LCX is not completely extracted. The case is successfully determined as “LD” after the expert

extended the LCX manually. For 41 (97.6%) of the 42 manually refined CATs, the DT detection method correctly identifies their DTs. Only one (2.4%) manually refined CAT of a LD case is wrongly detected as a RD due to the wrong identification of the main branches by the automatic identification method. This manually refined CAT is manually set as LD before calculating the quality score.

With the automatically identified DTs, the proposed quality score is applied on all automatically extracted and manually refined CATs and the results are shown in Figure 3.6. The manually refined extractions get a higher average quality scores and a lower standard deviation (88.9±5.4) compared to the automatic extractions (82.0±15.8). In all automatic extractions, two CATs have very low scores which are shown as two outliers in Figure 3.6 (a). In one of the two outliers, the CAT has a score of 0 since the automatic extraction was failed. This CAT is manually refined with a final score of 82.1. The other CAT has a score of 22.3 because the RCA is not automatically extracted. This case is shown in Figure 3.7(a) as an example.

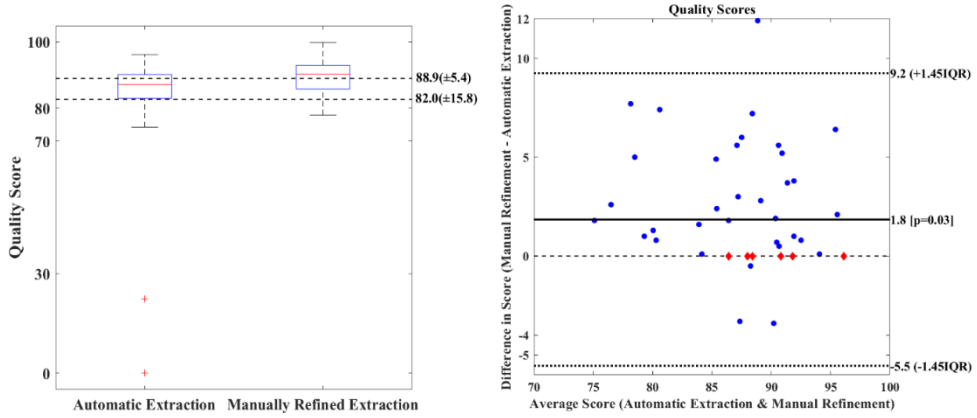

(a) (b)

Figure 3.6 Quality scores of the automatic extraction and manual refinement for 42 cases. (a) 82.0 (±15.8) and 88.9 (±5.4) are the average quality scores of automatic extractions and manually refined extractions for all cases; (b) the differences of scores in the manual refinement and the automatic extraction. Red diamonds are the 6 cases that experts didn't correct anything.

From Figure 3.6(b), in 33 (78.6%) of the 42 cases, the extraction after the manual refinement has a higher score than the automatic extraction. 6 (14.3%) cases have the same scores in the automatic extraction and the manually refined extraction since experts didn't correct anything for these cases. Three (7.1%) cases have lower scores after manual refinement. In one of the three cases, two additional small branches are added (less than 3 mm) when the expert extended the LAD resulting in six vessels without a label on the LAD which lowered the quality score (less than 4 points in a 100-point scale). For the remaining two cases, the vessels labeled as RPDA in the automatic extractions were removed by the expert which results in a

lower *S1*; in the meantime, a lot of wrong extractions were removed by the expert which results in a higher *S2*. Since *S1* has a higher score weight factor than *S2*, the final score *S* is still lower than the automatic extraction.

Table 3.3 Scores of automatically extracted and manual improved CAT from the 18 datasets

Case NO.	Automatic Extraction			Manually Refined Extraction			Automatically Detected DT
	S	*S1*	*S2*	*S*	*S1*	*S2*	
0	**88.4**	85.6	100.0	**88.4**	85.6	100.0	RD
1	90.4	93.5	77.8	90.9	93.5	80.8	RD
2	22.3	16.0	47.6	91.8	98.1	66.7	RD
3	89.0	86.3	100.0	85.7	86.3	83.3	RD
4	76.9	77.3	75.0	84.3	85.9	87.5	RD
5	**91.8**	89.7	100.0	**91.8**	89.7	100.0	RD
6	74.2	84.8	31.9	76.0	82.4	61.5	RD
7	89.5	93.5	68.4	88.0	90.1	80.0	RD
8	91.4	95.2	76.2	92.4	95.2	81.3	RD
9	92.2	98.1	68.4	98.6	99.8	100.0	RD
10	**90.8**	95.2	73.3	**90.8**	95.2	91.7	RD
11	84.8	86.3	78.9	92.0	93.7	85.0	RD
12	84.2	86.9	73.3	86.6	87.0	84.6	RD
13	83.1	88.0	63.7	84.7	88.0	71.6	RD
14	78.8	82.4	64.3	79.8	82.4	69.2	RD
15	79.9	81.4	73.7	80.7	81.4	77.8	RD
16	84.3	89.0	65.4	89.9	89.0	93.3	LD
17	85.7	91.8	61.5	88.7	93.3	80.0	LD
Average (±SD)	82.0 (±15.8)	84.5 (±17.9)	72.2 (±17.1)	88.5 (±5.3)	89.8 (±5.4)	83.0 (±11.3)	

Note: Bold numbers are cases with same score after manual refinement. Underlined numbers are cases with lower score between the automatic extraction and manually refined extraction. SD=standard deviation; DT=Dominance Type; LD= Left Dominant; RD= Right Dominant.

Details of the *S1*, *S2* and *S* for the automatically extracted and manually refined CATs from the 18 datasets (NO.0-17) are listed in Table 3.3. *S2* of an extracted CAT could reach 100 if no pathline is longer than the maximum length, no bifurcation angle is larger than 120 degrees,

and the number of vessels without a label is in the range of [minimum, maximum]. With the same scores in vessels without a label (*S2*), a higher score in vessels with labels (*S1*) results in a higher extraction quality (Case NO.10 vs Case NO.12). Even with the *S2*=100 (such as Case NO.0), the final score *S* of the case is 88.1 (*S1*=85.6, *S2*=100). This is lower than the case with the *S2*=77.8 (Case NO.1) but the final score *S* is 90.4 (*S1*=93.5, *S2*=77.8).

Furthermore, Figure 3.7 shows an example that an automatically extracted CAT is improved by different manual operations. The CATs in Figure 3.7(a)-(d) have different quality which is also indicated by the different scores.

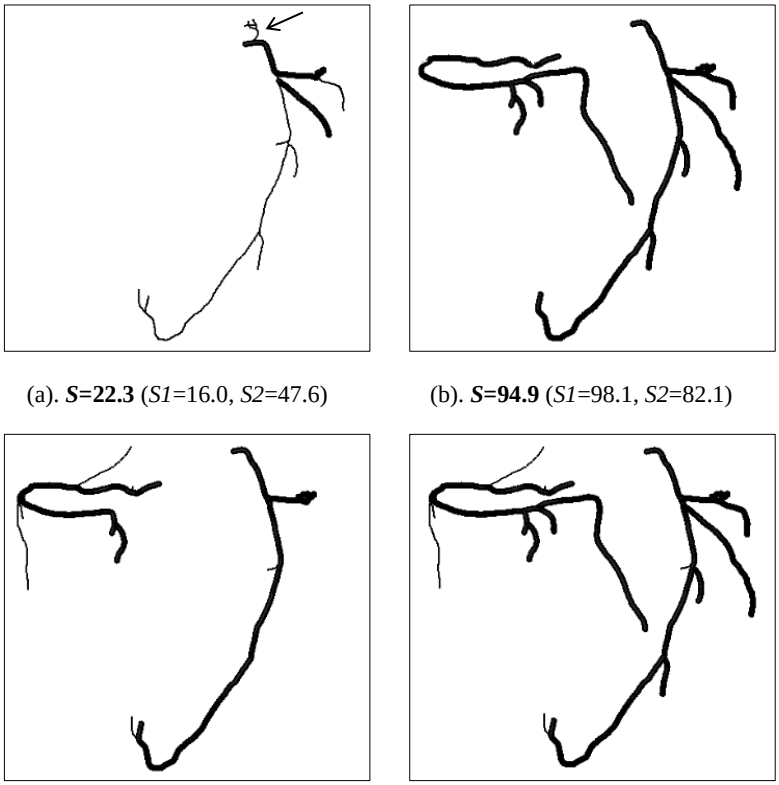

(a). ***S*=22.3** (*S1*=16.0, *S2*=47.6) (b). ***S*=94.9** (*S1*=98.1, *S2*=82.1)

(c). ***S*=79.6** (*S1*=74.5, *S2*=100.0) (d). ***S*=98.5** (*S1*=98.1, *S2*=100.0)

Figure 3.7 Extracted coronary artery trees of a case with different quality and corresponding scores. (a) one sub-tree (RCA) not extracted; (b) with all labels but no vessels without a label; (c) no side branch with labels (d) all possible arteries extracted. Vessels with labels are represented as bold lines. Extractions with wrong angles are pointed at by an arrow in (a).

CONCLUSION AND DISCUSSION

In this paper, a quality score for coronary artery tree (CAT) extractions from the coronary computed tomography angiography (CCTA) images is designed based on generated anatomical statistical models.

An automatic dominance type (DT) detection method is also developed to enable the automatic application of the proposed score in the CATs from different coronary dominances. The results show that the presented DT detection method correctly identified the DTs for 97.6% of the 42 manually refined CATs. The DT detection method failed on only one CAT due to the wrong identification of the main branches. The DT of the CAT was afterwards correctly determined with the manually identified main branches.

Evaluation of the proposed quality score on the automatically extracted and manually refined CATs illustrates that the scoring method generated higher values for the extracted CATs with manual refinements and had the same values when there were no manual refinements in 92.9% of the cases. Details of the two sub-scores from the quality score in Table 3.3 point out that the two sub-scores can be used separately regarding the importance of the clinical significance and the completeness of the CAT. The quality score will benefit the automatic processing of the CAT extractions in large cohorts.

However, we noticed that three (7.1%) cases have lower quality scores even after the manual refinement. In one of the three cases, the distal part of the left anterior descending artery (dLAD) was not fully extracted in the automatic extraction. The expert connected the distal part to the automatic extracted dLAD in the manual refinement. The connected part contained two small side branches (<3 mm) which were not considered important by the expert. The proposed score treated these two small side branches as mistakes and showed as a small quality decrease. Similar scores can be expected if the expert and the score system make a consistent view in small branches. For the remaining two cases, the vessels in the automatic extractions were mislabeled as right posterior descending artery (RPDA) by the automatic identification method from Cao et al. [58]. The two vessels were then removed by the expert in the manually refined CATs. Since the RPDA has a large effect on the quality score, the two manually refined CATs ended up with lower scores compared to the corresponding automatic extractions. These will be eliminated if the automatic identification method is improved. Furthermore, it should be noted that the manual refinements were made with the purpose of stenosis detection and focused on the refinement of vessels with high clinical significance instead of the completeness of the extractions.

In future work, experts' opinions will serve as a reference for the quality of a CAT extraction to evaluate the proposed quality score. Anatomical models that contain more segments could also be built to provide more information on the extracted CATs. Furthermore, the proposed quality score will be used to measure the performance of a potential automatic refinement process for the coronary tree extraction.

CHAPTER 4

A Model-guided Method for Improving Coronary Artery Tree Extractions From CCTA Images

Qing Cao, Alexander Broersen, Pieter H. Kitslaar, Boudewijn P.F. Lelieveldt, Jouke Dijkstra

Int J Comput Assist Radiol Surg, vol. 14, no. 2, pp. 373-383, Feb, 2019

ABSTRACT

Purpose: Automatically extracted coronary artery trees (CATs) from coronary computed tomography angiography images could contain incorrect extractions which require manual corrections before they can be used in clinical practice. A model-guided method for improving the extracted CAT is described to automatically detect potential incorrect extractions and improve them.

Methods: The proposed method is a coarse-to-fine approach. A coarse improvement is first applied on all vessels in the extracted CAT, and then a fine improvement is applied only on vessels with higher clinical significance. Based upon a decision tree, the proposed method automatically and iteratively performs improvement operations for the entire extracted CAT until it meets the stop criteria. The improvement of the extraction quality obtained by the proposed method is measured using a scoring system. 18 datasets were used to determine optimal values for the parameters involved in the model-guided method and 122 datasets were used for evaluation.

Results: Compared to the initial automatic extractions, the proposed method improves the CATs for 122 datasets from an average quality score of 87±6 to 93±4. The developed method is able to run within 2 minutes on a typical workstation. The difference in extraction quality after automatic improvement is negatively correlated with the initial extraction quality (R=-0.694, P<0.001).

Conclusion: Without deteriorating the initially extracted CATs, the presented method automatically detects incorrect extractions and improves the CATs to an average quality score of 93 guided by anatomical statistical models.

INTRODUCTION

Coronary computed tomography angiography (CCTA) is an established technique for the assessment of patients with suspected coronary artery disease (CAD) [76]. In order to diagnose CAD on CCTA images, the coronary artery tree (CAT) is often extracted. Automatic CAT extraction methods based on minimum path techniques have been widely used due to their simplicity and computational efficiency [26, 28, 30]. The minimum path searching is often performed on a vesselness image which is typically created by applying a modified Frangi's vesselness filter to CCTA images [35, 37].

However, severe occlusion or low contrast in coronary arteries can result in gaps in the vesselness image. Furthermore, surrounding veins could be wrongly extracted as arteries because of their similar appearance. These situations can create undesirable shorter or longer extractions which require manual corrections from experts. Han et al. [49]proposed active searching to solve the discontinuity in automatically extracted CATs using a statistical branch occurrence location model which predicts the position of a branch. However, their model is used only for the left main artery and discontinuity detection was not described. Zheng et al. [50] used a 3D coronary tree model to predict the initial position of the major centerlines while side branch information is not included.

This paper presents a model-guided method for improving the extracted CAT from CCTA images. Guided-by anatomical statistical models, the proposed method automatically detects potential incorrect extractions and improves the extracted CAT. A recently proposed scoring system by Cao et al. [44] is exploited to monitor the quality of the CAT improved by the proposed method.

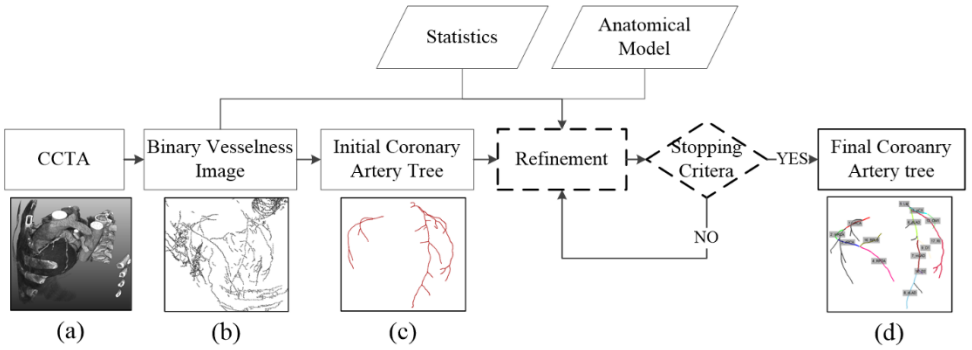

Figure 4.1 Pipeline of the model-guided method for improving coronary artery tree extractions. Modules in dashed boxes are described in more detail in this paper. (a) Coronary Computed Tomography Angiography image. (b) Binary vesselness image. (c) Fully automatically extracted coronary artery tree. (d) Automatically improved extraction using the proposed model-guided method.

METHODS

Figure 4.1 gives an overview of the proposed method. On the CCTA image (a), an improved Frangi's vesselness filter is applied to create a binary vesselness image (b). Next, an initial CAT (c) is extracted using a fully automatic extraction method presented by Yang et al. [37]. Then, the proposed method based upon the anatomical statistical model and binary vesselness image is applied to the initial CAT. The improvement process is iteratively performed by adding missing arteries and removing wrong extractions until the stop criteria are met. The automatically improved CAT together with the anatomical names assigned to the corresponding coronary artery segments is shown in (d). Details of the model-guided improvement method are described in the following sections. We first introduce some prior knowledge in the next section.

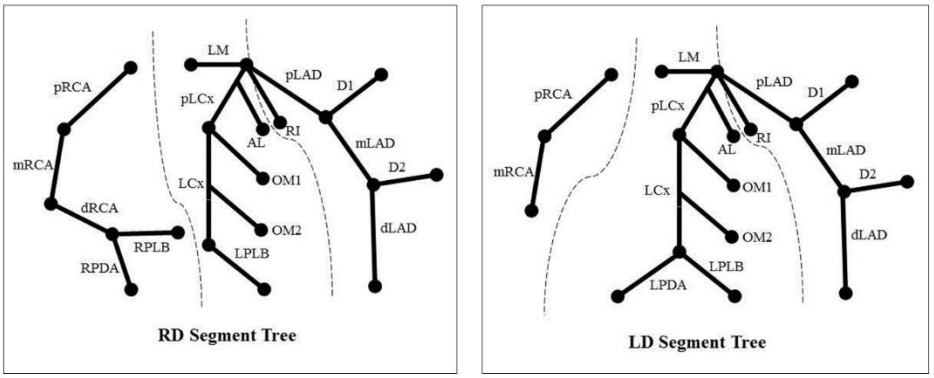

Figure 4.2 RD and LD coronary artery tree segments. Dashed lines represent division between sub-trees RCA, LAD, and LCX. RCA=Right coronary artery; LAD=Left Anterior Descending; LCX=Left Circumflex; LD= Left Dominant; RD= Right Dominant

Coronary Artery Tree

A CAT is composed of three main branches, right coronary artery (RCA), left anterior descending (LAD) and left circumflex (LCX), and their side-branches. The main branch that supplies the posterior descending artery (PDA) determines the CAT dominance type [77]: right dominant (RD), left dominant (LD), and balanced type. Different dominance types have different geometrical topologies. To report CAD on CCTA images, the modified 17-segments model defined by the American Heart Association (AHA) is widely used in clinical practice [23, 65]. Figure 4.2 shows the AHA models for RD and LD cases as two separate schematic figures. The balanced type will be treated as RD which is the most prevalent dominance type. Main branches are divided into proximal (p-), mid (m-), and distal (d-) segments and these segments are represented as parent-child relationships.

The Initial Extraction. The initial CAT is extracted using the automatic centerline extraction method proposed by Yang et al. [37]. Additionally, a binary vesselness image containing the

central axes of the vessel-like structures of the CCTA image is created during the extraction process (Figure 4.1(b)).

The Statistical Models. Cao et al. [44] defined separate anatomical statistical models for RD and LD cases which contain global information for all vessels in a CAT as well as local information for each specific segment in the AHA model. In the statistical models, each label has a weight to represent its importance. An important label has a higher weight and weight values for each label can be found in Supplementary Material Section 1. The deviations of the extracted CAT from the anatomical statistical models indicate the locations of the incorrect extractions.

The Model-guided Method

Guided by the statistical models mentioned above, the initial CAT extractions are improved using a coarse-to-fine approach, starting with the coarse improvement on all vessels in the extracted CAT followed by the fine improvement only on the segments with corresponding anatomical definitions in the AHA model which are further referred as *vessels-with-labels.*

Coarse Improvement

The coarse improvement removes incorrectly extracted segments in three steps. First, vessel-like structures in the initial CAT not connected with the left and right ostia are removed. Second, pathlines longer than the corresponding global maximum length from the statistical model are pruned to the maximum length. Pathlines shorter than 1 mm are considered as not important and removed. Third, vessels in the initial CAT with angles larger than expected from the statistical model are removed. The angle between the parent branch along the blood flow direction and the side branch direction is calculated and the vessel is removed when the angle is larger than 120°. Examples of applying coarse improvement on CATs can be found in Supplementary Materials Section 2.

Fine Improvement

Coarse-improvement operations are mainly shortening and removing while the fine-improvement performs a more precise analysis on *vessels-with-labels* to verify correctness of the anatomical positions and to extract missing arteries in a CAT.

Automatic detection of inaccurate extractions. On the coarsely improved CAT, anatomical labels are automatically assigned using the labeling method of Cao et al. [58]. By comparing all anatomical labels in the model with *vessels-with-labels* in the extracted CAT, their presence and absence in the extracted CAT are obtained. If an anatomical label is present in the CAT but the length of the segment is outside the anatomical statistical model range for this specific label, it will be marked as too short or too long. If an anatomical label is absent, it could be a missed extraction or a normal variation since some labels appear more often than the others. We use the label weight to decide the probability of a miss-extraction when the

label is absent. To improve the above identified inaccurate extractions, two improvement operations, deletion and extension, are performed.

Deletion

If a labeled segment is too long, a deletion operation similar to the one described in the coarse improvement section is performed. The segment is deleted from where it starts exceeding the maximum length. Since other improvements can alter the topology of a CAT, the vessel angles are computed again and labeled segments with angles larger than 120° are deleted. Figure 4.3 shows an extracted CAT which is improved by the deletion operation.

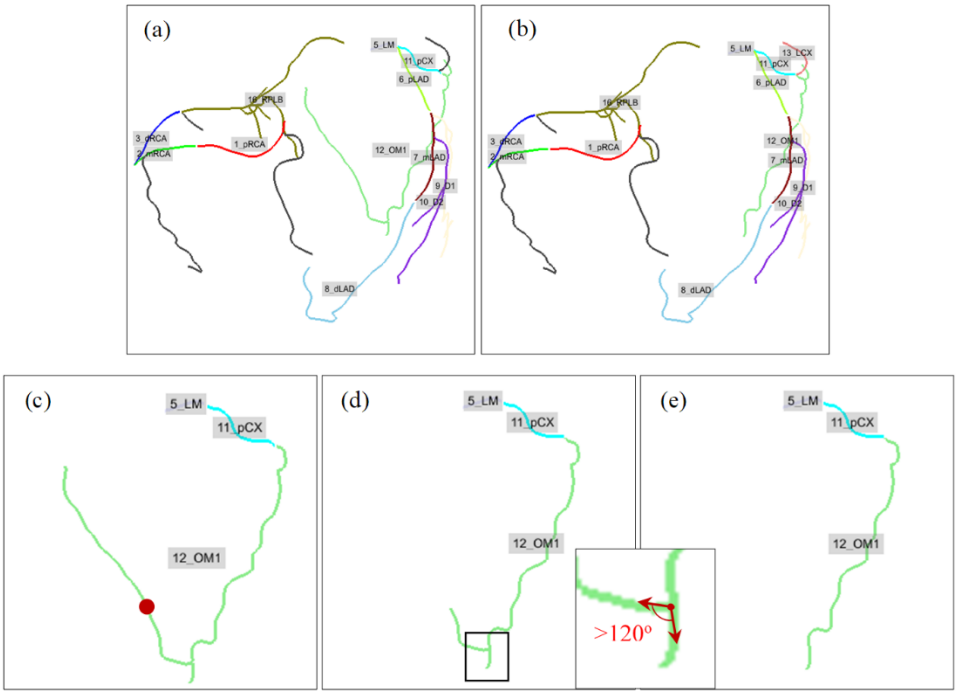

Figure 4.3 Automatic long vessel deletion and angle improvement. (a) Initially extracted CAT with labels. (b) Automatically improved CAT; (c)-(e) zoom in image of the OM1. (c) Red point on OM1 shows the position of the maximum length of the OM1. (d) Shortened OM1 with side branch bifurcation angle larger than 120°. (e) OM1 after length and angle improvement. CAT= Coronary Artery Tree; OM1= first Obtuse Marginal branch

Extension

If a labeled segment is too short or an important label is absent, an extension operation is performed to bridge the gaps in the binary vesselness image. Yang et al. [37] presented branch searching on the binary vesselness image using a wave propagation algorithm with a fixed searching distance. Their method considers all points in the extracted CAT with a large change in curvature as starting points. Since the inclusion of all points is computing-intensive

and a fixed search distance cannot deal with gaps of different sizes, we introduce an improved branch searching algorithm using automatically determined start points and an adaptively-set searching distance.

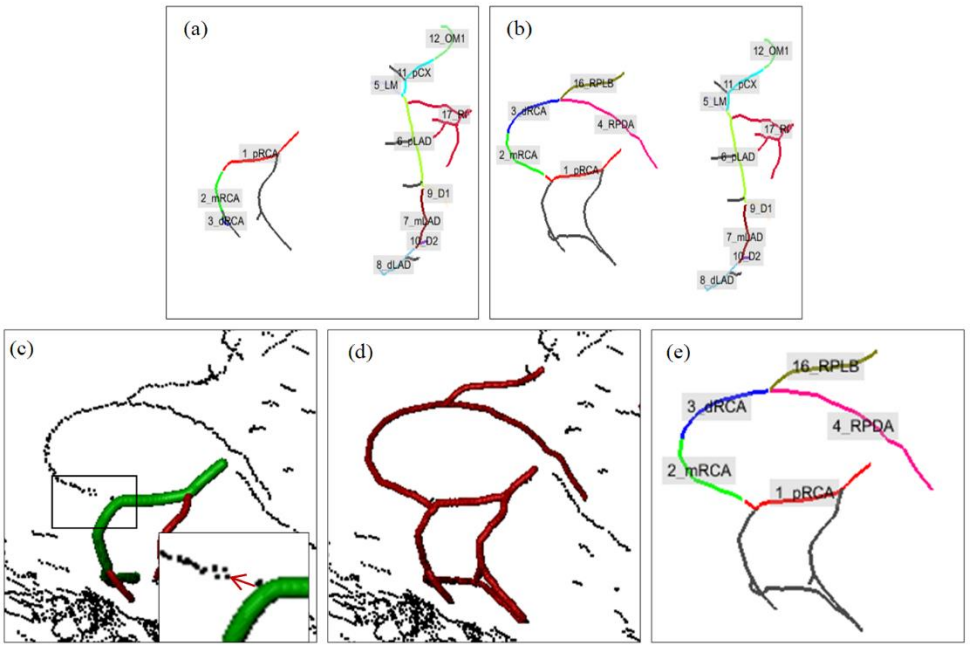

Figure 4.4 Automatic improvement to get RPDA and RPLB for a RD case by extension. (a) Initially extracted CAT with labels. (b) An automatically improved CAT. (c)-(e) zoom-in image of the sub-tree RCA. (c) Initially extracted RCA on the binary vesselness image; the green part shows the labeled segments and the red part shows the unlabeled segments; the box shows a zoom-in image of searching area, and the red arrow points out the extension direction. (d) Automatically extended RCA (red) on the binary vesselness image. (e) Extended RCA with labels. RPDA= Right Posterior Descending Artery; RPLB= Right Posterior Lateral Branch; RD= Right Dominant; CAT= Coronary Artery Tree; RCA= Right Coronary Artery

Improved Branch Searching. The improved branch searching method selects the start points depending on the situation. (1) If a side branch label is absent, all points on the parent label with a large curvature are selected as start points. (2) If a main branch label, such as mRCA, is absent, all points on the extracted main branch with large curvature are used as start points. This is because the identification of the whole main branch could be incorrect if a main branch segment is absent as mentioned in the automatic identification method [58]. An example is presented in Supplementary Material Section 3.1 to illustrate the difference in selecting starting points to search for a main branch label. (3) If a labeled segment is too short, the end point of this segment is selected as the start point.

From the automatically selected start-points, unconnected vessel-like structures are searched iteratively starting with an initial searching distance and increasing by a step in each iteration. The search continues until unconnected parts are found or the maximum search distance is reached. Figure 4.4 shows an example of an extension operation for a RD case.

The Decision Tree

Since different operations might be needed for the overall improvement of a CAT, the decision tree in Figure 4.5 shows the order of improvement operations according to the importance of a label in the topology of the CAT and its influence on successive steps.

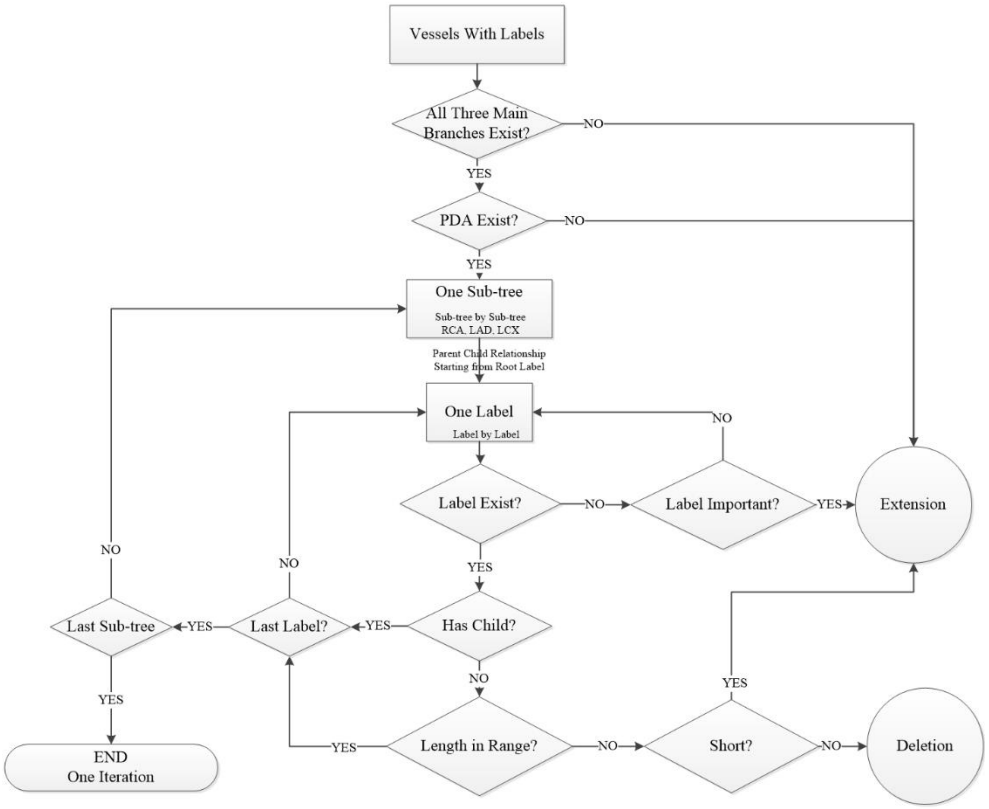

Figure 4.5 The decision tree for the improvement process. PDA= Posterior Descending Artery; RCA= Right Coronary Artery; LAD= Left Anterior Descending artery; LCX= Left Circumflex artery

The top level detects the three main branches. If any of the three main branches is absent, the improvement operation will be performed until all of them are extracted.

The next level evaluates the dominance type since it determines which anatomical model to use. We use the automatic method proposed by Cao et al. [44] to decide the dominance type. However, their method determines a CAT as RD when both the LCX and RCA are not fully extracted. Therefore, the automatically determined dominance type is evaluated by checking

the presence and correctness of the PDA since in the RD case it should be present in the RCA while in the LD case it should present in the LCX [77]. If the PDA is absent or its length is incorrect, the corresponding improvement operation is performed until it is found and has a correct length.

The remaining levels of the decision tree are as follows. Based upon the three main branches (RCA, LAD and LCX), the CAT is split into three sub-trees. Each sub-tree contains one main branch and several side branches (Figure 4.2). The improvement process will traverse sub-tree by sub-tree. In each sub-tree, the process starts from the root label to the leaf label. For each label, its presence, length and direction is evaluated and improved if necessary. If the current label has a child which is also present, the improvement step will move forward until reaching a leaf label. For example, if the mLAD is present and its child dLAD is also present, the improvement process checks the correctness of dLAD instead of the mLAD. If all labels in the current sub-tree are evaluated and improved, the process moves to the next sub-tree.

The improvement for all sub-trees, which might include several improvement operations, is counted as one iteration. The improvement process is performed iteratively in order to achieve a CAT with a better quality. This requires a quality measurement for evaluation and some criteria to stop the iterative process.

Stopping Criteria

A quality score for a CAT is calculated using the scoring system proposed by Cao et al. [44]. The quality scores before and after an improvement operation are represented as S_{old} and S_{new} respectively and $S_\Delta=(S_{new}-S_{old})$ describes the change in quality after one improvement operation. If $S_\Delta>0$, the improvement operation increases the quality of the CAT and the process moves to the next step. The improvement process stops when $S_\Delta=0$ in one iteration.

If $S_\Delta<0$, the improvement operation deteriorates the extracted CAT. To constrain the deterioration, a threshold $T_{S\Delta}$ ($T_{S\Delta}<0$) is used. If $S_\Delta>T_{S\Delta}$, the current improvement operation is kept since a small quality score decrease could be improved by a later improvement operation. If $S_\Delta<T_{S\Delta}$, the current improvement operation will be reverted. Moreover, this improvement operation is skipped and the improvement process moves to the next step. After each step, the improved CAT is stored so the process can be reverted. The value of the $T_{S\Delta}$ is determined by a training process which can be found in Supplementary Material Section 3.

To prevent the extraction quality from continuously decreasing within the threshold ($S_\Delta>T_{S\Delta}$) after each improvement operation, the accumulated score difference $\sum S_\Delta$ is computed and when $\sum S_\Delta<T_{S\Delta}$, the automatic improvement process stops.

Additionally, a maximum number of iterations is set to prevent the improvement process from over-extracting artery-like structures due to unforeseen circumstances. The intermediate results of the improvements are stored and the extraction with the highest score will be the final extraction.

Statistical Analysis

Descriptive data are expressed as the average ± standard deviation (SD). The correlation between the quality score of the initial extraction and the score difference after automatic improvement is evaluated using Spearman correlation coefficient. The statistical computations were performed in SPSS (Version 20.0; IBM Corp, Armonk, NY). A 2-tailed P-value less than 0.05 was considered to be statistically significant.

EXPERIMENTS AND RESULTS

Experiments

The performance of the proposed algorithm was assessed on two cohorts. The first cohort consists of 42 datasets (No. 0-41) from the MICCAI segmentation challenge workshop [75] which were distributed over five calcium categories to have a representative population for undergoing CTA examination. Patients with pacemaker or CTA of non-diagnostic image quality, such as motion artifacts, were excluded.

The second cohort consists of 98 cases (60 RD and 38 LD). The average image and voxel size of the datasets was 512x512x512 and 0.307x0.307x0.25 mm, respectively. These cases did not include severe lesions at the proximal part of main branches or coronary anomalies.

The initial CATs for all cases were extracted using the method of Yang et al. [37]. The model-guided method is applied to improve these initial CATs. To set up references for the proposed method, experts manually corrected all initial CATs if necessary. The first 18 datasets (No. 0-17) from the first cohort were used to optimize parameters (see the results in Supplementary Material Section 4). The remaining 24 datasets from the first cohort were used to test the performance of the proposed method using these settings. The proposed method is applied on the other cohort (98 cases) to evaluate its performance in a different cohort.

Results

The proposed method was implemented in MeVisLab-2.7.1. In general, improving a CAT takes less than 2 minutes on a typical workstation with a 2.67 GHz Intel quad-core processor.

In total 122 cases, 24 testing cases from the first cohort and 98 cases from the second cohort were used to validate the proposed method. For all 122 automatically extracted CATs, the model-guided method was able to improve their average quality score from 87±6 to 93±4.

MICCAI challenge cohort

For 24 (No.18-41) cases from the first cohort, quality scores for the initially extracted, manually improved, and automatically improved CATs are listed in Table 4.1. The developed model-guided method improved the 24 initial CATs to an average quality score of 93±5. It shows 21 CATs were improved with a quality score increase of at least 1. The remaining 3 (12%) showed no score change indicating no improvement.

Table 4.1 Quality scores of the initially extracted, manually improved and automatically improved coronary artery trees for 24 testing cases from the first cohort

Case No.	Quality Score				
	Initial Extraction	Manual Improvement	Automatic Improvement	DIF (Manual - Init)	DIF (Auto - Init)
18	76	81	78	5	2
19	77	85	81	8	4
20	88	86	96	-2	8
21	94	97	97	3	3
22	90	90	91	0	1
23	84	89	96	5	12
24	94	94	95	0	1
25	94	93	96	-1	2
26	97	97	98	0	1
27	93	94	95	1	2
28	95	95	95	0	**0**
29	92	95	93	3	1
30	81	95	86	14	5
31	76	81	88	5	12
32	88	93	97	5	9
33	87	90	92	3	5
34	83	90	89	7	6
35	91	88	92	-3	1
36	87	94	91	7	4
37	96	93	96	-3	**0**
38	96	96	96	0	**0**
39	90	95	95	5	5
40	92	95	96	3	4
41	82	82	92	0	10
Min	76	81	78	-3	0
Max	97	97	98	14	12
Median	90	93	95	2	3
Average (±SD)	88 (±6)	91 (±5)	93 (±5)	3 (±4)	4 (±4)

Note: Bold numbers are cases with same score after automatic improvement. DIF represents the difference in the quality score between the manually or automatically improved CAT and the initial CAT. Min=Minimum; Max=Maximum; SD=Standard Deviation.

The last column of Table 4.1 in the main document displays the difference in quality score between the initial extractions and automatically improved CATs. The highest score increase (12) was for cases No.23 and No.31. For both cases, the dominance types could not automatically be determined since both the RCA and LCX were not completely extracted. For example, the "RD" dominance type is used initially in case No.23 but after the automatic improvement, it was successfully detected as LD.

A different cohort for robustness

On the second cohort (98 cases), the robustness of the proposed method to different cohorts was measured. For the 98 cases, 89 initial CATs were automatically extracted without user interaction while the initial extraction for 9 (9%) cases failed due to a wide-field of view CCTA scanning. The initial CATs for these 9 cases were semi-automatically extracted with manually set aorta centers (6 cases) or ostia positions (3 cases).

Quality scores of the automatically extracted, manually improved and automatically improved CATs for the 98 cases are shown in Figure 4.6. Box-plots in Figure 4.6(a) show the quality score distributions among 98 cases. Compared to the automatic extractions, all improved CATs have either the same (10 cases) or a higher quality score (88 cases). The average quality score for all 98 automatically improved CATs is 93±4. Two cases had a final quality score of 100 after the automatic improvement, since they are the same as the designed anatomical statistical models.

In Figure 4.6(a), 3 initial CATs have $S<75$ which are shown as outliers. The outlier with $S=70$ is a case that the LM did not exist, which is a coronary artery anomaly (represented as a green + in Figure 4.6a). This case is also shown as an outlier among the results from the manual improvement and automatic improvement. The case with the initial $S=57$ had its LAD not automatically extracted (represented as red * in Figure 4.6a). The experts manually corrected this to a score of $S=68$. The proposed method automatically extended LAD and improved this CAT to $S=89$ which contributed to the maximum score increase $S_{\Delta}=32$ among all datasets. The remaining outlier is a RD case for which only the proximal part of RCA was extracted which resulted in a lower score of $S=73$ (represented as blue + in Figure 4.6a). The proposed method automatically added the remaining part of the RCA including the RPDA into this extracted CAT which results in a quality score of 87. In the automatically improved CATs, there is another outlier ($S=83$, represented as red diamond in Figure 4.6a) except from the coronary artery anomaly case. In this case, a vein was located near the LCx in such a way that the vesselness filter could not distinguish between them and the LCx was detected as a vein. Due to lack of information in the binary vesselness image, our method couldn't automatically extract the LCx.

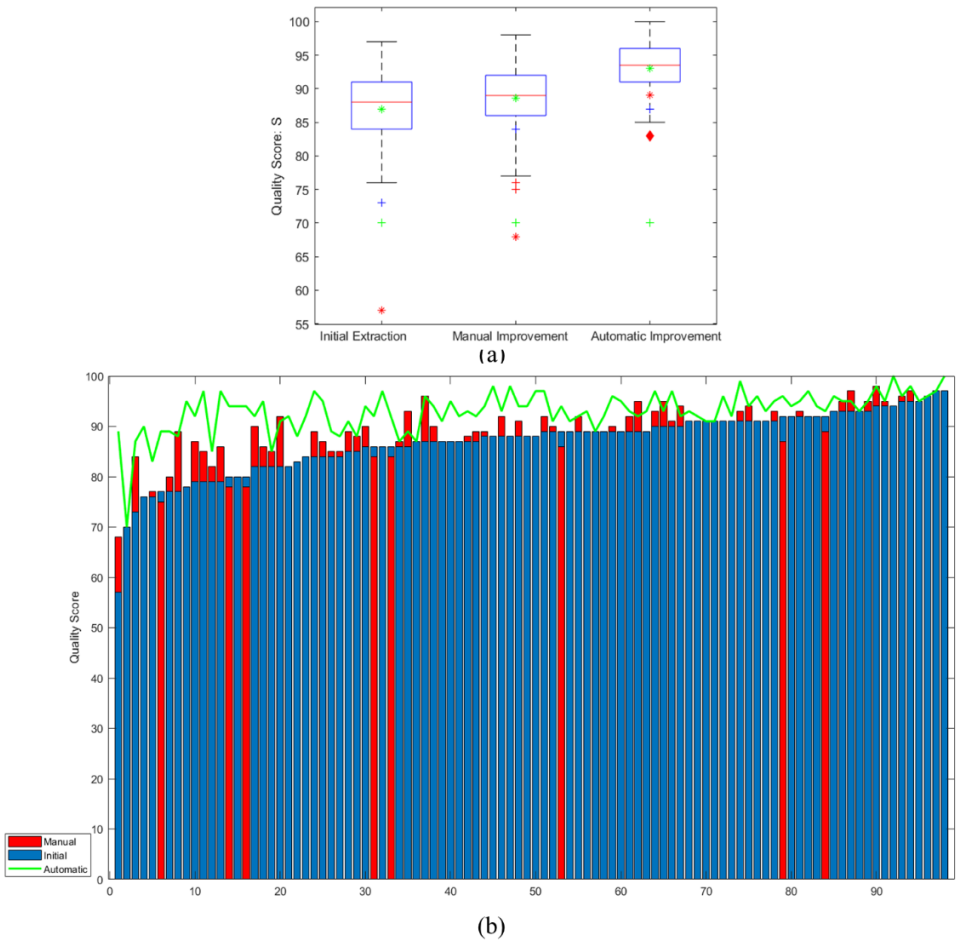

Figure 4.6 Quality scores of the initial extractions, manual improvements and automatic improvements. (a) Box-plots of the quality scores for initial extractions, manually improved and automatically improved extractions with their medians as 88, 89 and 94. Green * shows their average quality scores which are 87±6, 89±6, and 93±4. For outliers, green + represents a case that the LM is not existed which is a coronary artery anomaly; red * represents a case that the LAD is not automatically extracted; blue + represents a RD case that only the proximal part of the RCA was extracted; red diamond represents a case that the distal part of the LCX could not be extracted. (b) Bar-plots of the quality scores sorted by the scores of the initial extractions. Red, blue bars show the scores for the manually improved and initial extractions; green line shows the scores of automatically improved extractions. LM= Left Main Artery; LAD= Left Anterior Artery; LCX= Left Circumflex; RD= Right Dominant

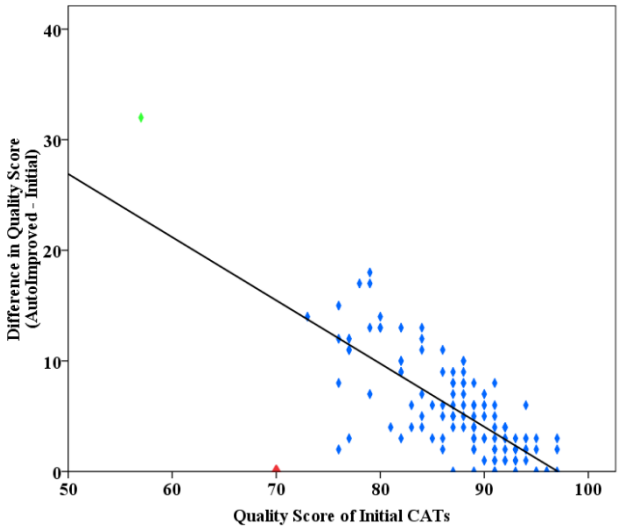

Figure 4.7 Correlation between the quality score of initial CATs and the difference in quality scores (R=-0.694, P<0.001) for 122 cases. The difference in quality scores is (the score of automatically improved CAT – the score of the initial CAT). Green diamond is the case with the LAD not automatically extracted. Red diamond is the case without LM. CATs= Coronary Artery Trees. LAD= Left Anterior Descending artery; LM=Left Main

DISCUSSION AND CONCLUSION

In this paper, an automatic method for improving coronary artery tree (CAT) extractions is described. Guided by anatomic statistical models, the proposed method is able to identify and improve incorrect extractions for automatically extracted CATs without deterioration. Although the initial extractions and binary vesselness images were extracted using a specific extraction method, the presented approach could also be applied to improve CATs extracted by other methods which can produce a candidate-list of vessel-like structures [2-5]. Automatically correcting CATs will reduce or even avoid the manual corrections for the radiologists or cardiologists. By providing a precise and complete CAT, the model-guided method will also help clinicians save time in performing analysis. Furthermore, automatically improved CATs will not introduce manual bias which are more reproducible. The proposed method can be safely applied and may facilitate the automatic analysis of coronary artery disease.

Searching distance. The improved branch searching is performed with an optimally selected initial searching distance and increasing step-size. If the searching distance is too small, no vessel-like structures are found; if the searching distance is too large, a lot of vessel-like structures are connected to the CAT and the search takes more time. Additionally, the

presented method is able to improve the extracted CAT for cases with chronic total occlusion with a lesion length shorter than the maximum searching distance (15 mm).

Weight of the label. Only the absence of a label with a high weight is treated as an incorrect extraction and the proposed method is applied to improve it. This reduces the searching time and the risk of including non-artery structures. The label weight threshold is empirically set as 0.4. Potentially, the miss-extractions on a low weight label could be missed while a miss-extraction on a high weight label could be over-extracted.

Stopping criteria. We defined the stopping criteria since it is difficult to set a generic standard score to judge the quality of extracted CATs from different scans. The change of the quality score after each improvement operation indicates the performance of one improvement action. The score decreasing threshold is used to ensure that the improvement operations don't deteriorate the quality of the CAT too much. However, we should also point out that some vessel-like structures might be included in the automatically improved results.

Comparison with manual corrections. We also included the manually corrected CATs as a reference. In general, more vessels are included in the automatically improved CAT compared to the corresponding manually corrected CAT. The manual correction was focused on removing veins and vessel-crossings while the model-guided method improves the CAT by considering not only the removal of wrong extractions but also the extension to generate a more complete CAT.

Due to the large anatomical variation in CATs among the general population, it is not possible to define a generally applicable cut-off of the quality score to indicate which case needs corrections. Furthermore, it should be noted that improving a CAT to a score of 100 is not the goal of the proposed method since only a CAT with exactly the same topology as defined in the anatomical statistical model will achieve 100.

Limitations

For vessels not in the AHA model, only corrections on the pathline length and vessel directions could be made. Additional features, such as anatomical locations, should be exploited. Also, the proposed method could not be performed when the initial extraction failed due to a wide-field of view CCTA scanning. It is to be expected that initial extractions will be successful by cropping the CCTA images around the heart which will improve the performance of the proposed method. Finally, no comparison between the improved coronary artery trees and the results from the experts was made due to the difficulty in obtaining ground-truth manual extractions from experts. Experts may focus on different aspects of a CAT or may have a different purpose with the extracted trees.

SUPPLEMENTARY DOCUMENT

1. Anatomical statistical models

The weight for each label in the 17-segments AHA model based on the occurrence of each label to describe its clinical significance (Figure 4.8).

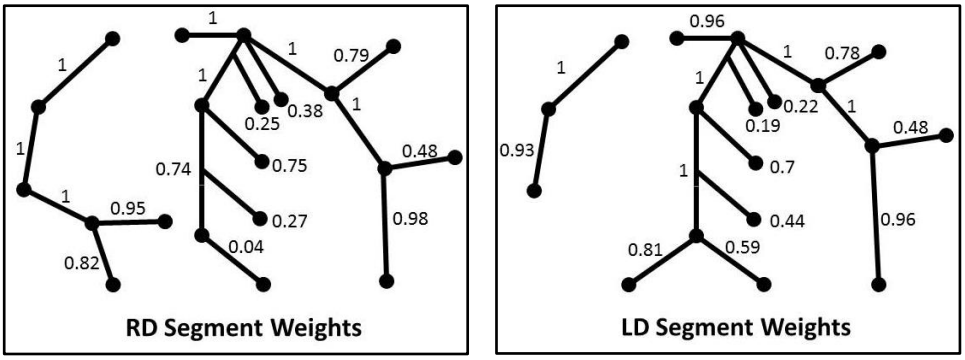

(a) (b)

Figure 4.8 The weight for each label in the 17-segments AHA model for both RD and LD cases. LD= Left Dominant; RD= Right Dominant

2. Coarse Improvement

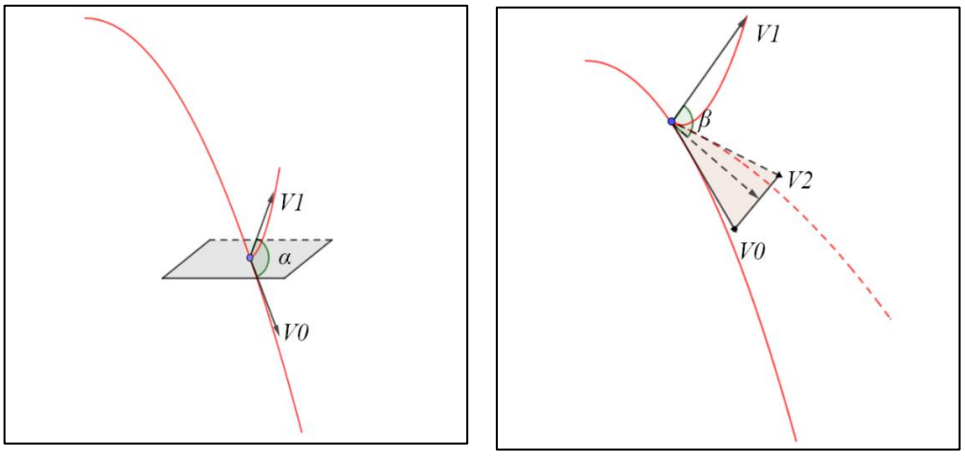

(a) (b)

Figure 4.9 The bifurcation angle α and the surface angle β of a vessel. (a) The bifurcation angle α of a vessel between vessel direction vector *V1* and the main branch direction vector *V0*. (b) The surface angle β between vessel direction vector *V1* and the plane defined by the main branch direction *V0* and the other vessel direction vector *V2*

Two angles are involved in the coarse improvement process. Along the blood flow direction, the angle between the parent branch direction *V0* and the side branch direction *V1* is calculated as the bifurcation angle α of this side branch (Figure 4.9a). When α>120°, the vessel is removed since it indicates a sudden change in direction. If multiple vessels bifurcate from the same position on a branch, the surface angle β of a side branch is calculated as the angle between *V1* and the plane defined by *V0* and *V2* (the other vessel direction) (Figure 4.9b). Vessels with β>120° are removed.

Figure 4.10 shows some examples of the coarse improvements applying on automatically extracted CATs. Blue lines show the extractions removed by coarse improvement operations.

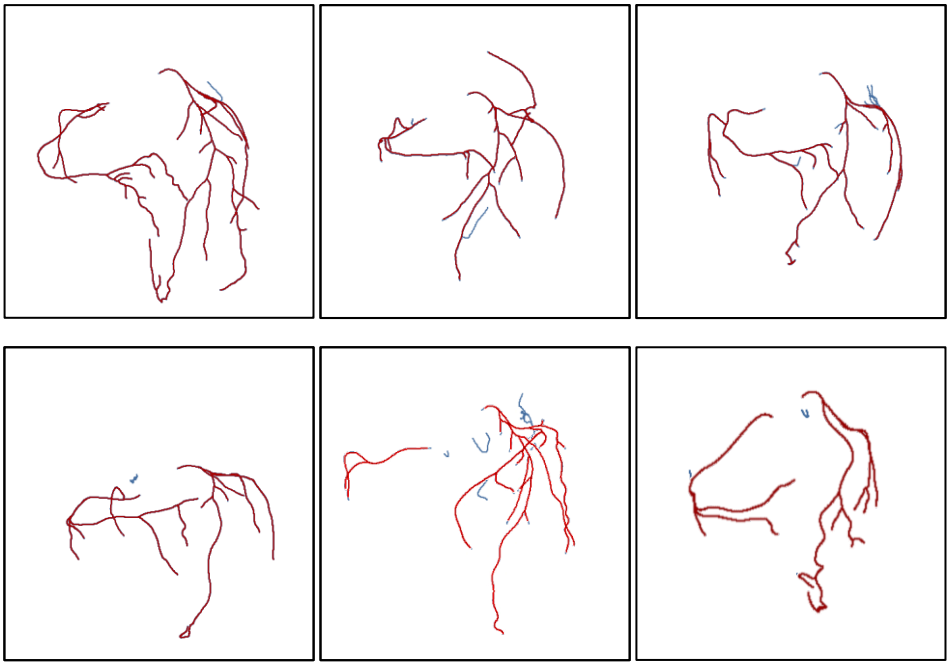

Figure 4.10 Coarsely improved 6 CATs. Blue lines are the vessel-like structures removed by coarse improvement operations.

3. Sensitivity Analysis of the Parameters

The proposed method involves four parameters, namely, l_0 and μ to initiate, increase and constrain the size of the searching distance; $T_{S\Delta}$ as a threshold to limit the quality score decrease and the maximum number of the iterations N_{iter}. The first 18 datasets (No. 0-17) from the first cohort were used to optimize all 4 parameters. Their values are listed in Table 1 with which the highest average score was achieved.

For a fast and accurate branch searching, the initial searching distance l_0 is set as 6 mm after training on 18 training sets. The step μ is set as 2.5 mm to allow some cases with larger gaps. In practice, a small initial searching distance (e.g., l_0=2 mm) can be used and increased by a step size μ=1 mm in case of including too many non-artery structures in the CAT which is a trade-off with time. A maximum searching distance of L_{max}=15 mm is still set to avoid extracting surrounding tissues as arteries. Moreover, if there is no limitation for the L, the searching time and also the risk of extracting surrounding tissues or veins as arteries increase. Absent labels in extracted CATs with weights larger than a threshold T_{weight} are marked as important and need to be improved. T_{weight} is set to 0.4 with which all main branch segments, the first marginal (OM1) and the first diagonal (D1) are considered as important.

Table 4.2 Parameters setting for the model-guided improvement method

Parameters	Value
l_0 (mm)	6
μ (mm)	2.5
$T_{S\Delta}$	-4
N_{iter}	4
T_{weight}	0.4

To evaluate the performance of the proposed method, different starting points, searching distances, quality score thresholds and number of iterations are explored and their derived improvement results are analyzed.

3.1 The selection of different start points

Figure 4.11 illustrates the process of extending from different start points to improve an extracted CAT. Firstly, the extracted CAT (Figure 4.11a) is automatically determined as a RD case. Then, the labels in the AHA model are automatically assigned to corresponding segments in the extracted CAT as shown in Figure 4.11d. After the comparison with the RD anatomical model, the absence of RPLB is detected. The extension operation is performed since the RPLB with a weight of 0.95 is important as being a RD case.

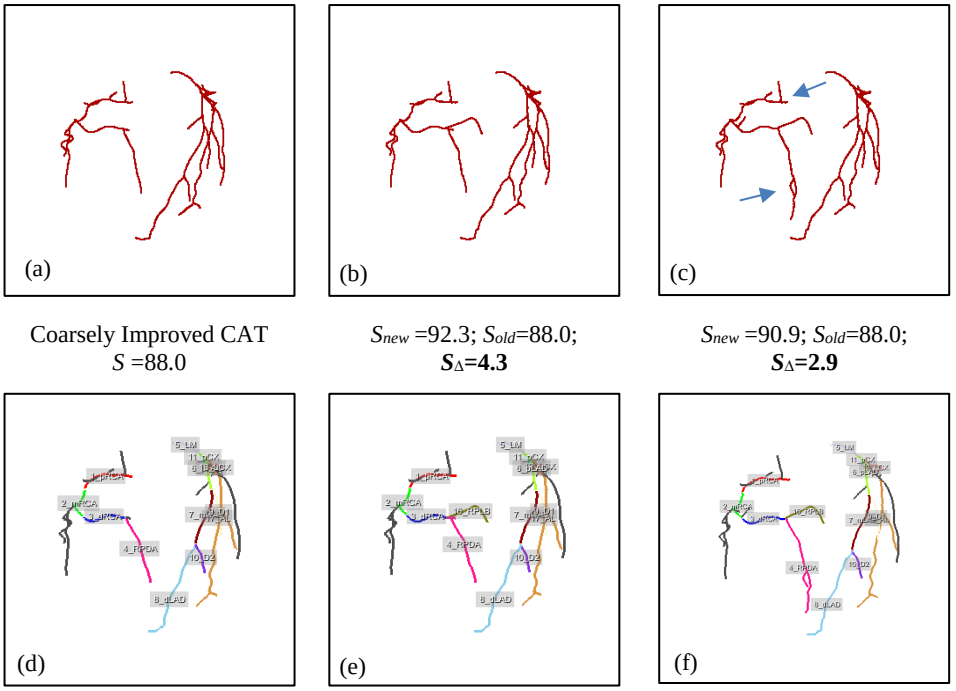

Figure 4.11 Extending from different starting points to get the RPLB. (a) The coarsely improved CAT. (b) The improved CAT extending from the dRCA. (c) The improved CAT extending from the whole RCA. Snew, Sold and SΔ are the quality scores after one improvement operation, before one improvement operation, and also their difference. The second row (d-f) shows the CATs with labels corresponding to the CATs in the first row (a-c). RPLB= Right Posterior Lateral Branch; CAT= Coronary Artery Tree; RCA= Right Coronary Artery; dRCA= distal Right Coronary Artery.

The points on the parent label (dRCA) of RPLB are selected as starting points for extension as described in the methods part. The RPLB is extracted and shown in Figure 4.11b and e. To illustrate the extension differences in selecting different start points, Figure 4.11c is the result of the extension using all points on the RCA as starting points. Even though the RPLB

is extracted in Figure 4.11c, several non-vessel structures are also included in the RCA (pointed out by blue arrows). Moreover, if more points are used as starting points, the searching time increases compared with the extension only from the dRCA. For better understanding, the second row from Figure 4.11d-f show the CATs with labels corresponding to the CATs in the first row (Figure 4.11a-c).

Different from the approach to extend a side branch, if a main branch label is absent, all points with large curvatures on the extracted part of the main branch are used as starting points. Figure 4.12 shows an example of the extension to get the RPDA and RPLB for a RD case. Figure 4.12a and d show a coarsely improved CAT in which the dRCA is assigned to an incorrect position since the real dRCA is not extracted. If the branch searching starts from segment dRCA (the part between the two red points in Figure 4.12d), the real RCA branch cannot be extracted, as can be seen from Figure 4.12b and e. A search from the whole RCA will successfully extract the real RCA branch (Figure 4.12c and f).

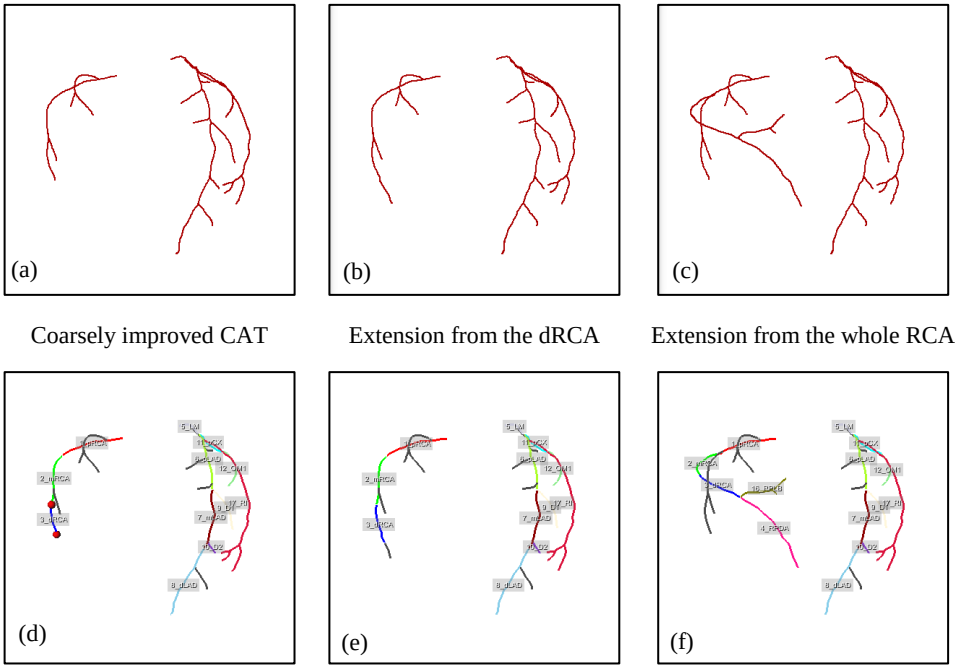

Figure 4.12 Extending from the main branch to get the RPDA and RPLB for a RD case. (a) The coarsely improved CAT. (b) The improved CAT extending from the dRCA. (c) The improved CAT extending from the whole RCA. The second row (d-f) shows the CATs with labels corresponding to the CATs in the first row (a-c); the two red points in (d) show the start and end points of the segment dRCA. RPDA= Right Posterior Descending Artery; RPLB= Right Posterior Lateral Branch; RD= Right Dominant; CAT= Coronary Artery Tree; RCA= Right Coronary Artery; dRCA= distal Right Coronary Artery.

Figure 4.13 shows another example of automatically searching for D1 and the difference between extending from the pLAD and the whole LAD. On the coarsely improved CAT (Figure 4.13a and d), the proposed method searches from the points on the pLAD (pointed out by two red points in Figure 4.13d to find the D1. One vessel-like branch is added (the blue arrow in Figure 4.13b) after the extension which is not the wanted D1, as can be seen from Figure 4.13e. However, the quality score remains the same since the added one branch have small effects on the quality score. Searching from the whole LAD results in extracting more unwanted vessel-like structures as arteries, seen in Figure 4.13c and f. These added structures affect the topology of the CAT leading to an incorrect automatic labeling for the CAT in Figure 4.13f.

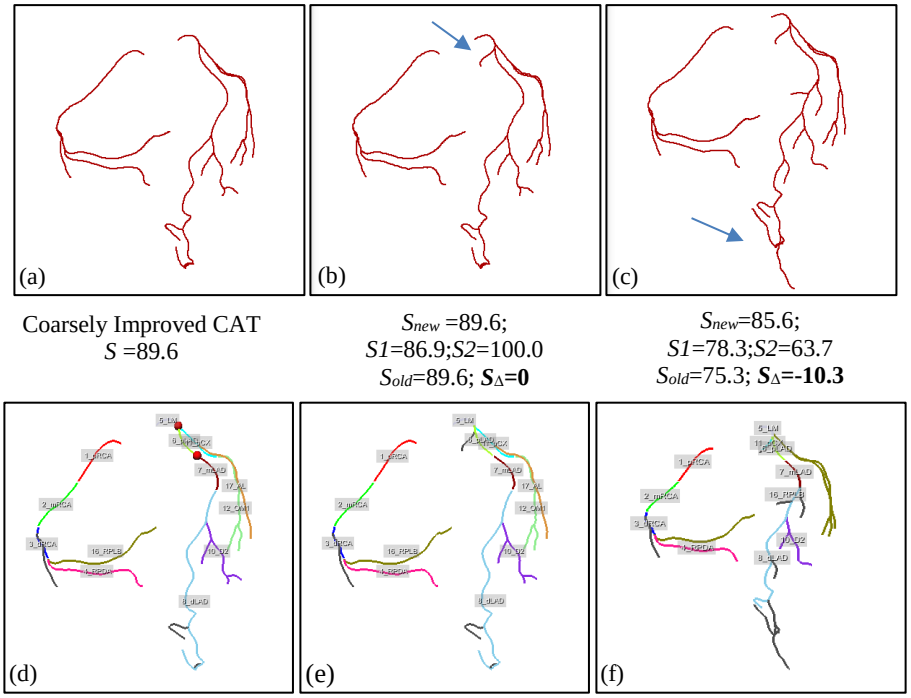

Figure 4.13 Extending from different start points to get the D1. (a) The coarsely improved CAT. (b) The improved CAT extending from the pLAD with one vessel-like structure added; the blue arrow points at the added branch which is not the D1 branch. (c) The improved CAT extending from the whole LAD with too many incorrect extractions added; blue arrows point at the added branches which are not the D1. The second row (d-f) shows the CATs with labels corresponding to the CATs in the first row (a-c); the two red points in (d) point at the segment pLAD. S_{new}, S_{old} and S_{Δ} are the quality scores after one improvement operation, before one improvement operation, and also their difference. *S1*, *S2* are the sub-quality scores for the *vessels-with-labels* and the *vessels-without-a-label*. The lower *S2*=63.7 from (c) compared to the *S2*=100.0 in (b) is caused by the added wrong extractions. D1= first Diagonal; CAT= Coronary Artery Tree; pLAD= proximal Left Anterior Descending branch.

3.2 Searching distance

From the automatically selected starting points, unconnected vessel-like structures in the corresponding binary vesselness image are searched iteratively starting with an initial searching distance $L=l_0$ and increasing in each iteration with step μ ($L=L+\mu$). The searching continues until unconnected parts are found or the maximum search distance L_{max} is reached. If multiple unconnected parts are found, the unconnected part with the most and the longest side branches is selected and connected to the extracted CAT.

Figure 4.14 shows the automatic improvement process for an extracted CAT extending with different searching distances. The initial CAT (Figure 4.14a and e) is automatically determined as a RD case. A coarse improvement is first performed to remove the vessels with wrong directions which are pointed out by two blue arrows in Figure 4.14a. A further detection reports that an extension of the RCA to get the RPDA and RPLB is needed for this RD case. As can be seen from Figure 4.14, extending with different searching distances from the same start points, different results will be obtained.

When the searching distance L<5 mm, no vessel-like structures are found and connected (Figure 4.14b and f). Figure 4.14c and d show the result of searching with L=6 mm which added both the RPDA and RPLB. When L=12 mm, the RPDA and RPLB are extracted while some unwanted vessel-like structures are also connected to the CAT (see blue arrows in Figure 4.14d). The score of the CAT in Figure 4.14d is lower than Figure 4.14c because additional *vessels-without-a-label* are included. Additionally, the searching takes more time.

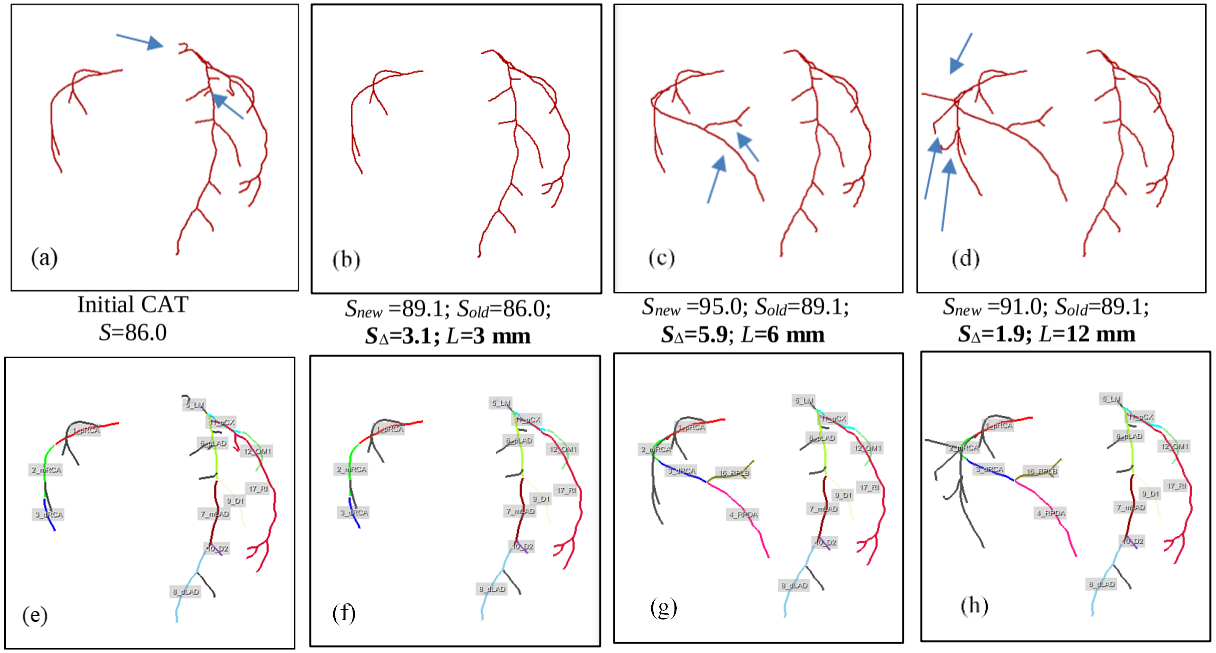

Figure 4.14 Extending the RCA with different searching distances. (a) Automatically extracted CAT; blue arrows point at vessels with wrong directions which will be removed by the coarse improvement before extending. (b) Extending the RCA for the coarsely improved CAT with the L=3 mm and no vessels are added. (c) Extending the RCA with L= 6 mm and two vessels are added; blue arrows point at the added two branches: the RPDA and the RPLB. (d) Extending the RCA with L=12 mm and two vessels are added together with several additional vessel-like structures which are pointed out by blue arrows. The second row (e-h) shows the CATs with labels corresponding to the CATs in the first row (a-d). S_{new}, S_{old} and S_{Δ} are the quality scores after one improvement operation, before one improvement operation, and also their difference. RCA= Right Coronary Artery; CAT= Coronary Artery Tree; RPDA= Right Posterior Descending Artery; RPLB= Right Posterior Lateral Branch.

3.3 Changes in quality scores

Figure 4.15 shows the process of an extracted CAT improved by several improvement operations. The quality scores of the CAT after each improvement operation are calculated. In order to get the RPLB and RPDA, the extension of the RCA in Figure 4.15b-d shows that the score decreased by 3.5, 0.3, and 7.3, respectively. Without the constraint for the changes in quality scores after each improvement operation or the accumulated score differences, the improvement process continuously worsen the extraction quality.

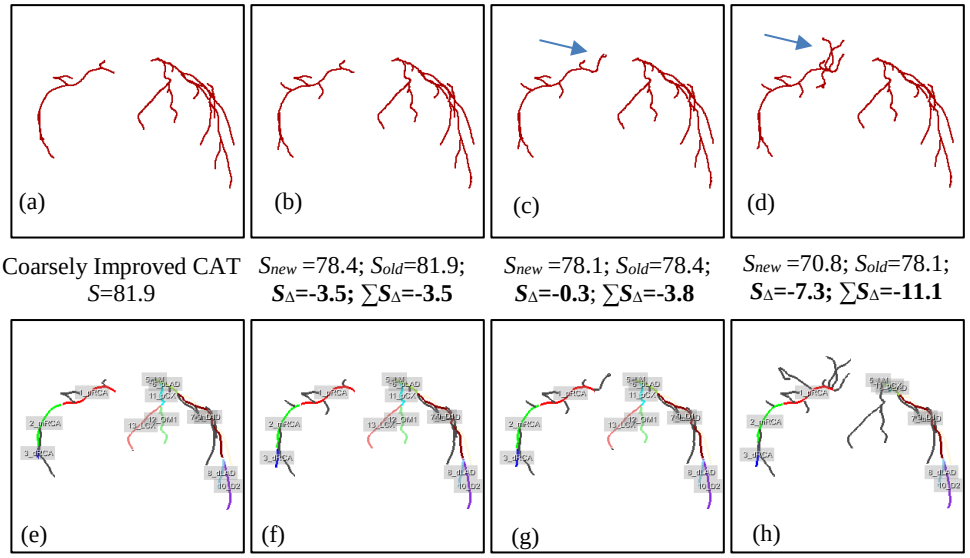

Figure 4.15 The changes in quality scores by several improvement operations to extend the RCA in order to extract RPDA and RPLB. (a) The coarsely improved CAT. (b-d) are the improved CATs extending for the first, second and third time, respectively. The RPDA and RPLB are not extracted while several unwanted vessel-like structures are added to the CATs (pointed out by blue arrows). The second row (e-h) shows the CATs with labels corresponding to the CATs in the first row (a-d). S_{new}, S_{old} and S_{Δ} are the quality scores after one improvement operation, before one improvement operation, and also their difference. $\sum S_{\Delta}$ is the accumulated score difference during the improvement process. RCA= Right Coronary Artery; RPDA= Right Posterior Descending Artery; RPLB= Right Posterior Lateral Branch.

3.4 The number of iterations

Figure 4.16 shows the automatically improved results for an extracted CAT within different iterations. On the coarsely improved and labeled CAT (Figure 4.16a and e), the absence of OM1 is detected which requires an extension. Points on the parent label (pCx) of the OM1 are used as starting points to do the extension (l_0=6 mm; μ =2.5 mm). After doing the branch searching for 3 iterations, there were no vessel-like structures added to the LCX subtree (Figure 4.16b). Actually, this case doesn't have an OM1. Without the constraint on the number of iterations, the extension will not stop. After 6 and 9 iterations in the branch searching, some unwanted vessel-like structures are added to the LCX subtree which are pointed out by the blue arrows in Figure 4.16c and d.

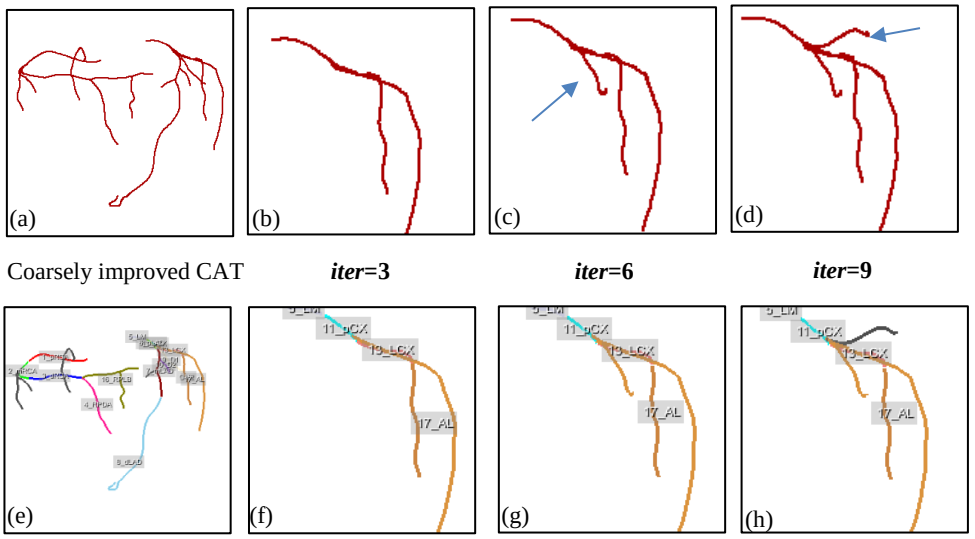

Figure 4.16 Extending from the pCx to get the OM1 within different iterations. (a) The coarsely improved CAT. (b-d) A close-up of the LCX subtree which shows the LCX subtree after extending in 3, 6 and 9 iterations, respectively; blue arrows point at the added branches. The second row (e-h) shows the CATs with labels corresponding to the CATs in the first row (a-d). pCx= proximal left Circumflex; OM1= first Obtuse Marginal; CAT= Coronary Artery tree; LCX= Left Circumflex.

4. Results for the 18 training cases

Quality scores of the CATs from the 18 training cases before and after the automatic improvement are calculated and shown in Table 4.3. The average quality score of the 18 training datasets is improved from 84 to 93 with the standard deviation decreasing from 16 to 4.

Table 4.3 Quality scores of the initially extracted, manually improved and automatically improved CATs for the 18 training cases (Case No. 0-17)

Case No.	Quality Score				
	Initial Extraction	Manual Improvement	Automatic Improvement	DIF (Manual - Init)	DIF (Auto-Init)
0	88	88	93	0	5
1	87	91	88	4	1
2	22	92	95	71	73
3	89	86	97	0	8
4	77	84	86	7	9
5	88	88	89	0	1
6	75	74	85	-1	10
7	93	88	95	-5	2
8	90	92	100	2	10
9	92	99	99	7	7
10	92	91	96	-1	4
11	86	92	95	6	9
12	86	87	95	1	9
13	91	85	96	-6	5
14	84	80	86	-4	2
15	89	81	97	-8	8
16	86	90	91	4	5
17	89	89	97	0	8
Min	22	75	85	-5	1
Max	93	97	100	74	73
Median	88	90	95	2	7
Average (±SD)	84 (±16)	90 (±5)	93 (±4)	6 (±17)	10 (±16)

Note: DIF represents the difference in the quality score between the manually or automatically improved CAT and the initial CAT. Min=Minimum; Max=Maximum; SD=Standard Deviation.

5. Automatic Tree Recovery

To further assess the performance of the proposed model-guided method, we artificially pruned 5 fully extracted CATs and then applied the proposed method to improve them. The proposed method completely recovered the 5 artificially pruned CATs to their initial CATs step by step based on the designed decisions tree. We show one of the 5 cases as an example (Figure 4.17) to demonstrate the process of the model-guided method recovering an artificially pruned CAT to the initial fully extracted CAT.

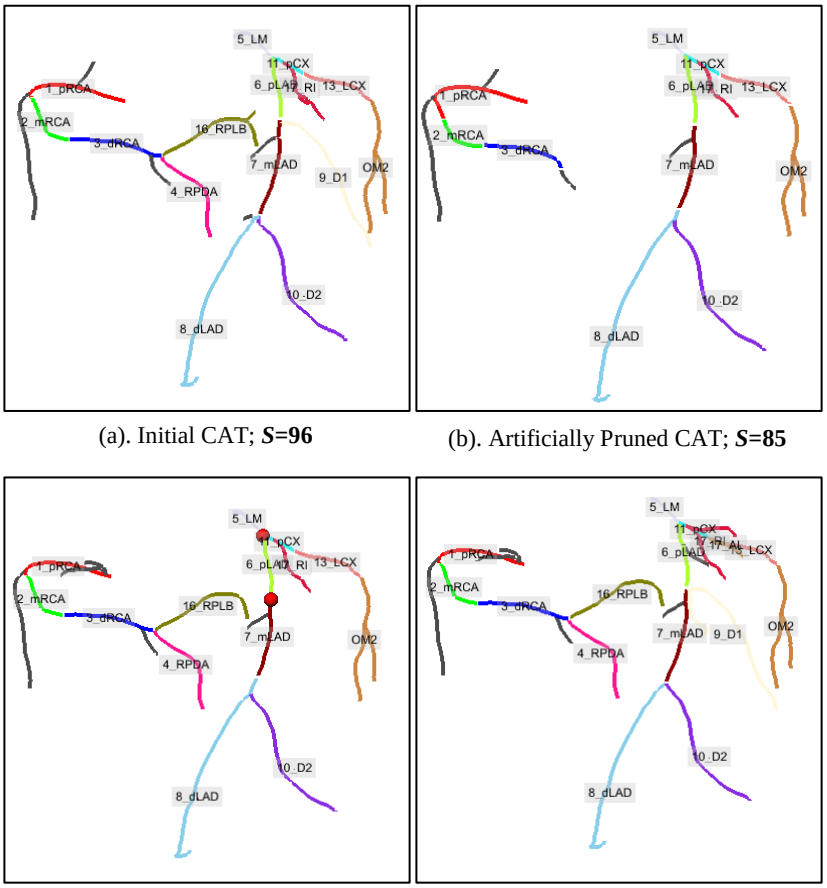

(a). Initial CAT; ***S*=96** (b). Artificially Pruned CAT; ***S*=85**

(c). Auto-Recovered CAT; ***S*=91** (d). Auto-Recovered Final CAT; ***S*=96**

Figure 4.17 Automatically recover an artificially pruned CAT to its initial fully extracted CAT. (a) A fully extracted CAT. (b) The artificially pruned CAT by removing the RPDA, RPLB and D1 branch. (c) The automatically improved CAT extending from the RCA to get the RPDA and RPLB. (d) The automatically improved CAT extending from the pLAD to get the D1. *S* is the quality score for each CAT. CAT= Coronary Artery Tree. RPDA= Right Posterior Descending Artery; RPLB= Right Posterior Lateral Branch; RD= Right Dominant; CAT= Coronary Artery Tree; RCA= Right Coronary Artery.

A fully extracted CAT (Figure 4.17a) is artificially pruned to the CAT in Figure 4.17bby removing the RPDA, RPLB and D1 branch. The automatic tree recovery process has the following steps. Firstly, the dominance type of this case is automatically detected as RD. With the information that the RPDA is absent in this RD case, the RCA is selected to be extended. Branch searching is performed on the binary vesselness image from points on the RCA and the result is shown in Figure 4.17c. The RPDA and RPLB were extracted in Figure 4.17c with its quality score as 91. Later in the process, in the LAD subtree, the absence of D1 requires an extension due to its high weight. Points on the parent label pLAD of the D1 (Figure 4.17c, marked as two red points) are used as searching starting points. The D1 is connected by the extension (Figure 4.17d) with the final quality score of the extracted CAT as 96. There are subtle differences in some branches, such as side branches on the pRCA, but these small branches are not important and they are below the maxima for the coarse improvement. These small branches are kept in the extraction. All the removed branches are recovered successfully.

We didn't perform experiments for the remaining 93 cases, since it is to be expected that similar to the 5 selected cases, the proposed method is able to fully recover a CAT if there are continuous vessel-like structures in the binary vesselness image.

CHAPTER 5

Automatic Coronary Artery Plaque Thickness Comparison Between Baseline and Follow-up CCTA images

Qing Cao, Alexander Broersen, Pieter H. Kitslaar, Mingyuan Yuan, Boudewijn P.F. Lelieveldt, Jouke Dijkstra

Accepted by Medical Physics, Nov., 2019

ABSTRACT

Purpose: Currently, coronary plaque changes are manually compared between a baseline and follow-up coronary computed tomography angiography (CCTA) images for long-term coronary plaque development investigation. We propose an automatic method to measure the plaque thickness change over time.

Methods: We model the lumen and vessel wall for both the baseline coronary artery tree (*CAT-BL*) and follow-up coronary artery tree (*CAT-FU*) as smooth 3D surfaces using a subdivision fitting scheme with the same coarse meshes by which the correspondence among these surface points is generated. Specifically, a rigid point set registration is used to transform the coarse mesh from the *CAT-FU* to *CAT-BL*. The plaque thickness and the thickness difference is calculated as the distance between corresponding surface points. To evaluate the registration accuracy, the average distance between manually defined markers on clinical scans is calculated. Artificial *CAT-BL* and *CAT-FU* pairs were created to simulate the plaque decrease and increase over time.

Results: For 116 pairs of markers from 9 clinical scans, the average marker distance after registration was 0.95 ± 0.98 mm (two times the voxel size). On the 10 artificial pairs of datasets, the proposed method successfully located the plaque changes. The average of the calculated plaque thickness difference is the same as the corresponding created value (standard deviation ±0.1mm).

Conclusion: The proposed method automatically calculates local coronary plaque thickness differences over time and can be used for 3D visualization of plaque differences. The analysis and reporting of coronary plaque progression and regression will benefit from an automatic plaque thickness comparison.

INTRODUCTION

Coronary artery disease (CAD) is still one of the leading causes of death worldwide [1] and is caused by the buildup of plaque in the walls of the coronary arteries that supply blood to the heart muscle. To diagnose suspected CAD, coronary computed tomography angiography (CCTA) has been widely used. For the assessment of coronary artery plaques on CCTA images, different parameters can be measured, such as the minimum lumen diameter, minimum lumen area, and plaque volume which are calculated per coronary segment, per plaque, or even per patient [45, 46]. Just lumen diameter assessment may lead to misinterpretation due to an irregular lumen shape caused by the plaque while area or volume assessment ignore local details. Furthermore, measurements based on the lumen do not consider the situation that the lumen remains the same while the plaque buildup enlarges the vessel wall (positive remodeling).

Automated quantification of coronary plaques on CCTA images has become feasible due to the development of automatic extraction, labeling, quality assessment and lumen and vessel wall segmentation methods for coronary artery trees (CATs) [39, 43, 44]. Coronary lumen and vessel wall contours are detected in the multi-plane reformatted. Based on the detected lumen and vessel wall contours, the plaque thickness at a certain location in an artery can be calculated as the distance from lumen to the vessel wall (Figure 5.1, the close-up image in green box).

Plaque changes between a baseline coronary artery tree (*CAT-BL*) and follow-up coronary artery tree (*CAT-FU*) are assessed on CCTA images to investigate the plaque development after a treatment, or to study the association with long-term mortality [47, 48]. Currently, plaque changes are measured manually as illustrated in Figure 5.1. The corresponding arteries from the *CAT-BL* and *CAT-FU* are first visually assessed from a similar longitudinal viewing angle, and then aligned using anatomical landmarks, for instance, bifurcation points. Afterwards, coronary plaque differences are calculated based on the 2D transversal view and experts visually assess and grade the changes [45]. However, manually selecting a viewing angle and landmarks for the alignment is time consuming and potentially introduces bias. It is difficult to decide whether the difference is a plaque change or caused by a slightly different viewing angle (Figure 5.1, pointed out by yellow arrows). Moreover, calculating plaque changes in 2D does not utilize the 3D topology information.

Previous studies have demonstrated the feasibility of automatically registering 3D CATs from CCTA images [78-80] which reduces manual alignment bias. However, most of these studies focused on registering CATs from different cardiac phases. Recently, Zeng et al. [79] presented a method to align CATs from two time points but the changes of lumen and vessel wall were not considered.

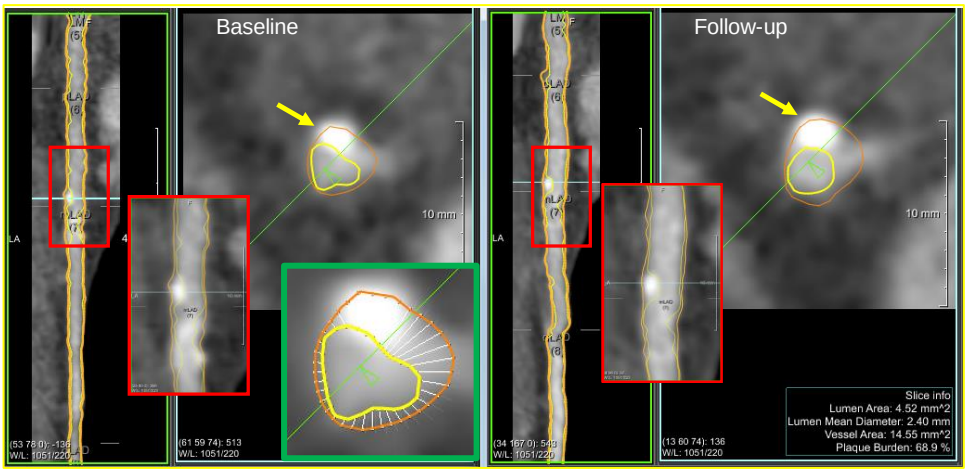

Figure 5.1 Traditional way of calculating the plaque thickness on a 2D slice and doing the baseline and the follow-up plaque thickness comparison. Similar viewing angles were selected manually for assessing plaque changes in an artery between baseline and follow-up; the red boxes include the location with coronary plaques and the close-up image of the location; the yellow arrows point at the coronary plaque which is difficult to determine if the plaque changed. The viewing intensity window width and level are the same for the baseline and follow-up images. The green box shows a close-up image of calculating the plaque thickness on a 2D slice. The yellow color is the lumen contour and the red color is the vessel wall contour; the white straight lines are the distances between the lumen and the vessel wall contour measured every 10º around the lumen center.

To the best of our knowledge, automatic calculation of local changes in coronary plaque over time has not been studied in CCTA. Similar work on magnetic resonance imaging (MRI) images for automatically assessing local changes in carotid plaque morphology was presented by van 't Klooster et al. [81]. However, compared to carotid arteries, coronary arteries are smaller in size and have more complex topologies which results in a more challenging task.

In this paper, we propose a novel method to automatically calculate and visualize the local changes in plaque thickness between *CAT-BL* and *CAT-FU*. The contribution of the manuscript is as follows,

(1). The plaque thickness is calculated and shown on each location on the 3D surface of the coronary arteries instead of on the traditional 2D transversal slices.

(2). A rigid registration method is used to match corresponding points on the baseline and follow-up coronary surfaces.

(3). Artificial baseline and follow-up datasets are created to evaluate the proposed method in a well-controlled environment. Multi-center and multi-vendor clinical datasets are used to evaluate the feasibility of the proposed method in clinical practice.

METHODS

The workflow of the proposed automatic method for calculating the plaque thickness difference is shown in Figure 5.2. We first calculate the plaque thickness for the *CAT-FU* where the lumen and vessel wall are modeled as subdivision surfaces using the same coarse mesh. Then, the *CAT-FU* coarse mesh is mapped to the *CAT-BL* coordinate space using a transformation vector which is obtained from a point set registration on their lumen centerline points. Using the same coarse mesh, the *CAT-BL* and *CAT-FU* subdivision surfaces are created on which their plaque thicknesses are computed. In the end, the difference in the plaque thickness is calculated between corresponding *CAT-BL* and *CAT-FU* surface point. In the next section, we describe the creation of coronary subdivision surfaces.

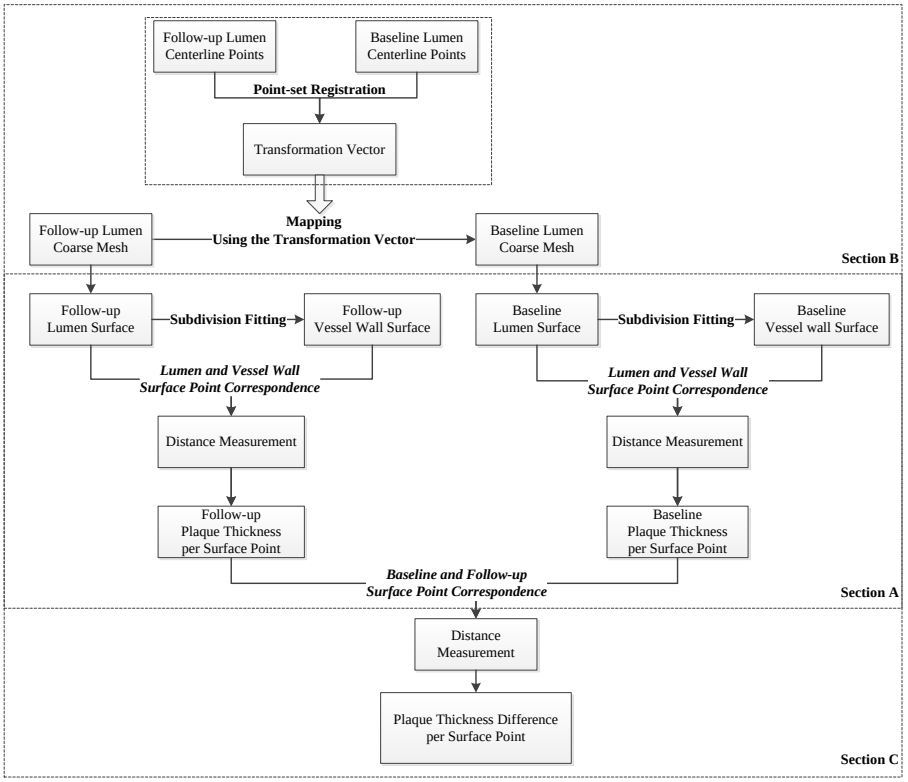

Figure 5.2 Workflow of the proposed method.

Plaque Thickness on Subdivision Surface Point

Coronary subdivision surface

We use the so-called "subdivision technique" to model the coronary lumen and vessel wall as smooth 3D surfaces. This technique allows to create a 3D surface from a coarse to a more fine-grained mesh by repeatedly adding new vertices and edges according to certain

subdivision rules [82]. In this way a high-resolution surface can be created from a low-resolution initialization. Kitslaar et al. [83] used the subdivision technique for coronary artery segmentation and showed the efficiency in modeling coronary arteries from CCTA images.

In our application, subdivision surfaces are initialized by hexagonal rings [82, 83] that define a tubular shaped structure. The initial mesh will grow towards the target contours iteratively pushed by a force factor. The force factor indicates how a mesh point on the subdivision surface moves to the target contour, which is defined as the distance to the contour along the normal direction of the surface in the proposed method. Figure 5.3 shows an example process of generating coronary lumen and vessel wall surfaces by subdivision fitting to contours.

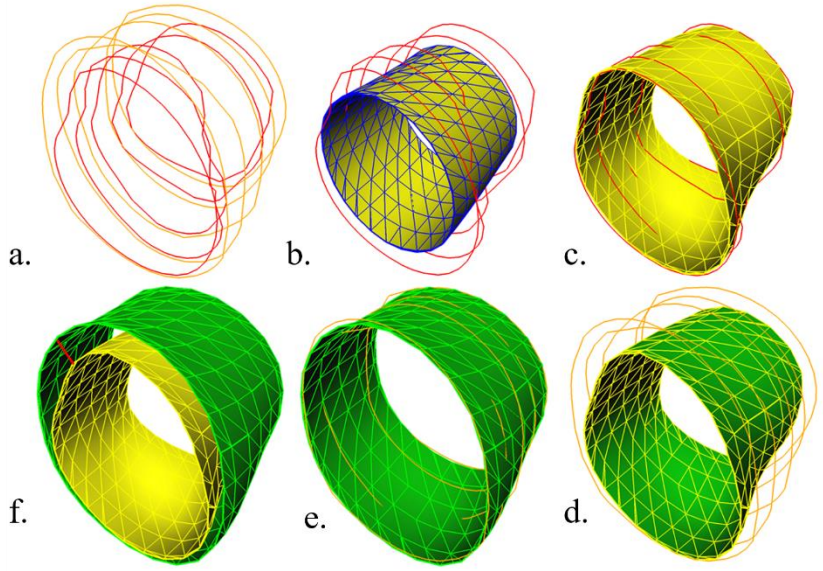

Figure 5.3 A process of generating coronary lumen and vessel wall surfaces by subdivision fitting to contours. From the top-left subfigure to the bottom-left subfigure in a clockwise direction are (a) lumen (red) and vessel wall contours (orange); (b) the initial lumen surface (blue) inside the lumen contours (red); (c) the final lumen surface (yellow) fitted to the lumen contours; (d) the initial vessel wall surface (green) inside the vessel wall contours (orange), and the initial vessel wall surface is actually the final lumen surface (the yellow surface in (c)); (e) the final vessel wall surface (green) fitted to the vessel wall contours; (f) the plaque thickness (red straight line) on subdivision surfaces which is the distance between two mesh points on the final lumen and vessel wall surfaces. Legend: red=lumen contours, orange=vessel wall contours, blue=initial surface, yellow=lumen surface, green=vessel wall surface.

Based on the created coarse mesh, a subdivision fitting scheme is applied to generate a smooth coronary lumen surface. To start the fitting process, we create a subdivision surface by subdividing every coarse mesh one time which results in a 12-point polygon. The 12-point polygon is called the level-1 subdivision surface. Next, we update the positions of the points on the level-1 subdivision surface towards the delineated contour by a force factor. This force

factor indicates how a point on the level-1 subdivision surface moves to the target position which is defined as the distance to the contour along the normal direction of the surface. Furthermore, considering that the contours have irregular shapes, we choose to update the point positions iteratively using a small step size (0.125 mm) in the guidance of the force factor. Several iterations could be needed until all points reach their target positions. Figure 5.3a shows the process of a level-1 subdivision surface fitting to a lumen contour for several iterations. In this way, we obtain the final position of the subdivision surface points which approximates the coronary lumen surface.

By subdividing a level-1 surface, a level-2 subdivision surface is generated which contains more surface points. Subdivision fitting on level-2 doesn't improve the approximation of the coronary artery surfaces. Still, for the purpose of measuring more detailed information, we visualize the final results as level-2 subdivision surfaces without the fitting step.

Plaque thickness of a coronary artery tree

Similar to the traditional plaque thickness calculation on the contours (Figure 5.1a), we calculate the plaque thickness for a coronary subdivision surface point as the distance from the lumen surface point to the corresponding vessel wall surface point. Before we can calculate the plaque thickness, we need to find the correspondence between the lumen surface point and vessel wall surface point. In our method, the correspondence is obtained by using the same coarse mesh for both the lumen and vessel wall to initiate the subdivision fitting.

After the creation of the lumen subdivision surface (as described in the above section), we use it as the initialization for the vessel wall subdivision surface (Figure 5.3d). The lumen subdivision surface moves outwards from the lumen and fits to the vessel wall contours hereby generating the vessel wall subdivision surface (Figure 5.3e). In this way, the correspondence between the lumen and vessel wall surface points remains.

Finally, the plaque thickness for a lumen surface point is calculated as the distance to the corresponding vessel wall surface point which is depicted as a red straight line in Figure 5.3f.

Baseline and Follow-up Surface Points Correspondence

For the plaque thickness differences calculation between *CAT-BL* and *CAT-FU*, we first need to obtain the correspondence between the *CAT-BL* and *CAT-FU* surface points. Here, a similar approach as calculating the lumen and vessel wall surface point correspondence is adopted. We use the same coarse mesh to generate both *CAT-BL* and *CAT-FU* subdivision surfaces, so that only the mesh point position differs while their correspondence remains.

However, it should be realized that the *CAT-BL* and *CAT-FU* are in different coordinate spaces. We use a registration method to transform the coarse mesh between the *CAT-BL* and the *CAT-FU* coordinates. Here, we simplify the surface registration by first registering the centerline points and then using the obtained transformation vector to transform the surfaces.

Coronary artery centerline points

Lumen centerline points are automatically detected from the coronary lumen contours using the method presented by Antiga et al. [84]. For all points on the extracted centerlines, a cubic spline interpolation is performed based on their absolute distances to the extracted ostia point and then down-sampled to a point spacing of 0.5 mm.

Coronary centerline points registration

In this work, we use the coherent point drift (CPD) point set registration method [66] to register the centerline points from *CAT-BL* and *CAT-FU*. CPD registration has been widely applied in tree matching, and an important benefit of this method is that points are forced to move coherently as a group to preserve the topological structure of the point sets. The CPD algorithm contains both rigid and non-rigid point set registration schemes.

Considering the movements of the coronary arteries caused by the complex heart motion, non-rigid registrations were preferred by previous studies for matching CATs since it allows more elastic deformations [78, 79]. CCTA images can be reconstructed from different phases of the cardiac cycle in which heart motion is involved resulting in shape deformations. Moreover, the extracted CATs can have different topologies, such as that some branches are missing in one of the CATs. Also, centerline points can shift between *CAT-BL* and *CAT-FU* due to the plaque size increase or decrease over time. However, these differences are treated as outliers or noise in the non-rigid CPD registrations which deteriorate the registration results and increase the registration time. Furthermore, non-rigid CPD allows the point spacing to change which increases the risk that points from different locations in the *CAT-BL* and *CAT-FU* are matched. After a comparison with the non-rigid registration, we use a rigid CPD registration in favor of the speed, robustness in noise and outliers, and point space preservation.

In the rigid CPD registration, we aim to align *CAT-FU* and *CAT-BL* using the following notations: $X=(x_1,\ldots,x_M)^T$, $Y=(y_1,\ldots,y_N)^T$ which refers to points in *CAT-FU* (the moving image) and *CAT-BL* (the fixed image), respectively. *X* and *Y* are an *M*-sized and a *N*-sized vector of 3D points. $T(X)$ represents the transformation vector for transforming *X* to match *Y*. After the rigid CPD registration, point correspondences are obtained. The obtained point correspondences are a *many-to-one* relationship which means that many points in the *CAT-FU* (the moving image) could correspond to the same point in *CAT-BL* (the fixed image). The *many-to-one* relationship is due to the potential difference in the number of points in the two point sets caused by the extraction. However, we want a *one-to-one* point correspondence to be able to do a precise comparison in a following procedure. Therefore, for a point y_k in *CAT-BL* which corresponds with one or more points from *CAT-FU*, we find the closet match x_i t and define the transformation vector as $T(x_i) = (y_k - x_i)$. In this way, a *one-to-one* point correspondence between *CAT-BL* and *CAT-FU* is determined. We choose to transform the *CAT-FU* to the *CAT-BL* coordinates since a lumen decrease (plaque progression) in the *CAT-FU* is more common than a lumen increase (plaque regression).

Coronary artery surface mapping

To transform the *CAT-FU* coarse mesh to the *CAT-BL* space, we project the centerline points correspondence to the coarse mesh points. As was described in **Coronary Subdivision Surface** section, coarse meshes are hexagonal rings along the centerline of a coronary artery, we use x_i^j, $j \in [1,6]$, to denote the hexagonal ring of a centerline point x_i. For two corresponding centerline points x_i (in *CAT-FU*) and y_k (in *CAT-BL*) with their transformation as $T(x_i) = (y_k - x_i)$, we transform the hexagonal ring from *CAT-FU* to *CAT-BL* with $y_k^j = T(x_i) + x_i^j$. y_k^j is the transformed x_i^j in *CAT-BL* coordinates, $j \in [1,6]$. We perform the transformation for all hexagonal rings to achieve the coarse mesh transformation.

The transformed *CAT-FU* coarse mesh is used as the coarse mesh for the subdivision fitting to get the *CAT-BL* subdivision surfaces. During the subdivision fitting procedure, the point correspondence between the coarse mesh of the *CAT-BL* and *CAT-FU* remains. Hence, the correspondence between subdivision surface points on the *CAT-BL* and *CAT-FU* also remains.

Plaque Thickness Difference

The plaque thickness is calculated for each lumen surface point of the *CAT-BL* and *CAT-FU* which are represented as *BL_Thic* and *FU_Thic*. The plaque thickness differences between corresponding *CAT-BL* and *CAT-FU* surface points are calculated as $DIF_{thickness} = (BL\_Thic - FU\_Thic)$.

For visualization purposes, the plaque thickness differences are mapped to different colors to show the changes over time as shown in Figure 5.6(c).

EXPERIMENTS AND RESULTS

The proposed method was implemented as a module in MeVisLab 2.7.1 (MeVis Medical Solutions AG, Bremen, Germany). The experiments were performed on a PC, with a 2.67 GHz CPU, 12 GB memory and a 64-bit Windows 10 system. The total procedure for calculating the plaque thickness difference between a coronary artery tree at baseline and at follow-up can be finished within 5 minutes.

For the evaluation, we used both clinical scans and artificial datasets which were created based on clinical scans. We did the experiments to evaluate the points correspondence accuracy and the subdivision surface fitting accuracy. Furthermore, experiments were performed on clinical scans to assess the feasibility of the method in clinical practice.

Datasets

In total, 12 multi-center, multi-vendor pairs of scans were used for the experiments, and we categorize them into 3 groups for different evaluation purposes. To enable the automatic coronary extraction and plaque comparison, the 12 pairs of scans used in this study were

carefully checked by two experts that there were no large motion artifacts present that would interfere with a correct analysis. The lumen and vessel wall contours were extracted using the method presented by Boogers et al.[4] and were manually corrected if needed by an expert.

To test the effect of different lumen and vessel wall contouring strategies, GROUP1 and GROUP2 were defined. GROUP1 contains 5 pairs of scans in which the vessel wall contours were always positioned outside the lumen contours, therefore resulting a thickness value always greater than zero. GROUP2 has 3 pairs of scans in which the vessel wall contours were positioned on the same location as the lumen contours when no plaques were present (resulting in zero thickness); If a plaque was present, the vessel wall contours were positioned outside the plaque. The follow-up scans in GROUP1 and GROUP2 were done within an average period of 2 years ± 1.6 months.

Table 5.1 Datasets

GROUP (number of scans)	Time Point	Voxel Size (x,y) (mm)	Slice Thickness (mm)	Scanner List
1 (5)	BL	0.43 x 0.43	0.45	Brilliance 64
	FU	0.34 x 0.34		
2 (3)	BL	0.35 x 0.35	(0.25, 0.625)	LightSpeed VCT SOMATOM Force SOMATOM Definition AS Aquillion ONE
	FU	0.37 x 0.37		
3 (4)	ED and ES	0.45 x 0.45	0.625	Revolution CT

Note: BL=Baseline; FU=Follow-up; ED=End of Diastolic; ES=End of Systolic; Voxel sizes are the average sizes of all data in one GROUP. For the slice thickness, the minimum and maximum values are presented when there are thickness differences within a group of the datasets. For some scans from GROUP2, the follow-up scan was done with a different scanner from the baseline.

Finally, we defined GROUP3, consisting of 4 pairs of end-of-diastolic (*ED*) and end-of-systolic (*ES*) scans, in which the lumen and vessel wall contours were placed using the same rule as for GROUP1. The plaque thickness does not change between *ED* and *ES* scans which are used to assess the systematic bias of the proposed method. Detailed information for the 12 pairs of scans can be found in Table 5.1.

Additionally, one clinical scan was used to create 10 artificial pairs of *CAT-BL* and *CAT-FU*. The clinical scan is the first case in the training datasets (dataset00) from the MICCAI 2008 Coronary Artery Tracking Challenge with a voxel size of 0.32 x 0.32 x 0.4 mm [75].

All the datasets in Group1 and Group2 were reconstructed at the mid-to-end diastolic phase (350ms before the next R-wave or at 65% to 70% of the R-R interval). The *ES* and *ED* datasets in Group3 were reconstructed at the 45% and 75% of the R-R interval, respectively

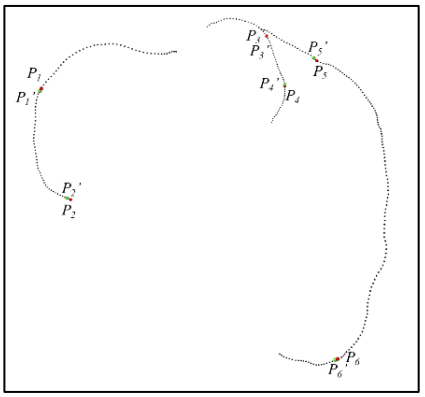

(a)

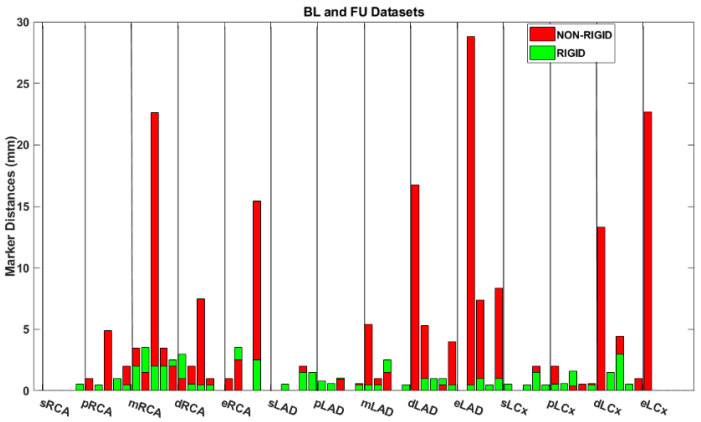

(b)

Figure 5.4 Distances between corresponding markers. (a) an example of markers on a *CAT-BL* and the corresponding *CAT-FU* markers after the registration. Markers on *CAT-BL* (p_i) and the registered markers (p_i') from *CAT-FU* are denoted as red and green points respectively. (b) Distances between markers on *CAT-BL* and the registered markers from *CAT-FU*. Y-axis represents the calculated distances between registered markers. On x-axis, markers are grouped by their positions on the artery. In each group, such as pRCA group, each bar represents the distance between two registered markers for one pair of datasets. Red bars denote the registered markers distances after non-rigid registration. Green bars denote the registered markers distances after rigid registration. s-, p-, m-, d-, e- represent the start, proximal, middle, distal and end of the coronary artery on the bifurcation. RCA= Right Coronary Artery; LAD= Left Anterior Descending artery; LCx= Left Circumflex artery. BL= Baseline; FU =Follow-up.

Points Correspondence Accuracy Evaluation

To evaluate the calculated points correspondence accuracy, centerline points were transformed using the obtained transformation vector and compared with ground truth correspondence. Therefore, markers were placed at the corresponding centerline points for both *CAT-BL* and *CAT-FU* by experts to create the ground truth. Corresponding markers were assigned to the start, proximal, middle, distal and end parts of the arteries on bifurcation points. Expert 1 independently assigned all corresponding markers, and subsequently expert 2 checked the location and applied a correction if needed after a consensus reading with expert 1. Both experts were blinded to the registration results. For each pair of markers, we calculated the Euclidean distance between the corresponding points x_i in *CAT-FU* and y_j in *CAT-BL* using the equation: $D_i = \| T(x_i) - y_j \|$, where T is the obtained transformation vector. Furthermore, we compared rigid registration with non-rigid CPD registration for illustrating the advantages of using rigid CPD in this work.

Figure 5.7 demonstrates the measured plaque thickness differences between *CAT-BL* and *CAT-FU* for a scan from GROUP2. In total, for 27867 mesh points on the generated *CAT-BL* and *CAT-FU* subdivision surfaces, the minimum and maximum for *BL_Thic* and *FU_Thic* are 0.00 mm and 0.85 mm, respectively. The measured minimum and maximum $DIF_{thickness}$ are -0.57 mm and 0.77 mm respectively. In Figure 5.7b, close-up images for a plaque are shown where the thickness values for corresponding mesh points on *CAT-BL*, *CAT-FU* and the plaque thickness differences images are highlighted. As can be seen from Figure 5.7b, there was a plaque in *CAT-BL*, and the plaque is still present at *CAT-FU* while the plaque size increased on a location (pointed by a red arrow) distally along the blood stream direction.

For the *ED* and *ES* scans from GROUP3 in which the $DIF_{thickness}$= 0.00 mm, the average of the calculated $DIF_{thickness}$ is -0.00 mm with a SD= ± 0.18 mm. Values of the calculated plaque thickness differences for each pair of the 4 scans in GROUP3 can be found in Table 5.2.

For the point correspondence evaluation, 9 pairs of scans (GROUP1 and GROUP3) were used. Since the markers were put in the start, proximal, middle, distal and end of the arteries and there are three main arteries in a coronary artery tree, an average of 14 markers were assigned to each pair of scans. In total 116 markers were included for the 9 pairs of scans. In Fig. 4b, each bar shows the distance for each pair of markers after the rigid (green) and non-rigid CPD registration (red) in GROUP1. The bars are divided into 14 groups based on the markers position using the black solid lines (Figure 5.4b). For example, the markers on mRCA, rigid registration shows better performance over the first, the third and the fourth case while it has a slightly worse performance on the second and the fifth case. In general, regardless of the marker position, rigid CPD has a more stable and shorter distance over all 116 markers than the non-rigid CPD with the mean distance of 0.95 ± 0.98 mm vs 2.70 ± 5.10 mm, respectively. Specifically, rigid CPD has a slightly better performance on scans from GROUP1 (0.89 ± 0.92 mm) than GROUP3 (1.01 ± 1.04 mm).

Subdivision Surface Fitting Accuracy Evaluation with Artificial Pairs of Datasets

A set of artificial datasets was created to evaluate the proposed method for calculating thickness changes for plaques with different sizes or plaques at different locations of the vessels.

We use a clinical scan as *CAT-BL* and manually edited its lumen or vessel contours to create a new CAT and then paired them up as "*CAT-BL*" and "*CAT-FU*". In total, we created 10 artificial pairs of *CAT-BL* and *CAT-FU* datasets with a known plaque thickness. For evaluating the ability to measure plaque changes, we decreased the lumen radius with different sizes and different lengths along the vessel direction to simulate different degree of plaque progression. Similarly, we increased the lumen radius to simulate plaque regression. To simulate the plaque positive remodeling, we increased the vessel wall radius while the lumen radius remained unchanged. We put these created plaques at different locations in a coronary artery and in different arteries to determine the robustness in measuring plaque changes at different locations. Furthermore, the lumen and vessel wall radius were increased with the same size to simulate the lumen increase with no change in plaque thickness. Details of the 10 artificial datasets can be found in Table 5.2.

For the 10 pairs of artificial datasets, the proposed method successfully found plaque thickness differences between *CAT-BL* and *CAT-FU* datasets. In general, on the location where we created the plaque thickness difference, the average of the calculated plaque thickness difference is the same as the ground truth value with the standard deviation (SD) of ± 0.10 mm. For cases where we created plaque increase with different lengths (No. 1, 2 and 3), the calculated average $DIF_{thickness}$ is 0.42 ± 0.06 mm. Varying position of the plaque (No. 7 and No. 8) still results in the calculated average $DIF_{thickness}$ = 0.43 ± 0.07 mm. For case No. 9 where the expected $DIF_{thickness}$ = 0.00 mm, the proposed method calculated the average plaque thickness difference as 0.00 mm with the minimum and maximum plaque thickness as - 0.08 mm and 0.13 mm, respectively. Details of the calculated plaque thickness differences for each pair are listed in the last column of Table 5.2.

Figure 5.5 shows examples of calculated plaque thickness differences for case No. 4, 5 and 6 which represent 0.25 mm increase, 1.00 mm increase, and 0.50 mm decrease of plaque thickness, respectively. For all mesh points along the artery (x-axis), the proposed method located the plaque changes exactly at the targeted position. The average of the measured *BL_Thic*, *FU_Thic* and $DIF_{thickness}$ (y-axis) are the same as the corresponding manually created values.

Table 5.2 Datasets description and results for artificial datasets and ED-ES scans

No.	Variable	Simulation	Created $DIF_{thickness}$ (mm)	Calculated Average $DIF_{thickness}$ (mm)
1	L= 4.00 mm ΔR_{lumen}= - 0.50 mm	Plaque increase with different lengths	+ 0.50	0.42 ± 0.08
2	L= 6.00 mm ΔR_{lumen}= - 0.50 mm		+ 0.50	0.45 ± 0.05
3	L= 2.00 mm ΔR_{lumen}= - 0.50 mm		+ 0.50	0.41 ± 0.05
4	L= 4.00 mm ΔR_{lumen}= - 0.25 mm	Plaque thickness increase with differences in transversal direction	+ 0.25	0.21 ± 0.09
5	L= 4.00 mm ΔR_{lumen} = -1.00 mm		+ 1.00	0.88 ± 0.17
6	L= 4.00 mm ΔR_{lumen} = + 0.5 mm	Plaque thickness decrease in transversal direction	- 0.50	-0.46 ± 0.06
7	L= 4.00 mm N_{plaque} = 3	Plaque thickness increase on the proximal, middle and distal part of an artery	+ 0.50	0.42 ± 0.08 (proximal) 0.43 ± 0.07 (middle) 0.44 ± 0.06 (distal)
8	L= 4.00 mm N_{plaque} = 3	Plaque thickness increase on the RCA, LAD and LCx	+ 0.50	0.42 ± 0.08 (RCA) 0.43 ± 0.07 (LAD) 0.43 ± 0.07 (LCx)
9	L= 4.00 mm ΔR_{vessel}= + 0.50 mm	Plaque increase with vessel wall size increase	+ 0.50	0.43 ± 0.09
10	L= 4.00 mm ΔR_{lumen}= + 0.50 mm ΔR_{vessel}= + 0.50 mm	Increase both lumen and vessel wall with plaque thickness difference as 0	0.00	-0.00 ± 0.03
ED and ES-01			0.00	-0.02 ± 0.21
ED and ES-02			0.00	-0.01 ± 0.21
ED and ES-03			0.00	0.02 ± 0.15
ED and ES-04			0.00	- 0.02 ± 0.16

Note: L=Length of a plaque along the vessel direction; N_{plaque} =Number of plaques; $DIF_{thickness}$=Difference in plaque thickness; ΔR_{lumen} = Lumen increase/decrease radius; ΔR_{vessel} =Vessel wall increase/decrease radius; RCA=Right Coronary Artery; LAD=Left Anterior Descending artery; LCx=Left Circumflex artery; ED=End of Diastolic; ES=End of Systolic.

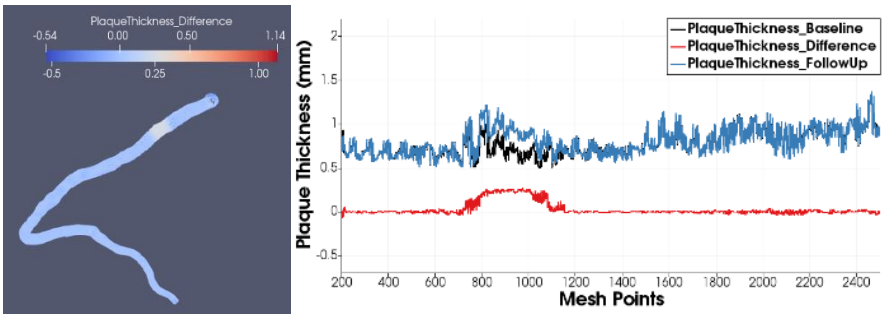

(a) No. 4

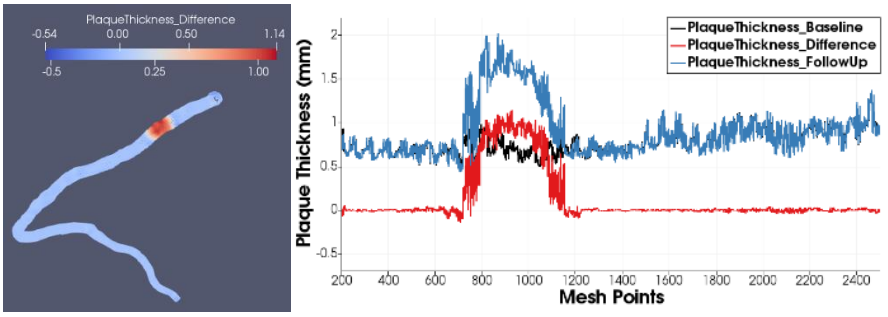

(b) No. 5

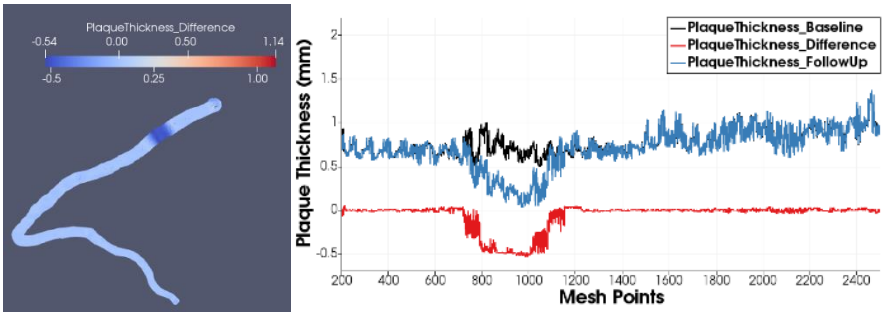

(c) No. 6

Figure 5.5 Plaque thickness calculated by the proposed method for artificially created baseline and follow-up pairs for No. 4, 5, and 6 in Table 5.2 with their average plaque thickness as 0.21 ± 0.09 mm, 0.88 ± 0.17mm, and -0.46 ± 0.06 mm, respectively. The left column is the measured plaque thickness difference with color coding on the modeled coronary subdivision surfaces, and the right column shows the plaque thickness for baseline, follow-up and their differences for each mesh point along this artery.

Plaque Thickness Differences on Clinical Scans

For 12 pairs of clinical scans (GROUP1, -2, and -3), the proposed method was performed to calculate the differences in plaque thickness for each surface point.

Figure 5.6 shows an overview of the baseline and follow-up comparison for a case from GROUP1 in the traditional way and using the proposed method. On Figure 5.6 (a-b), 3D views of the plaque thickness changes between baseline and follow-up are presented. For this case from GROUP1, the automatic results by the presented method showed that there is a plaque thickness change at every location of the CAT (seen from Figure 5.6a) which is caused by the manual bias during the delineating of the lumen and vessel wall contours for *CAT-BL* and *CAT-FU*. For a better visualization purpose, a threshold (||0.5|| mm) is selected as a cut-off value to focus on large plaque thickness changes. Figure 5.6b, the calculated $DIF_{thickness}$ in the range [-0.5 mm, 0.5 mm] is denoted as no plaque change. The calculated $DIF_{thickness}$< -0.5 mm is described as a decrease of a plaque while the calculated $DIF_{thickness}$ > 0.5 mm is described as an increase of a plaque. The plaque increase is denoted by red and the plaque decrease is denoted by yellow which provides a straightforward overview for the users (Figure 5.6b).

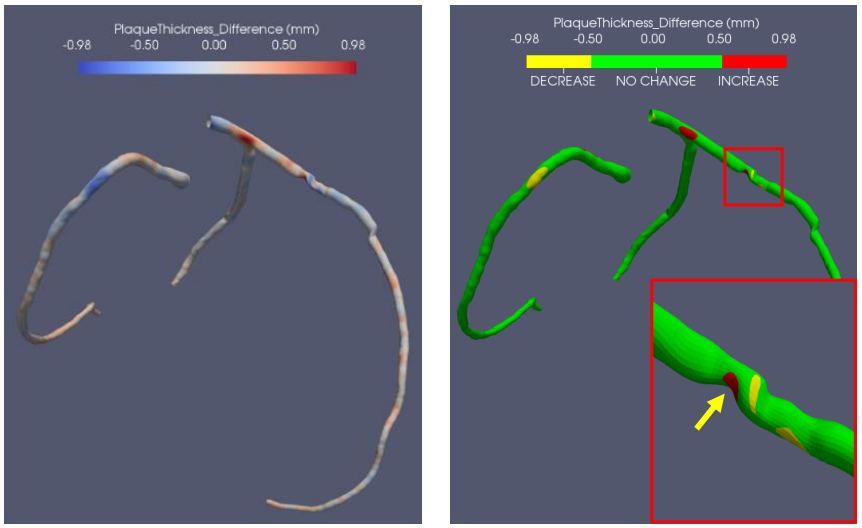

(a) (b)

Figure 5.6 The proposed way of baseline and follow-up plaque thickness difference assessment and the automatic quantification of plaque thickness changes. (a) The automatically calculated plaque thickness changes with color coding on coronary subdivision lumen surface points. (b) The 3D visualization of large plaque thickness increase/decrease using a threshold 0.5 mm; The red box includes the close-up image of the plaques with the yellow arrow pointing at the same plaque as shown in Figure 5.1.

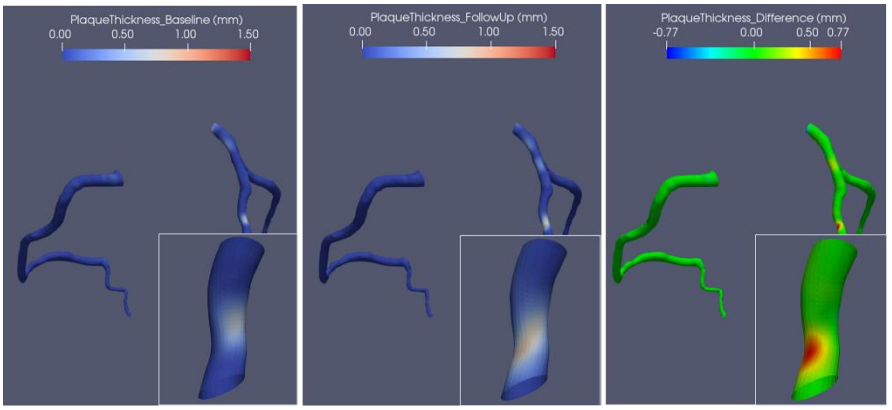

(a)

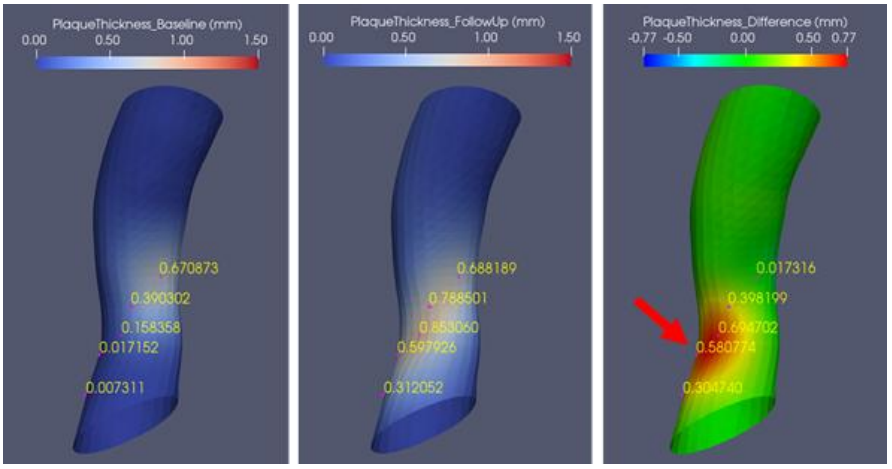

(b)

Figure 5.7 3D coronary subdivision surfaces with the plaque thickness for baseline, follow-up and their differences color coded. (a) An overview of a case for the plaque thickness at baseline, follow-up and their differences; (b) Close-up images of the plaque in (a), on corresponding mesh points, the plaque thickness values were assigned. The red arrow points at the position where there is a plaque size increase along the coronary blood stream.

Figure 5.7 demonstrates the measured plaque thickness differences between *CAT-BL* and *CAT-FU* for a scan from GROUP2. In total, for 27867 mesh points on the generated *CAT-BL* and *CAT-FU* subdivision surfaces, the minimum and maximum for *BL_Thic* and *FU_Thic* are 0.00 mm and 0.85 mm, respectively. The measured minimum and maximum $DIF_{thickness}$ are -0.57 mm and 0.77 mm respectively. In Figure 5.7b, close-up images for a plaque are shown where the thickness values for corresponding mesh points on CAT-BL, CAT-FU and the plaque thickness differences images are highlighted. As can be seen from Figure 5.7b,

there was a plaque in CAT-BL, and the plaque is still present at CAT-FU while the plaque size increased on a location (pointed by a red arrow) distally along the blood stream direction.

For the *ED* and *ES* scans from GROUP3 in which the $DIF_{thickness}$= 0.00 mm, the average of the calculated $DIF_{thickness}$ is -0.00 mm with a SD= ± 0.18 mm. Values of the calculated plaque thickness differences for each pair of the 4 scans in GROUP3 can be found in Table 5.2.

DISCUSSION

In this paper, a method to automatically calculate local plaque thickness differences between a coronary artery tree on baseline and follow-up CCTA images is presented.

A rigid CPD registration was used in this work due to its high accuracy and robustness in coronary trees acquired at two time points (*CAT-BL* and *CAT-FU*) or two phases (*ED* and *ES*). Even though non-rigid CPD registration allows more deformations which could find an exact match for each point, the purpose of this work is to find a list of *one-to-one* corresponding points without changing the centerline point spacing. By first doing a rigid CPD registration and then calculating the closest point, we are able to find corresponding points with the local changes between two CATs preserved. According to the experiments, the proposed method generates points correspondence within 1 mm deviation which is within two voxels. The registration performed slightly worse on scans from two cardiac phases than scans from a baseline and follow-up which is probably due to more coronary shape deformations between scans from two phases. The matching results for the distal part of coronaries are slightly less accurate compared to the proximal parts. It could be caused by differences in the extraction of distal parts due to less contrast in distal part of the artery. From a clinical point of view, plaques in the distal part of a coronary artery are not that relevant for clinical decision making.

We find the surface point correspondence of two CATs by subdivision fitting with the same coarse meshes. The *CAT-FU* coarse meshes are transformed to *CAT-BL* coordinates and used as the coarse mesh for *CAT-BL*. With the same coarse meshes as an initialization for the subdivision fitting, the mesh point correspondences were obtained directly. We choose to transfer *CAT-FU* to *CAT-BL* since plaque progression is more common than plaque regression, resulting in a smaller lumen in a follow-up CAT which fits our idea of creating a coarse mesh entirely inside of the lumen. However, the subdivision fitting is also able to grow towards the inside of the lumen which means transforming *CAT-BL* to *CAT-FU* should not affect the final calculation of the plaque thickness.

Our experiments on artificially created *CAT-BL* and *CAT-FU* pairs showed that the calculated plaque thickness has an average deviation of 0.10 mm from the expected values. The deviation is caused by the approximation of the subdivision fitting process for modeling the coronary surfaces. Furthermore, it should be noted that potential motion artifacts could still exist in the CATs but these do not have a big influence on the final results. Accordingly, the

average of the calculated plaque thickness differences for *ED* and *ES* scans is zero with a SD of 0.18 mm which could be caused by the lumen and vessel wall contour delineation, the registration and also the surface subdivision fitting and potential motion artifacts.

For the visualization purpose, we used a fixed threshold as a cut-off value to focus on the large plaque thickness increase and decrease in Figure 5.6d. The threshold (0.5 mm) is obtained based on the calculated plaque thickness differences of all scans in GROUP1 which is related to the delineation of the lumen and vessel wall contours. From the calculation for artificial datasets (SD ± 0.10 mm) and *ED* and *ES* scans (SD ± 0.18 mm), the systematic bias was about 0.18 mm. Therefore, the threshold should be large enough to be able to visualize plaque changes. To determine the plaque progression or regression, a smaller value can be used depending on the presence of a systematic bias. Furthermore, the systematic bias of the whole process was about 0.18 mm which is half of the voxel size of the CCTA images.

To the best of our knowledge, the current tools in PACS calculate the plaque thickness on 2D slices the same as illustrated by the Figure 5.1 (the close-up image in green box) which could be performed in a few seconds. The comparison of the plaque thickness between the baseline and the follow-up is performed manually by selecting an artery, and then the corresponding slice, which is shown in Fig.1. However, this process could make the calculation non-reproducible and could take very long time to manually find the corresponding location and viewing angle in 2D slice. The proposed method calculates the plaque thickness at multiple locations in multiple slices for the entire coronary arteries automatically and the calculation is reproducible

Limitations. The proposed method relies on the delineated lumen and vessel wall contours which in this method were first created by the automatic software and afterwards corrected by experts.

CONCLUSION

The presented automatic plaque thickness comparison method can successfully locate, calculate and visualize the changes of coronary plaque thickness over time for a specific location in the coronary artery. This will benefit the automatic analysis and reporting of the coronary plaque progression and regression.

CHAPTER 6

Summary and Discussion

SUMMARY

The main purpose of this thesis is to facilitate the automatic lesion reporting and risk stratification in a large cohort of patients and allow automatic follow-up comparison of quantitative parameters in coronary segments or coronary arteries on coronary computed tomography angiography (CCTA) images.

In clinical practice, radiologists and cardiologists usually report pathological findings from CCTA images per artery or per segment. To facilitate the automatic lesion reporting and risk stratification, in **Chapter 2**, a labeling algorithm was presented to automatically identify the anatomical segments of the extracted coronary artery tree (CAT) centerlines from CCTA images. 3-dimension models for both right dominant (RD) and left dominant (LD) coronary circulations were designed which contain the average length, location and average bifurcation angle of each anatomical label. Based on the designed models, we proposed a labeling method to automatically identify and assign anatomical labels to CAT segments with an average precision of 91% in comparison with the manual annotations of two experts.

However, we needed to manually determine the dominance type of a CAT, and then select the corresponding average model to do the labeling (**Chapter 2**). Therefore, an automatic dominance type detection method for an extracted CAT was presented in **Chapter 3** which successfully identified the dominance type for 41 out of 42 automatically extracted CATs.

CATs are often extracted beforehand to aid the fully automatic analysis of coronary artery disease (CAD) on CCTA images. **Chapter 3 and Chapter 4** pay particular attention to the quality of the extracted CATs since the extraction quality will affect the successive steps.

For the coronary artery tree segments identification method, 100 CCTA scans, consisting of 68 RD and 32 LD cases, were included and two observers did the manual labeling as the ground truth for the evaluation. On these manually labeled CATs, we created statistical coronary models for both RD and LD CATs (**Chapter 3**) which are an improvement compared to the average coronary models presented in **Chapter 2**. Based on the statistical models, we designed a scoring system to assess the quality of the extracted CAT (**Chapter 3**). The presented score measures the extraction quality from the clinical significance of the arteries as defined in the American Heart Association (AHA) model and the completeness of the extracted CAT. On a 100-point scale, for 39 (92%) out of 42 datasets, the quality score system measured the quality of the manually refined CATs with higher scores than automatically extracted CATs with an average score as 82.0 (±15.8) and 88.9 (±5.4), respectively.

During the development of the scoring system, we noticed that the statistical models we created not only revealed the potential incorrect extractions on a CAT but also indicated the location of incorrect extractions. Therefore, guided by the statistical model and combined with the scoring system, we proposed a method to automatically detect the potential incorrect extractions and improve them in **Chapter 4**. A coarse improvement on all vessels in the

extracted CAT is performed to mainly remove incorrect extractions. After this, a fine improvement is applied only on the vessels-with-labels to extend short or missing branches due to a stenosis or low contrast, and removing over-extracted branches due to the similarity with surrounding tissues or veins. Focus was placed on the robustness of the method with various evaluations. For 122 automatically extracted CATs, without deteriorating the initial extractions, an average extraction quality score of 93 was achieved on a 100-point scale. The improvement could be done within 2 minutes on a typical workstation. Additionally, the difference in extraction quality after automatic improvement is negatively correlated with the initial extraction quality (R=-0.694, P<0.001) which means with a better initial extraction quality, there is limited space for the model-guided method to do an improvement.

For long-term coronary plaque development or risk investigation, plaque changes between a coronary artery tree at baseline (*CAT-BL*) and a coronary artery tree at follow-up (*CAT-FU*) are assessed on CCTA images. Traditionally, experts either visually select a similar viewing angle to do the comparison on 2D images, or compare the plaque volume changes of an entire artery. We proposed a method to automatically calculate local plaque thickness differences between *CAT-BL* and *CAT-FU* (**Chapter 5**). The coronary arteries are modeled as 3D surfaces using the subdivision fitting technique to enable the calculation of the local plaque thickness changes. By using the same coarse mesh for the subdivision fitting of coronary surfaces, we build the lumen and vessel wall surface point correspondence to calculate the plaque thickness; *CAT-BL* and *CAT-FU* surface point correspondence to calculate the differences in plaque thickness. Specifically, to solve the coordinate space differences between *CAT-BL* and *CAT-FU* coarse meshes, the transformation between them is obtained using a point-set registration method. Automatically matching *CAT-BL* and *CAT-FU* in 3D reduces the bias of a 2-dimenson manual alignment. A 3D visualization of the plaque changes in coronary arteries was also provided to give clinicians a straightforward view. The calculated plaque thickness difference is the same as the ground truth value with only a 0.1 mm deviation. The analysis and reporting of coronary plaque progression and regression will benefit from the presented automatic plaque thickness comparison method.

DISCUSSION

So far, approaches for quantitative analysis of coronary arteries on CCTA images have been studied and developed for different purposes. The extraction of the centerlines of the CAT, the quality assessment of the extractions, the improvements for the extractions, the detection and identification of the extracted coronary artery segments, the quantification of the coronary plaques and potential changes over time. Many factors prevent these approaches of being successful in all cases, such as the large variation in the population and the difference in scan quality.

Hereby, a focus is placed on a detailed discussion of the remaining challenges in developing approaches for automatic analysis of coronary arteries on CCTA images.

Ground Truth

Effective datasets with sufficient data and image quality are required for designing automatic approaches for the analysis of coronary arteries on CCTA images. The design and building of the average or statistical CAT models requires the collection of information, especially the ground truth data with experts' annotation.

Multiple well-trained observers are needed to analyze the image data, and also perform consensus reading. Sometimes, inter-observer differences still exist even after the consensus reading, as discussed in **Chapter 2**. Accordingly, acquiring ground truth data needs a lot of effort and takes a lot of time, especially for cohorts containing large datasets.

Another problem is that the ground truth data sometimes cannot be reused to evaluate extractions or analysis for different purposes. In **Chapter 3** and **4**, we used the MICCAI 2012 stenosis challenge data [75] for the evaluation of the automatic tree extraction improvement. However, our improvement is applied both on the vessels with high clinical significance and the completeness of the extractions while the manual refinements were only focused on the vessels with high clinical significance. Therefore, the automatically improved CAT (**Chapter 4**) often included more branches than the manually corrected CAT, and therefore showed a potential higher quality score (**Chapter 3**).

Chapter 5 showed the feasibility of automatically quantifying local coronary plaque thickness changes over time. For better visualization, a fixed threshold was used to filter out the systematic bias and focus on the large changes of the plaque thickness. Depending on the presence of a systematic bias, a threshold can also be used to determine the plaque progression or regression. However, the systematic bias includes the manual bias in delineating lumen and vessel wall contours for *CAT-BL* and *CAT-FU*, registration error and the surface modeling approximation. If ground truth information of the plaque progression or regression for each case exists, a more accurate quantification for the plaque progression and regression will be achieved.

Evaluation Measurements

One straightforward way of evaluating the automatic analysis methods is by comparison with the results from the experts. However, creating manual annotations for large cohorts is time-consuming, labor-intensive and most of the time cannot be reused (discussed in "**Ground Truth**" Section). Alternatively, statistical information or models can also be exploited to evaluate the automatic analysis methods. Collecting datasets, analyzing and organizing information from these datasets will build a reference for the targeted purpose. In **Chapter 3**, we performed a statistical analysis to generate the anatomical information for CATs which showed the normal variation and the possible outliers of a CAT in the whole population. The comparison of an automatically extracted CAT with this statistical model was described as a score to show the quality of the extraction.

Informative Features Exploitation

In order to extract the centerlines of the CATs, or calculate the plaque changes in the coronary arteries, image features of the targeted objects are analyzed and then used as a priori knowledge. Automatic CAT extraction methods based on minimum path techniques have been widely used due to their simplicity and computational efficiency [26, 28, 30]. The minimum path searching method is often performed on a vesselness image which is typically created by applying a modified Frangi's vesselness filter to CCTA images [35, 37]. However, these filters and models are based on the assumptions about the observed appearance and may not fully grasp all the information available in data. To reduce manual corrections from experts, approaches to automatically detect and correct undesirable shorter or longer extractions were presented [43, 49, 50].

However, these methods require prior information from training datasets, such as that in **Chapter 4**, where a statistical model is combined with a scoring system to provide a guide to detect the potential incorrect extractions and improve them automatically. Still, for *vessels-without-a-label*, only corrections on the pathline length and vessel directions could be made. Accordingly, additional features, such as anatomical locations for *vessels-without-a-label*, should be exploited.

Error Propagation

The propagation of the errors among different quantitative analyses within one workflow is an important issue to be considered.

On extracted CATs, coronary artery segments identification (**Chapter 2**) was performed which will helps the automated lesion reporting and risk stratification. However, the quality of the tree labeling is highly dependent on the automatic extraction results. In other words, the wrong extractions will lead to worse labeling results.

A quality score (**Chapter 3)** and a model-guided method (**Chapter 4**) were designed to assess the quality and improve the automatically extracted CATs. In order to automatically apply the scoring method and the model-guided method for tree improvement, we use the automatic labeling method (**Chapter 2**) to identify the extracted coronary artery segments. Therefore, the quality score also relied on the automatic identification method. An assignment of a high weight label on an incorrectly extracted artery will end up with a high score for the extracted CAT while it should be a lower quality tree. These will be eliminated if the automatic identification method is improved. The plaque thickness comparison method relies on the delineated lumen and vessel wall contours which in this method were first created by the automatic software and afterwards corrected by experts. Therefore, to develop methods with less inter-steps will solve the error propagation problem.

In summary, this thesis describes several novel approaches to achieve automatic analysis for coronary arteries on CCTA images. Therefore, the main goal of this thesis as set out in the introduction, has been reached.

FUTURE PERSPECTIVES

CCTA in Intervention Planning

When a patient has a high plaque burden, or a coronary event happens, an intervention is needed in the catheterization room. To decrease the procedure time and thus reduce the dose exposure and patient discomfort, a good intervention planning is needed. Thanks to new imaging techniques and dose reduction strategies, suspected CAD is more and more diagnosed using CCTA. Using CCTA in the planning stage for percutaneous coronary intervention (PCI) could help the fast localization of the lesion, and automatically find the optimal viewing angle. Therefore, methods to enable the usage of CCTA in intervention planning is an interesting future research topic, for instance the real-time registration of coronary arteries from CCTA images to X-ray angiography images. Additionally, the introduction of multispectral computed tomography (CT) might help to improve the plaque detection and classification.

Multi-time Point Study

Most of the previous studies in CCTA image processing were restricted to the image from one time point or the images within different cardiac cycles. The new developments in dose reduction of CCTA also allow a patient to be scanned multiple times over time which enables the longitudinal studies of CAD using CCTA. The analysis of the patients' data over different time points could help predict the development of the CAD. Moreover, with the collection of more follow-up cohort data could enable long-term population studies into the natural course of coronary artery disease, and potentially leading to a coronary event prediction.

Multi-modality Integration

A main difference of the automatic quantitative analyses described in this thesis from clinical decision making is the fact that the automatic quantitative analysis focuses on one factor. Clinicians often can combine multiple information resources in their diagnostic workflow from patient records to various imaging data to do analysis and diagnosis. Therefore, in the future, automatic quantitative analysis will benefit from the combination of different information resources, such as the magnetic resonance imaging (MRI), CT image and patient records. Furthermore, similar to the multidisciplinary team meeting for diagnosis/treatment, the combination of pathological findings from different disciplines will help to further automate the diagnosis.

End-to-End Approaches

The current workflow to do the automatic analysis of coronary arteries on CCTA images starting from the extraction of CATs followed by lumen/vessel wall detection, and then plaque detection, characterization, quantification and reporting. The error from the previous step propagates to the following steps. To solve the error propagation issue, novel "End-to-End" approaches should be developed to perform the plaque quantification, plaque reporting or even the risk stratification directly. The rapid developments in large memory graphics processing unit (GPU) and computing capacity bring the spring for deep learning techniques and therefore a wide application in medical image processing. Neural networks that can take inputs from medical images and output the quantitative analysis or even the reporting of pathological findings will be of high interest.

Combination of Traditional Image Processing and Deep Learning

Despite that deep learning techniques enable the development of end-to-end approaches, combining with the traditional medical image processing methods could be a possible direction to improve the automatic analysis of coronary arteries on CCTA images. For example, the coronary artery centerlines from the traditional image processing methods could be used as part of the input for the coronary artery lumen/vessel wall extraction to build a semi-supervised or weakly supervised neural network. Semi-supervised, weakly supervised or self-supervised learning will reduce the large burden of ground truth data in medical image processing using deep learning techniques. Furthermore, the evaluation in deep neural networks is quite limited which is normally using similarity metrics, such as a dice coefficient. In the meantime, studies of evaluation measurements in traditional image processing is quite comprehensive. Applying the evaluation measurements from traditional image processing methods could be a way to improve the training efficiency of a neural network, and thus improve the automatic analysis of the coronary arteries in CCTA images.

HOOFDSTUCK 6

Samenvatting en Discussie

SAMENVATTING

Het belangrijkste doel van dit proefschrift is om de automatische laesierapportage en risicostratificatie in een groot cohort van patiënten te faciliteren en om een automatisch vergelijk mogelijk te maken tussen kwantitatieve parameters uit segmenten van de kransslagaderen en die uit vervolgcontroles op coronaire computertomografie-angiografie (CCTA) beelden.

In de klinische praktijk rapporteren radiologen en cardiologen meetstal pathologische bevindingen uit CCTA-beelden per slagader of per segment. Om de automatische laesierapportage en risico stratificatie te faciliteren, werd er in **Hoofdstuk 2** een label-algoritme gepresenteerd dat automatisch de anatomische segmenten van geëxtraheerde middellijnen van kransslagaderbomen (coronary artery trees, of CAT) uit CCTA-beelden identificeert. Driedimensionale (3D) modellen voor zowel rechtsdominant (RD) als linksdominant (LD) coronaire circulaties werden ontworpen die de gemiddelde lengte, de locatie en de gemiddelde bifurcatiehoek van elk anatomisch label bevatten. Op basis van de ontworpen modellen hebben we een labelmethode voorgesteld om anatomische labels automatisch te identificeren en toe te wijzen aan CAT-segmenten met een gemiddelde precisie van 91% in vergelijking met de handmatige annotaties van twee experts.

Desalniettemin, moesten we het dominantietype van een CAT handmatig bepalen en vervolgens het overeenkomstige model met gemiddelden selecteren om labels toe te kennen (**Hoofdstuk 2**). Hiervoor is in **Hoofdstuk 3** een automatische methode om het dominantie type te detecteren gepresenteerd dat 41 van de 42 automatische geëxtraheerde CAT's succesvol wist te identificeren.

CAT's worden vaak vooraf geëxtraheerd ten behoeve van de volledig automatische analyse van coronaire hartziekte (coronary artery disease, of CAD) op CCTA-beelden. In **Hoofdstuk 3 en Hoofdstuk 4** wordt bijzondere aandacht besteed aan de kwaliteit van de geëxtraheerde CAT's omdat de extractiekwaliteit de opeenvolgende stappen zal beïnvloeden.

Voor de identificatiemethode van de kransslagaderboom-segmenten werden 100 CCTA-scans opgenomen, bestaande uit 68 RD- en 32 LD-gevallen. Twee waarnemers hebben handmatig de labels toegekend als gouden standaard voor de evaluatie. Op deze handmatig gelabelde CAT's hebben we statistische coronaire modellen gemaakt voor zowel RD- als LD CAT's (**Hoofdstuk 3**). Deze waren een verbetering ten opzichte van de coronaire modellen met gemiddelden die in **Hoofdstuk 2** zijn gepresenteerd. Op basis van de statistische modellen hebben we een scoresysteem ontworpen om de kwaliteit van de geëxtraheerde CAT te beoordelen (**Hoofdstuk 3**). De gepresenteerde score meet de extractiekwaliteit met betrekking tot de klinische betekenis van de slagaders zoals gedefinieerd in het model van de American Heart Association en de volledigheid van de geëxtraheerde CAT. Voor 39 (92%) van de 42 datasets, mat het kwaliteitsscore-systeem de kwaliteit van de handmatig aangepaste

CAT's met hogere scores dan automatisch geëxtraheerde CAT's met een gemiddelde score als 82,0 (± 15,8) en 88,9 (± 5,4), respectievelijk op een 100-puntenschaal.

Tijdens de ontwikkeling van het scoresysteem hebben we gemerkt dat de statistische modellen die we hebben gemaakt, niet alleen de mogelijke onjuiste extracties op een CAT zichtbaar maakten, maar ook de locatie aangaf van onjuiste extracties. Daarom hebben we in **Hoofdstuk 4** een methode voorgesteld om de potentieel onjuiste extracties automatisch te detecteren en te verbeteren geleid door het statistische model en in combinatie met het scoresysteem. Eerst wordt er een grove verbetering op alle vaten in de geëxtraheerde CAT uitgevoerd om voornamelijk onjuiste extracties te verwijderen. Hierna wordt een fijne verbetering toegepast om alleen de vaten met labels te verlengen die korte of ontbrekende takken hebben vanwege een stenose of verminderd contrast. Ook wordt het teveel aan geëxtraheerde takken verwijderd die een gelijkenis hebben met het omliggende weefsel of aders. De nadruk werd gelegd op de robuustheid van de methode en is op verschillende manieren geëvalueerd. Voor 122 automatisch geëxtraheerde CAT's werd een gemiddelde extractiekwaliteitsscore van 93 behaald op een 100-puntensschaal zonder de initiële extracties te verslechteren. De verbetering kon binnen 2 minuten op een typisch werkstation worden uitgevoerd. Bovendien is het verschil in extractiekwaliteit na automatische verbetering negatief gecorreleerd met de initiële extractiekwaliteit ($R=-0.694$, $P<0.001$), wat betekent dat met een betere initiële extractiekwaliteit er beperkte ruimte is voor een verbetering door de model-gestuurde methode.

Voor de ontwikkeling van coronaire plaque op lange termijn of risico-onderzoek worden plaque-veranderingen tussen kransslagaderbomen op CCTA-beelden op een eerste tijdspunt (CAT-baseline, of CAT-BL) en kransslagaderbomen op een volgend tijdspunt (CAT-follow-up, of CAT-FU) beoordeeld. Van oudsher selecteren experts visueel een vergelijkbare kijkhoek om de vergelijking tussen de 2D-afbeeldingen te kunnen maken, of ze vergelijken de veranderingen in het plaquevolume over de gehele slagader. We stelden een methode voor om automatisch lokale plaquedikte verschillen tussen CAT-BL en CAT-FU te berekenen (**Hoofdstuk 5**). De kransslagaders worden gemodelleerd als gladde 3D oppervlakken met behulp van een onderverdelingstechniek om de lokale plaquedikte veranderingen te kunnen berekenen. Door dezelfde grove oppervlakverdeling te gebruiken voor het benaderen van de oppervlakteonderverdeling van coronair vaten, kunnen we de puntcorrespondentie tussen het lumen en de vaatwand gebruiken om de plaquedikte te berekenen. De puntcorrespondentie tussen CAT-BL en CAT-FU wordt gebruikt om de verschillen in plaquedikte te berekenen. Om de coördinaatruimteverschillen tussen de grove oppervlakten van de CAT-BL en CAT-FU in het bijzonder op te lossen, wordt de transformatie daartussen verkregen met behulp van een punten-set registratiemethode. Het automatisch laten overeenkomen van CAT-BL en CAT-FU in 3D vermindert de fout van een tweedimensionale (2D) handmatige uitlijning. Er werd ook een 3D-visualisatie gemaakt van de plaque-veranderingen in de kransslagaders om clinici een eenvoudig beeld te geven. Het berekende verschil in plaquedikte is hetzelfde als de gouden standaard met slechts een afwijking van 0.1 mm. De analyse en rapportage van de

progressie en regressie van coronaire plaque zal profiteren van de beschreven automatische vergelijkingsmethode voor plaquedikte.

DISCUSSIE

Tot nu toe zijn benaderingen voor kwantitatieve analyse van kransslagaders op CCTA-afbeeldingen onderzocht en ontwikkeld voor verschillende doeleinden. De extractie van de middellijn van de CAT, de kwaliteitsbeoordeling van de extracties, de verbeteringen in de extracties, de detectie en identificatie van de geëxtraheerde kransslagadersegmenten, de kwantificering van coronaire plaques en mogelijke veranderingen in de tijd. Veel factoren verhinderen dat deze benaderingen in alle gevallen succesvol zijn, zoals de grote variatie in de populatie en verschillen in scankwaliteit.

Hierbij wordt de nadruk gelegd op een gedetailleerde bespreking van de resterende uitdagingen bij het ontwikkelen van benaderingen voor automatische analyse van kransslagaders op CCTA-beelden.

Gouden standaard

Voor het ontwerpen van automatische benaderingen voor de analyse van kransslagaders op CCTA-beelden zijn effectieve datasets met voldoende data en beeldkwaliteit vereist. Het is nodig om informatie te verzamelen om gemiddelde of statistische CAT-modellen te kunnen ontwerpen en bouwen, met name de annotaties van experts die als gouden standaard dienen.

Meerdere goed opgeleide waarnemers zijn nodig om de beelden te analyseren en consensuslezingen uit te voeren. Soms blijven er verschillen bestaan tussen waarnemers, zelfs na de consensuslezing, zoals besproken in **Hoofdstuk 2**. Dienovereenkomstig vergt het verkrijgen van een gouden standaard veel inspanning en kost het veel tijd, vooral voor cohorten die een grote hoeveelheid data bevatten.

Een ander probleem is dat de gegevens van de gouden standaard soms niet kunnen worden hergebruikt om extracties of analyses met een ander doeleinde te evalueren. In **Hoofdstuk 3** en **4** hebben we de data van de MICCAI 2012 uitdaging voor stenose bepaling [1] gebruikt om de verbeteringen in de automatische boomextractie te evalueren. Onze verbetering wordt echter toegepast op zowel de vaten die klinisch belangrijk zijn als op de volledigheid van de extracties, terwijl de handmatige aanpassingen alleen gericht waren op de vaten die klinisch belangrijk zijn. Hierdoor bevatte de automatisch verbeterde CAT's (**Hoofdstuk 4**) vaak meer vertakkingen dan de handmatig gecorrigeerde CAT's en hadden daarom in theorie hogere kwaliteitsscore (**Hoofdstuk 3**).

Hoofdstuk 5 toonde de haalbaarheid aan van het automatisch kwantificeren van lokale veranderingen in de dikte van coronaire plaque in de tijd. Voor een betere visualisatie werd er een vaste drempelwaarde gebruikt om een systematische afwijking eruit te filteren en zo te focussen op de grote veranderingen in de plaquedikte. Afhankelijk van de aanwezigheid

van een systematische afwijking, kan een drempelwaarde ook worden gebruikt om plaque progressie of regressie te bepalen. De systematische afwijking omvat echter de handmatige aanpassingen bij het tekenen van de lumen- en vaatwandcontouren voor CAT-BL en CAT-FU, de registratiefout, de benadering van oppervlaktemodellering en is lastig te kwantificeren. Als er een gouden standaard bestaat voor plaqueprogressie of -regressie, zal het mogelijk zijn de plaqueprogressie en -regressie nauwkeuriger te kwantificeren.

Evaluatiemetingen

Een eenvoudige manier om de automatische analysemethoden te evalueren is door deze te vergelijken met de resultaten van de experts. Het maken van handmatige annotaties voor grote cohorten is echter tijdrovend, arbeidsintensief en kan meestal niet worden hergebruikt (besproken in de paragraaf "**Gouden standaard**"). Als alternatief kan sommige statistische informatie of modellen ook worden gebruikt om de automatische analysemethoden te evalueren. Door het verzamelen van datasets, het analyseren en organiseren van informatie uit deze datasets kan er een referentie standaard gevormd worden voor het beoogde doel. In **Hoofdstuk 3** hebben we statistische analyses uitgevoerd om anatomische informatie voor kransslagaderbomen te genereren die de normale variatie en de mogelijke uitschieters van een CAT onder de gehele populatie liet zien. Door een automatisch geëxtraheerde CAT met deze statistische model te vergelijken kan de kwaliteit van de extractie uitgedrukt worden in een score.

Gebruik maken van informatieve kenmerken

Om de middellijnen van de CAT's te extraheren, of plaqueveranderingen in de kransslagaders te berekenen, worden beeldkarakteristieken van de beoogde objecten geanalyseerd en vervolgens gebruikt als a priori kennis. Automatische CAT-extractiemethoden op basis van minimale pad-technieken zijn op grote schaal gebruikt vanwege hun eenvoud en efficiënte manier van berekenen [2-4]. De zoekmethode voor minimale paden wordt vaak uitgevoerd op een beeld van vaatstructuren dat meestal wordt gemaakt door het toepassen van een aangepast vaatstructuurfilter van Frangi op CCTA-beelden [5, 6]. Deze filters en modellen zijn echter gebaseerd op veronderstellingen over hoe het uiterlijk van een vat en bevat mogelijk niet alle informatie die in de data beschikbaar is. Om het aantal handmatige correcties van experts te verminderen, werden benaderingen gepresenteerd voor het automatisch detecteren en corrigeren van ongewenste kortere of langere vaatextracties [7-9].

Deze methoden vereisen echter voorafgaande informatie, meestal statistische informatie op basis van verzamelde data, zoals die in **Hoofdstuk 4**. Het statistische model wordt gecombineerd met het scoresysteem om een leidraad te geven voor het detecteren van mogelijke onjuiste extracties en deze automatisch te verbeteren. Toch kunnen er alleen maar correcties worden gedaan op de lengte van een pad-lijn en de richting van het vat voor de *vaten die geen label* hebben. Overeenkomstig moeten extra functies, zoals de anatomische locaties van de *vaten zonder label*, worden benut.

Foutpropagatie

Het doorwerken van de fouten tussen verschillende kwantitatieve analyses binnen één werkstroom is een belangrijk aandachtspunt.

De kransslagadersegmentidentificatie (**Hoofdstuk 2**) werd op geëxtraheerde CAT's uitgevoerd om de geautomatiseerde laesierapportage en risicostratificatie te ondersteunen. De kwaliteit van de segmentidentificatie is echter sterk afhankelijk van de resultaten van de automatische extractie. Met andere woorden, verkeerde extracties zullen leiden tot slechtere labelresultaten.

Een kwaliteitsscore (**Hoofdstuk 3**) en een model-gestuurde methode (**Hoofdstuk 4**) zijn ontworpen om de kwaliteit te beoordelen en de automatisch geëxtraheerde CAT's te verbeteren. Om de kwaliteitsscoremethode en de model-gestuurde methode voor boomverbeteringen automatisch toe te passen, moeten we de automatische labelmethode (**Hoofdstuk 2**) gebruiken om de geëxtraheerde kransslagadersegmenten te identificeren. Het boom-verbetersysteem en de kwaliteitsscore zijn gebaseerd op de automatische identificatiemethode. Het toewijzen van een label met een hoog gewicht aan een onjuist geëxtraheerde slagader zal resulteren in een hoge score voor de geëxtraheerde CAT, terwijl dit een boom met een lagere score zou moeten zijn. Deze worden verwijderd als de automatische identificatiemethode is verbeterd. De methode om de plaquedikten te vergelijken is gebaseerd op de afgebakende lumen- en vaatwandcontouren die voor deze methode eerst werden gecreëerd door de automatische software en nadien gecorrigeerd door experts. Als er methoden ontwikkeld zouden worden met minder tussenstappen zal daarom het probleem van het doorwerken van fouten opgelost worden.

Concluderend, deze thesis beschrijft verschillende nieuwe benaderingen om automatische analyse voor coronaire slagaders op CCTA beelden te bereiken. Het hoofddoel van dit proefschrift is daarom bereikt.

TOEKOMSTPERSPECTIEVEN

CCTA in interventieplanning

Wanneer een patiënt een aanzienlijke hoeveelheid plaque heeft, of er een coronaire complicatie plaatsvindt, is een interventie in de katheterisatiekamer nodig. Om de proceduretijd te verkorten en dus het ongemak van de blootstelling aan straling voor de patiënten te verminderen, is een goede interventieplanning nodig. Dankzij nieuwe beeldvormingstechnieken en dosisreductiestrategieën kan CAD steeds meer worden gediagnosticeerd door middel van CCTA. Het gebruik van CCTA in de planningsfase voor een percutane coronaire interventie kan helpen de laesie snel te lokaliseren en automatisch de optimale kijkhoek te vinden. Daarom kunnen methoden om het gebruik van CCTA in interventieplanning mogelijk te maken een toekomstig onderzoeksdoel zijn, zoals het onvertraagd registreren van de kransslagaders van CCTA-afbeeldingen op

röntgenangiografiebeelden. Bovendien kan de introductie van multi-spectrale computertomografie helpen de plaquedetectie en classificatie te verbeteren.

Multitijdpunt studie

De meeste van eerdere onderzoeken naar CCTA-beeldverwerking waren beperkt tot het beeld op één tijdstip of de beelden van verschillende hartcycli. Dankzij de nieuwe ontwikkelingen van CCTA kan een patiënt in de loop van de tijd meerdere keren worden gescand, waardoor lange termijn-studies voor CAD met behulp van CCTA mogelijk zijn. De analyse van de scans van de patiënten op verschillende tijdstippen kan de ontwikkeling van de CAD helpen voorspellen. Bovendien zou met het samenbrengen van datasets uit vervolgcontroles in een cohort een lange termijn-studie mogelijk maken en dus de voorspelling van coronaire gebeurtenissen kunnen faciliteren.

Multimodaliteit Integratie

Een belangrijk verschil met de huidige automatische kwantitatieve analyse van de clinici is dat een automatische kwantitatieve analyse zich op één doel richt. Artsen kunnen vaak informatiebronnen in diagnostische workflow informatie van patiëntendossiers tot verschillende doelen combineren om analyses en diagnoses te maken. Daarom zal in de toekomst een automatische kwantitatieve analyse profiteren van de combinatie van verschillende beeldvormingsmodaliteiten, zoals de magnetische-resonantiescan in combinatie met CCTA-beelden en patiëntendossiers. Bovendien zal de combinatie van pathologische bevindingen uit verschillende disciplines, net als een multidisciplinaire teambijeenkomst voor diagnose/behandeling, helpen bij de volledig automatische diagnose.

Eind-naar-eind benaderingen

De huidige manier van werken voor het automatisch analyseren van kransslagaders op CCTA-afbeeldingen start vanaf de extractie van CAT's gevolgd door lumen/vaatwanddetectie en vervolgens komt de plaquedetectie, karakterisering, kwantificering en rapportage. De fout uit de vorige stap wordt meegenomen in de volgende stappen. Om het probleem van de foutpropagatie op te lossen, is het tijd om een "eind-naar-eind" -benadering te gebruiken om de plaquekwantificering, plaquerapportage of zelfs de risicostratificatie rechtstreeks uit te voeren. De revolutie en ontwikkeling van het grote geheugen op de grafische kaart en rekencapaciteit vormen een springplank voor diepgaande leertechnieken en hebben dus een brede toepassing in de medische beeldverwerking. Neurale netwerken die als input medische beelden kunnen benutten en de kwantitatieve analyses of zelfs de rapportages van de pathologische bevindingen kunnen opleveren, zullen de groot belang zijn.

Combinatie van traditionele beeldverwerking en diepgaande leertechnieken

Ondanks dat diepgaande leertechnieken de ontwikkeling van eind-naar-eind benaderingen mogelijk maken, zou combinatie met de traditionele medische beeldverwerkingsmethoden een mogelijke richting kunnen zijn om de automatische analyse van kransslagaders op CCTA-afbeeldingen te verbeteren. De middenlijnen van de kransslagaders gemaakt door traditionele beeldverwerkingsmethoden kunnen bijvoorbeeld worden gebruikt als onderdeel van de input voor de extractie van het kransslagaderlumen/vaatwand om een semi-gecontroleerd of zwak gecontroleerd neuraal netwerk te bouwen. Semi-gecontroleerde of zwak gecontroleerde diepgaande leertechnieken zullen de grote last van een gouden standaard in de medische beeldverwerking verminderen. Bovendien is de evaluatie van diepgaande neurale netwerken vrij beperkt. Normaal gesproken maken zij gebruik van gelijkenisstatistieken, zoals het Dice-coëfficiënt. Ondertussen is het onderzoek naar evaluatiemetingen bij traditionele beeldverwerkingsmethoden vrij uitgebreid. Het toepassen van de evaluatiemetingen van traditionele beeldverwerkingsmethoden zou een manier kunnen zijn om de trainingsefficiëntie van een neuraal netwerk te verbeteren en zo de automatische analyse van de kransslagaders in CCTA-afbeeldingen te verbeteren.

BIBLIOGRAPHY

[1] F. Sanchis-Gomar, C. Perez-Quilis, R. Leischik et al., "Epidemiology of coronary heart disease and acute coronary syndrome," *Ann Transl Med,* vol. 4, no. 13, pp. 256, Jul, 2016.

[2] R. C. Schlant, R. W. Alexander, R. A. O'Rourke et al., *Hurst's the heart,* 8 ed., p.^pp. 63-93, New York: McGraw-Hill Education, 1994.

[3] F. Cademartiri, L. La Grutta, R. Malago et al., "Prevalence of anatomical variants and coronary anomalies in 543 consecutive patients studied with 64-slice CT coronary angiography," *Eur Radiol,* vol. 18, no. 4, pp. 781-791, Apr, 2008.

[4] C. E. Handy, C. S. Desai, Z. A. Dardari et al., "The Association of Coronary Artery Calcium With Noncardiovascular Disease: The Multi-Ethnic Study of Atherosclerosis," *JACC Cardiovasc Imaging,* vol. 9, no. 5, pp. 568-576, May, 2016.

[5] B. c. staff, "Medical gallery of Blausen Medical 2014," *WikiJournal of Medicine* vol. 1, no. 2, 2014.

[6] Y. Xie, H. Jin, M. Zeng et al., "Coronary Artery Plaque Imaging," *Curr Atheroscler Rep,* vol. 19, no. 9, pp. 37, Sep, 2017.

[7] A. Mangla, E. Oliveros, K. A. W. Sr. et al., "Cardiac imaging in the diagnosis of coronary artery disease," *Current Problems in Cardiology*, 2017.

[8] D. American College of Cardiology Foundation Task Force on Expert Consensus, D. B. Mark, D. S. Berman et al., "ACCF/ACR/AHA/NASCI/SAIP/SCAI/SCCT 2010 expert consensus document on coronary computed tomographic angiography: a report of the American College of Cardiology Foundation Task Force on Expert Consensus Documents," *J Am Coll Cardiol,* vol. 55, no. 23, pp. 2663-99, Jun 8, 2010.

[9] S. Cimen, A. Gooya, M. Grass et al., "Reconstruction of coronary arteries from X-ray angiography: A review," *Med Image Anal,* vol. 32, pp. 46-68, Aug, 2016.

[10] C. Fischer, E. Hulten, P. Belur et al., "Coronary CT angiography versus intravascular ultrasound for estimation of coronary stenosis and atherosclerotic plaque burden: a meta-analysis," *J Cardiovasc Comput Tomogr,* vol. 7, no. 4, pp. 256-66, Jul-Aug, 2013.

[11] G. J. Tearney, E. Regar, T. Akasaka et al., "Consensus standards for acquisition, measurement, and reporting of intravascular optical coherence tomography studies: a report from the International Working Group for Intravascular Optical Coherence Tomography Standardization and Validation," *J Am Coll Cardiol,* vol. 59, no. 12, pp. 1058-72, Mar 20, 2012.

[12] M. Horvath, P. Hajek, C. Stechovsky et al., "The role of near-infrared spectroscopy in the detection of vulnerable atherosclerotic plaques," *Arch Med Sci,* vol. 12, no. 6, pp. 1308-1316, Dec 1, 2016.

[13] M. E. Clouse, "Coronary plaque quantification: is there a "gold standard?"," *J Cardiovasc Comput Tomogr,* vol. 3, no. 1, pp. 32-4, Jan-Feb, 2009.

[14] M.-J. Bertrand, P. Lavoie-L'Allier, and J.-C. Tardif, "Near-Infrared Spectroscopy (NIRS): A Novel Tool for Intravascular Coronary Imaging," *Developments in Near-Infrared Spectroscopy*, K. Kyprianidis and J. Skvaril, eds., 2017.

[15] D. B. Mark, D. S. Berman, M. J. Budoff et al., "ACCF/ACR/AHA/NASCI/SAIP/SCAI/SCCT 2010 expert consensus document on coronary computed tomographic angiography: a report of the American College of Cardiology Foundation Task Force on Expert Consensus Documents," *J Am Coll Cardiol,* vol. 55, no. 23, pp. 2663-2699, 2010.

[16] M. C. Williams, A. Moss, E. Nicol et al., "Cardiac CT Improves Outcomes in Stable Coronary Heart Disease: Results of Recent Clinical Trials," *Curr Cardiovasc Imaging Rep,* vol. 10, no. 14, 2017.

[17] H. Sakuma, "Coronary CT versus MR angiography: the role of MR angiography," *Radiology,* vol. 258, no. 2, pp. 340-9, Feb, 2011.

[18] P. Knaapen, S. de Haan, O. S. Hoekstra et al., "Cardiac PET-CT: advanced hybrid imaging for the detection of coronary artery disease," *Neth Heart J,* vol. 18, no. 2, pp. 90-8, Feb, 2010.

[19] M. Poon, M. Cortegiano, A. J. Abramowicz et al., "Associations between routine coronary computed tomographic angiography and reduced unnecessary hospital admissions, length of stay, recidivism rates, and invasive coronary angiography in the emergency department triage of chest pain," *J Am Coll Cardiol,* vol. 62, no. 6, pp. 543-52, Aug 6, 2013.

[20] A. Sabarudin, and Z. Sun, "Coronary CT angiography: Dose reduction strategies," *World J Cardiol,* vol. 5, no. 12, pp. 465-72, Dec 26, 2013.

[21] C. E. Richards, S. Dorman, P. John et al., "Low-radiation and high image quality coronary computed tomography angiography in "real-world" unselected patients," *World J Radiol,* vol. 10, no. 10, pp. 135-142, Oct 28, 2018.

[22] G. L. Raff, A. Abidov, S. Achenbach et al., "SCCT guidelines for the interpretation and reporting of coronary computed tomographic angiography," *J Cardiovasc Comput Tomogr,* vol. 3, no. 2, pp. 122-36, Mar-Apr, 2009.

[23] J. Leipsic, S. Abbara, S. Achenbach et al., "SCCT guidelines for the interpretation and reporting of coronary CT angiography: A report of the Society of Cardiovascular Computed Tomography Guidelines Committee," *J Cardiovasc Comput Tomogr,* vol. 8, no. 5, pp. 342-358, Jul-Aug, 2014.

[24] J. X. Xie, R. C. Cury, J. Leipsi et al., "The Coronary Artery Disease–Reporting and Data System (CAD-RADS) Prognostic and Clinical Implications Associated With Standardized Coronary Computed Tomography Angiography Reporting," *JACC Cardiovasc Imaging,* vol. 11, no. 1, 2018.

[25] M. Schaap, C. T. Metz, T. van Walsum et al., "Standardized evaluation methodology and reference database for evaluating coronary artery centerline extraction algorithms," *Med Image Anal,* vol. 13, no. 5, pp. 701-714, Oct, 2009.

[26] Y. Chen, Y. Zhang, J. Yang et al., "Curve-like Structure Extraction Using Minimal Path Propagation with Back-tracing," *IEEE Trans Image Process,* vol. 25, no. 2, pp. 988-1003, 2016.

[27] Y. Chen, Q. Cao, G. Yang et al., "Centerline Constrained Minimal Path Propagation For Vessel Extraction." pp. 794-797, 2014.

[28] Y. Zheng, M. Loziczonek, B. Georgescu et al., "Machine learning based vesselness measurement for coronary artery segmentation in cardiac CT volumes." p. 79621K, 2011.

[29] Q. Cao, Y. Chen, G. Yang et al., "Coronary Vessel Extraction Method Using An Improved Minimum Path Based Region Growing," *International Conference on Biomedical Engineering and Informatics.* pp. 127-131, 2014.

[30] T. Boskamp, D. Rinck, F. Link et al., "New vessel analysis tool for morphometric quantification and visualization of vessels in CT and MR imaging data sets.," *Radiographics,* vol. 24, no. 1, pp. 287-297, 2004.

[31] M. A. Palomera-Pérez, M. E. Martinez-Perez, H. Benítez-Pérez et al., "Parallel multiscale feature extraction and region growing: application in retinal blood vessel detection," *IEEE transactions on information technology in biomedicine,* vol. 14, no. 2, pp. 500-506, 2010.

[32] J. M. Wolterink, R. W. V. Hamersvelt, M. A. Viergever et al., "Coronary artery centerline extraction in cardiac CT angiography using a CNN-based orientation classifier," *Med Image Anal,* vol. 51, pp. 46-60, Oct 22, 2018.

[33] F. Benmansour, and L. D. Cohen, "Tubular Structure Segmentation Based on Minimal Path Method and Anisotropic Enhancement," *International Journal of Computer Vision,* vol. 92, no. 2, pp. 192-210, Apr, 2011.

[34] D. Lesage, E. D. Angelini, I. Bloch et al., "A review of 3D vessel lumen segmentation techniques: models, features and extraction schemes," *Med Image Anal,* vol. 13, no. 6, pp. 819-45, Dec, 2009.

[35] A. F. Frangi, W. J. Niessen, K. L. Vincken et al., "Multiscale vessel enhancement filtering." pp. 130-137, 1998.

[36] C. T. Metz, M. Schaap, A. C. Weustink et al., "Coronary centerline extraction from CT coronary angiography images using a minimum cost path approach," *Medical Physics,* vol. 36, no. 12, pp. 5568-5579, Dec, 2009.

[37] G. Yang, P. Kitslaar, M. Frenay et al., "Automatic centerline extraction of coronary arteries in coronary computed tomographic angiography," *Int J Cardiovasc Imaging,* vol. 28, no. 4, pp. 921-933, Apr, 2012.

[38] H. A. Marquering, J. Dijkstra, P. J. H. de Koning et al., "Towards quantitative analysis of coronary CTA," *The International Journal of Cardiovascular Imaging,* vol. 21, no. 1, pp. 73-84, 2005.

[39] M. J. Boogers, A. Broersen, J. E. van Velzen et al., "Automated quantification of coronary plaque with computed tomography: comparison with intravascular ultrasound using a dedicated registration algorithm for fusion-based quantification," *Eur Heart J,* vol. 33, no. 8, pp. 1007-16, Apr, 2012.

[40] J. Karha, S. A. Murphy, A. J. Kirtane et al., "Evaluation of the association of proximal coronary culprit artery lesion location with clinical outcomes in acute myocardial infarction," *Am J Cardiol,* vol. 92, no. 8, pp. 913-8, Oct 15, 2003.

[41] K. J. Harjai, R. H. Mehta, G. W. Stone et al., “Does proximal location of culprit lesion confer worse prognosis in patients undergoing primary percutaneous coronary intervention for ST elevation myocardial infarction,” *J Interv Cardiol,* vol. 19, no. 4, pp. 285-94, 2006.

[42] G. Sianos, M. A. Morel, A. P. Kappetein et al., “The SYNTAX Score: an angiographic tool grading the complexity of coronary artery disease,” *EuroIntervention,* vol. 1, no. 2, pp. 219-227, Aug, 2005.

[43] Q. Cao, A. Broersen, P. H. Kitslaar et al., “A model-guided method for improving coronary artery tree extractions from CCTA images,” *Int J Comput Assist Radiol Surg,* vol. 14, no. 2, pp. 373-383, Feb, 2019.

[44] Q. Cao, A. Broersen, P. H. Kitslaar et al., "A quality score for coronary artery tree extraction results." p. 105750V, 2018.

[45] A. Arbab-Zadeh, and J. Hoe, “Quantification of coronary arterial stenoses by multidetector CT angiography in comparison with conventional angiography methods, caveats, and implications,” *JACC Cardiovasc Imaging,* vol. 4, no. 2, pp. 191-202, Feb, 2011.

[46] S. E. Lee, J. M. Sung, A. Rizvi et al., “Quantification of Coronary Atherosclerosis in the Assessment of Coronary Artery Disease,” *Circ Cardiovasc Imaging,* vol. 11, no. 7, pp. e007562, Jul, 2018.

[47] G. Ndrepepa, R. Iijima, S. Kufner et al., “Association of progression or regression of coronary artery atherosclerosis with long-term prognosis,” *American heart Journal,* 2016.

[48] V. Sandfort, D. A. Bluemke, J. Vargas et al., “Coronary Plaque Progression and Regression in Asymptomatic African American Chronic Cocaine Users with Obstructive Coronary Stenoses: A Preliminary Study,” *J Addict Med,* vol. 11, no. 2, pp. 126-137, Mar/Apr, 2017.

[49] D. Han, H. Shim, B. Jeon et al., “Automatic Coronary Artery Segmentation Using Active Search for Branches and Seemingly Disconnected Vessel Segments from Coronary CT Angiography,” *PLoS One,* vol. 11, no. 8, pp. e0156837, Aug 18, 2016.

[50] Y. Zheng, H. Tek, and G. Funka-Lea, "Robust and Accurate Coronary Artery Centerline Extraction in CTA by Combining Model-Driven and Data-Driven Approaches." pp. 74-81, 2013.

[51] C. Chalopin, G. Finet, and I. E. Magnin, “Modeling the 3D coronary tree for labeling purposes,” *Med Image Anal,* vol. 5, no. 4, pp. 301-15, Dec, 2001.

[52] M. S. Akinyemi A, Poole I, Roberts C. , "Automatic labeling of coronary arteries." pp. 1562-66.

[53] M. Gulsun, L. G. Funka, Y. Zheng et al., "CTA Coronary Labeling through Efficient Geodesics between Trees Using Anatomy Priors," *LNCS.* pp. 521-528, 2014.

[54] Yang G, Broersen A, Petr R et al., "Automatic coronary artery tree labeling in coronary computed tomographic angiography datasets," 2011.

[55] C. E. Veltman, F. R. de Graaf, J. M. van Werkhoven et al., “Prognostic value of coronary vessel dominance in relation to significant coronary artery disease determined with non-

invasive computed tomography coronary angiography," *Eur Heart J,* vol. 33, no. 11, pp. 1367-1377, Apr 5, 2012.

[56] N. I. Parikh, E. J. Rosenthal, E. Honeycutt et al., "Left-Dominant Coronary Artery Circulation Is Associated with Higher in-Hospital Mortality among Patients Undergoing Percutaneous Coronary Intervention in Acute Coronary Syndrome: Data from the American College of Cardiology National Cardiovascular Data Registry for Catheterization Percutaneous Coronary Intervention," *J Am Coll Cardiol,* vol. 57, no. 14, pp. E903-E903, Apr 5, 2011.

[57] E. Abu-Assi, M. Castineira-Busto, V. Gonzalez-Salvado et al., "Coronary Artery Dominance and Long-term Prognosis in Patients With ST-segment Elevation Myocardial Infarction Treated With Primary Angioplasty," *Rev Esp Cardiol (Engl Ed),* vol. 69, no. 1, pp. 19-27, Jan, 2016.

[58] Q. Cao, A. Broersen, M. A. de Graaf et al., "Automatic identification of coronary tree anatomy in coronary computed tomography angiography," *Int J Cardiovasc Imaging,* vol. 33, no. 11, pp. 1809-1819, Nov, 2017.

[59] J. T. Dodge, Jr., B. G. Brown, E. L. Bolson et al., "Intrathoracic spatial location of specified coronary segments on the normal human heart. Applications in quantitative arteriography, assessment of regional risk and contraction, and anatomic display," *Circulation,* vol. 78, no. 5, pp. 1167-1180, Nov, 1988.

[60] P. Medrano-gracia, J. Ormiston, M. Webster et al., "Construction of a Coronary Artery Atlas from CT Angiography," *LNCS.* pp. 513-520, 2014.

[61] R. C. Cury, S. Abbara, S. Achenbach et al., "CAD-RADS™ Coronary Artery Disease e Reporting and Data System. An expert consensus document of the Society of Cardiovascular Computed Tomography (SCCT), the American College of Radiology (ACR) and the North American Society for Cardiovascular Imaging (NASCI). Endorsed by the American College of Cardiology," *J Cardiovas Comput Tomogr,* vol. 10, pp. 269-281, 2016.

[62] R. Shahzad, H. Kirisli, C. Metz et al., "Automatic segmentation, detection and quantification of coronary artery stenoses on CTA," *Int J Cardiovasc Imaging,* vol. 29, no. 8, pp. 1847-59, Dec, 2013.

[63] M. A. de Graaf, A. Broersen, W. Ahmed et al., "Feasibility of an automated quantitative computed tomography angiography-derived risk score for risk stratification of patients with suspected coronary artery disease," *Am J Cardiol,* vol. 113, no. 12, pp. 1947-55, Jun 15, 2014.

[64] J. E. van Velzen, F. R. de Graaf, M. A. de Graaf et al., "Comprehensive assessment of spotty calcifications on computed tomography angiography: comparison to plaque characteristics on intravascular ultrasound with radiofrequency backscatter analysis," *J Nucl Cardiol,* vol. 18, no. 5, pp. 893-903, Oct, 2011.

[65] W. G. Austen, J. E. Edwards, R. L. Frye et al., "A reporting system on patients evaluated for coronary artery disease. Report of the Ad Hoc Committee for Grading of Coronary Artery Disease, Council on Cardiovascular Surgery, American Heart Association," *Circulation,* vol. 51, no. 4, pp. 5-40, Apr, 1975.

[66] A. Myronenko, and X. Song, “Point set registration: coherent point drift,” *IEEE Trans Pattern Anal Mach Intell,* vol. 32, no. 12, pp. 2262-75, Dec, 2010.

[67] D. M. Leaman, R. W. Brower, G. T. Meester et al., “Coronary artery atherosclerosis: severity of the disease, severity of angina pectoris and compromised left ventricular function,” *Circulation,* vol. 63, no. 2, pp. 285-299, Feb, 1981.

[68] C. F. de Azevedo, M. S. Hadlich, S. G. Bezerra et al., “Prognostic value of CT angiography in patients with inconclusive functional stress tests,” *JACC Cardiovasc Imaging,* vol. 4, no. 7, pp. 740-751, Jul, 2011.

[69] J. K. Min, L. J. Shaw, R. B. Devereux et al., “Prognostic value of multidetector coronary computed tomographic angiography for prediction of all-cause mortality,” *J Am Coll Cardiol,* vol. 50, no. 12, pp. 1161-70, Sep 18, 2007.

[70] X. Liu, F. Hou, H. Qin et al., “Robust Optimization-based Coronary Artery Labeling from X-Ray Angiograms,” *IEEE J Biomed Health Inform,* Oct 1, 2015.

[71] B. De Bruyne, W. F. Fearon, N. H. Pijls et al., “Fractional flow reserve-guided PCI for stable coronary artery disease,” *N Engl J Med,* vol. 371, no. 13, pp. 1208-1217, Sep 25, 2014.

[72] C. Tesche, C. N. De Cecco, M. H. Albrecht et al., “Coronary CT Angiography-derived Fractional Flow Reserve,” *Radiology,* vol. 285, no. 1, pp. 17-33, Oct, 2017.

[73] R. Nakanishi, and M. J. Budoff, “Noninvasive FFR derived from coronary CT angiography in the management of coronary artery disease: technology and clinical update,” *Vasc Health Risk Manag,* vol. 12, pp. 269-278, 2016.

[74] J. W. Tukey, “Exploratory data analysis,” 1977.

[75] H. A. Kirisli, M. Schaap, C. T. Metz et al., “Standardized evaluation framework for evaluating coronary artery stenosis detection, stenosis quantification and lumen segmentation algorithms in computed tomography angiography,” *Med Image Anal,* vol. 17, no. 8, pp. 859-876, Dec, 2013.

[76] M. C.Williams, A. Moss, E. Nicol et al., “Cardiac CT Improves Outcomes in Stable Coronary Heart Disease: Results of Recent Clinical Trials,” *Curr Cardiovasc Imaging Rep,* vol. 10, no. 14, 2017.

[77] A. D. Villa, E. Sammut, A. Nair et al., “Coronary artery anomalies overview: The normal and the abnormal,” *World J Radiol,* vol. 8, no. 6, pp. 537-55, Jun 28, 2016.

[78] S. Habert, P. Khurd, and C. Chefd'hotel, “Registration of multiple temporally related point sets using a novel variant of the coherent point drift algorithm: application to coronary tree matching,” vol. 8669, pp. 86690M, 2013.

[79] S. Zeng, J. Feng, Y. An et al., "Towards Accurate and Complete Registration of Coronary Arteries in CTA Images." pp. 419-427.

[80] X. Z. Wang, Y. J. Zhang, G. S. Fu et al., “One-year clinical outcomes and multislice computed tomography angiographic results following implantation of the NeoVas bioresorbable sirolimus-eluting scaffold in patients with single de novo coronary artery lesions,” *Catheter Cardiovasc Interv,* vol. 91, no. S1, pp. 617-622, Feb 15, 2018.

[81] R. van 't Klooster, M. T. Truijman, A. C. van Dijk et al., “Visualization of local changes in vessel wall morphology and plaque progression in serial carotid artery magnetic resonance imaging,” *Stroke,* vol. 45, no. 8, pp. e160-3, Aug, 2014.

[82] W. Ma, X. Ma, S.-K. Tso et al., “A direct approach for subdivision surface fitting from a dense triangle mesh,” *Computer-Aided Design,* vol. 36, no. 6, pp. 525-536, 2004.

[83] P. H. Kitslaar, R. van’t Klooster, M. Staring et al., "Segmentation of branching vascular structures using adaptive subdivision surface fitting." p. 94133Z.

[84] L. Antiga, and D. A. Steinman, “Robust and Objective Decomposition and Mapping of Bifurcating Vessels,” *IEEE Transactions on Medical Imaging,* vol. 23, no. 6, pp. 704-713, 2004.

PUBLICATIONS

JOURNAL ARTICLES

Cao, Q., Broersen, A., Kitslaar, P. H. et al., "Automatic Coronary Artery Plaque Thickness Comparison Between Baseline and Follow-up CCTA images," Accepted by Medical Physics.

Cao, Q., Broersen, A., Kitslaar, P. H. et al., "A model-guided method for improving coronary artery tree extractions from CCTA images," Int J Comput Assist Radiol Surg, 1-11 (2018).

Cao, Q., Broersen, A., de Graaf, M. A. et al., "Automatic identification of coronary tree anatomy in coronary computed tomography angiography," Int J Cardiovasc Imaging, 33(11), 1809-1819 (2017).

INTERNATIONAL CONFERENCE PROCEEDING

Cao, Q., Broersen, A., Kitslaar, P. H. et al., "A Quality Score for Coronary Artery Tree Extraction Results," In: Proc. SPIE 10575, Medical Imaging 2018: Computer-Aided Diagnosis, Houston, Texas United States, 27 February 2018. p 105750V.

OTHER ARTICLES

Chen, Y., Zhang, Y., Yang, J, **Cao, Q**. et al., "Curve-like Structure Extraction Using Minimal Path Propagation with Back-tracing," IEEE Trans Image Process, 25(2), 988-1003 (2016).

ACKNOWLEDGEMENTS

For the whole jouney as a PhD student, I would like to say it has been difficult and tough. But I appreciate the treasure it leaves in my life.

Being a PhD student and doing research was never my plan, but I like to make things work and especially put what I learn into practice. I would like to thank Guanyu Yang who shared with me the information that LKEB is doing application-oriented researches.

I would like to express my sincere gratitude and appreciations to my promotor Prof.dr.ir., Boudewijn Lelieveldt and my supervisor Jouke Dijkstra for your suggestions when I was wandering in the reseach fields. It is you who pulled me back and told me where to focus on, and when to stop. Alex, many thanks to you, your strictness and self-organization in working really changed me a lot in my research behavior. Our discussions related to research and paper writing really helped me a lot. Without your help and support, it would have been impossible for me to accomplish my PhD study.

For the last four years regular monthly CT tree-meeting with Xinpei, Jasper, Pieter, Hans, Boudewijn, Jouke and Alex. Thanks a lot for sharing ideas, discussions and suggestions from all of you. Deep learners Hessam, Mohamed, Sahar, Denis, and Marius, our bi-weekly paper reading and discussion kept me updated in the area of deep learning.

In LKEB, I have met so many nice collegues. Jeroen, you are always there when I need any help, regarding research and daily life. Dear Poortgebouw guys, Patrick (I will miss our daily 'fight'), Shengnan, and Niels, I enjoyed our working together, our talk and the Friday afternoon beer and oliebollen.

I am aslo grateful to my Terminalzaal roommates, Baldur for the life-wise talks and English grammar help, Thomas for the gym and healthy food advise, and Xiaowu for the daily life chat and plausible suggestions. Many thanks to the other main building LKEBers, Leo for your warm hug and new year face-kisses; Niels for our outings to concerts. Rob for our discussions related to panda and China; Michèle for your IT support; Leo, Els and Berend of your excellent concert perfomances; Zhiwei, Yuchuan and Zhuo for our discussion about new ideas of publishing papers; Qian, Ling Lin, Chenhong, Ningning, Lu Huang for our daily lunch meet-up together.

I really appreaciate that the ASCI graduate school provides a platform for all medical image processing PhD students in the Netherlands.In this way, I could meet Yaoyao, Chaoping, Yuanyuan and Hua Ma, these nice friends to be able to communicate with them and get my research life inspired.

Many thanks to my best friends, Xiaowu, Lingling Wen, Zexu, Yao Xiao, Zhiwei. It has been a great treasure to meet you here in the Netherlands. Monica, Runzhang, Erqian, I would like to thank you for the time we spent together for playing badminton and all kinds of

entertainments. A lot of thanks to my friends, Qing Shu, Zhikung Zhuang in China for your encourgement and kindful comfort when I was disappointed by the experiments.

A special gratitude to my dear friends Zhong and Xiaoyan, and their daughter yixin, having been lived together for 4 years already made us a family. Xiaoyan, thanks to your wise suggestions about the life, the skills in management; your patience and encouragement when my projects depressed me. Without all of these, I wouldn't have made it this far myself.

亲爱的爸爸妈妈和我最爱的妹妹佳佳，感谢你们的理解和无条件支持。你们的鼓励，你们的报喜不报忧，你们的独当一面，都让身在异国他乡的我能心无旁骛地前行。

As I've always told my friends, I was at an age that I would say I knew nothing about the world when I came to the Netherlands. Now at the end of my PhD journery, I am leaving with full of knowledge. And the journey still continues.

To the last 5 years and 133 days!

Qing Cao

2020.01.21

CURRICULUM VITAE

QING CAO was born in Jiangsu Taizhou, China, on 14 March, 1990. She received her bachelor degree in information management and information system in 2011 at China Pharmaceutical University. In the same year, she started her master projects in the computer science department at Southeast University, China, where she started her research career in medical image processing. In 2014, she got her master's degree and decided to continue her research in the medical imaging field as a PhD student in the Division of Image processing (LKEB) group in the Leiden University Medical Center. She worked in the "Vascular and Molecular Imaging" section and has been working on the "4D CTA analysis of the coronary arteries and cardiac structures" which includes the improvement of coronary tree extraction and analysis in multi-timepoint CTA data, automatic matching of baseline and follow-up CTA data and segmentation of cardiac structures in different cardiac cycles. The contributions are collected to construct this thesis. After she finished her PhD project, she realized her enthusiasm in making the research into real applications. In July 2019, she joined the General Electric (GE) Medical System (China) and works as a senior software engineer to develop new features for the cardiovascular ultrasound scanners. In the meantime, she also works in the Digital Science group in GE Healthcare (Norway) to develop deep learning models for automatic quantifications on the cardiovascular ultrasound images.